8-2007

Control of Nonlinear Mechatronic Systems

Enver Tatlicioglu
Clemson University, etatlic@clemson.edu

CONTROL OF NONLINEAR MECHATRONIC SYSTEMS

A Dissertation
Presented to
the Graduate School of
Clemson University

In Partial Fulfillment
of the Requirements for the Degree
Doctor of Philosophy
Electrical and Computer Engineering

---

by
Enver Tatlicioglu
August 2007

Accepted by:
Dr. Darren M. Dawson, Committee Chair
Dr. Ian D. Walker
Dr. John R. Wagner
Dr. Timothy C. Burg

ABSTRACT

This dissertation is divided into four self-contained chapters. In Chapter 1, an adaptive nonlinear tracking controller for kinematically redundant robot manipulators is presented. Past research efforts have focused on the end-effector tracking control of redundant robots because of their increased dexterity over their non-redundant counterparts. This work utilizes an adaptive full-state feedback quaternion based controller developed in [1] and focuses on the design of a general sub-task controller. This sub-task controller does not affect the position and orientation tracking control objectives, but instead projects a preference on the configuration of the manipulator based on sub-task objectives such as the following: singularity avoidance, joint limit avoidance, bounding the impact forces, and bounding the potential energy.

In Chapter 2, two controllers are developed for nonlinear haptic and teleoperator systems for coordination of the master and slave systems. The first controller is proven to yield a semi-global asymptotic result in the presence of parametric uncertainty in the master and the slave dynamic models provided the user and the environmental input forces are measurable. The second controller yields a global asymptotic result despite unmeasurable user and environmental input forces provided the dynamic models of the master and slave sytems are known. These controllers rely on a transformation and a flexible target system to allow the master system's impedance to be easily adjusted so that it matches a desired target system. This work also offers a structure to encode a velocity field assist mechanism to provide the user help in controlling the slave system in completing a pre-defined contour following task. For each controller, Lyapunov-based techniques are used to prove that both controllers provide passive coordination of the haptic/teleoperator system when the velocity field assist mechanism is disabled. When the velocity field assist mechanism is enabled, the analysis proves the coordination of the haptic/teleoperator system. Simulation results are presented for both controllers.

In Chapter 3, two controllers are developed for flat multi-input/multi-output nonlinear systems. First, a robust adaptive controller is proposed and proven to yield semi-global asymptotic tracking in the presence of additive disturbances and parametric uncertainty. In addition to guaranteeing an asymptotic output tracking result, it is also proven that the parameter estimate vector is driven to a constant vector. In the second part of the chapter, a learning controller is designed and proven to yield a semi-global asymptotic tracking result in the presence of additive disturbances where the desired trajectory is periodic. A continuous nonlinear integral feedback component is utilized in the design of both controllers and Lyapunov-based techniques are used to guarantee that the tracking error is asymptotically driven to zero. Numerical simulation results are presented for both controllers.

In Chapter 4, a new dynamic model for continuum robot manipulators is derived. The dynamic model is developed based on the geometric model of extensible continuum robot manipulators with no torsional effects. The development presented in this chapter is an extension of the dynamic model proposed in [2] (by Mochiyama and Suzuki) to include a class of extensible continuum robot manipulators. First, the kinetic energy of a slice of the continuum robot is evaluated. Next, the total kinetic energy of the manipulator is obtained by utilizing a limit operation (i.e., sum of the kinetic energy of all the slices). Then, the gravitational potential energy of the manipulator is derived. Next, the elastic potential energy of the manipulator is derived for both bending and extension. Finally, the dynamic model of a planar 3-section extensible continuum robot manipulator is derived by utilizing the Lagrange representation. Numerical simulation results are presented for a planar 3-section extensible continuum robot manipulator.

DEDICATION

This work is dedicated to my wife Şeyda.

ACKNOWLEDGMENTS

I would like thank my committee members Dr. Darren M. Dawson, Dr. John R. Wagner, Dr. Timothy C. Burg, and Dr. Ian D. Walker for their invaluable technical support and guidance through out my doctoral studies. In addition, I would like to express a deep gratitude to my advisor Dr. Dawson for his support and motivation through out my studies.

I would also like to express my thanks to all my colleagues who helped me during the entire course of doctoral research: Michael McIntyre, Nitendra Nath, DonBin Lee, Bin Xian, Warren Dixon, Bryan Jones, Vilas Chitrakaran, Jian Chen, Mohammad Salah, Hariprasad Kannan, Abhijit Baviskar, Apoorva Kapadia, and Saeid Bashash. My special thanks go to Dr. David Braganza for all the inspiring conversations we had and helping me out with software issues. I have to admit that after talking to him I always felt like I do not know anything about softwares!

TABLE OF CONTENTS

Table of Contents (Continued)

Page

Table of Contents (Continued)

Page

LIST OF FIGURES

List of Figures (Continued)

Figure Page

List of Figures (Continued)

Figure Page

CHAPTER 1
ADAPTIVE NONLINEAR TRACKING CONTROL OF KINEMATICALLY REDUNDANT ROBOT MANIPULATORS WITH SUB-TASK EXTENSIONS

Introduction

In many robotic applications, the desired task is naturally defined in terms of end-effector motion. As a result, the desired robot trajectory is described by the desired position and orientation of a Cartesian coordinate frame attached to the robot manipulator's end-effector with respect to the base frame, also referred to as the *task-space*. Control of robot motion is then performed using feedback of either the joint variables (relative position of each robot joint pair) or the task-space variables. Unfortunately, joint-based control has the undesirable feature of requiring the solution of the inverse kinematics to convert the desired task-space trajectory into the desired joint space trajectory. In contrast, task-space control does not require the inverse kinematics; however, the precise tracking control of the end-effector orientation complicates the problem. For example, several parameterizations exist to describe the orientation angles, including minimum three-parameter representations (*e.g.*, Euler angles, Rodrigues parameters, *etc.*) and the non-minimum four-parameter representation given by the unit quaternion. Whereas the three-parameter representations always exhibit singular orientations (*i.e.*, the orientation Jacobian matrix in the kinematic equation is singular for some orientations), the unit quaternion-based approach can be used to represent the end-effector orientation without singularities. Thus, despite significantly complicating the control design, the unit quaternion seems to be the preferred method of formulating the end-effector orientation tracking control problem. Some past work that deals with task-space control formulation can be found in [3], [4], and [5]. Specifically, an experimental assessment of different end-effector orientation parameterization for task-space robot control was provided in [3]. One

of the first results in task-space control of robot manipulators was presented in [4]. Resolved-rate and resolved-acceleration task-space controllers using the quaternion parameterization were proposed in [5].

In addition, the control problem is further complicated in the presence of kinematic redundancy. That is, to provide the end user with increased flexibility for executing sophisticated tasks, the next generation of robot manipulators will have more degrees of freedom than are required to perform an operation in the task-space. Since the number of joints in a redundant robot is greater than the dimension of the task-space, one can show that joint motion in the null-space of the Jacobian matrix exists that does not affect task-space motion (this phenomenon is commonly referred to as *self-motion*). As noted in [6], [7], and [8], there are generally an infinite number of solutions for the inverse kinematics of redundant robots. As a result, given a desired task-space trajectory, it is difficult to select a reasonable desired joint trajectory that satisfies the control requirements (*e.g.*, closed-loop stability and boundedness of all signals) and the sub-tasks (*e.g.*, singularity avoidance, joint limit avoidance, bounding the impact forces and bounding the potential energy). Thus, there is strong motivation for control of redundant robots to be done in the task-space. For work related to controllers for redundant robots, the reader is referred to [4], [9], [10], [11], [12], [13], [14] and the references therein.

This work utilizes the adaptive full-state feedback quaternion based controller developed in [1] and focuses on the design of a general sub-task controller. The novelty of this work is the systematic integration of the sub-task controller while simultaneously achieving end-effector tracking. Other efforts have been proposed in [1], [10] and [14], but in these approaches, the sub-task objective is an *add-on* to the tracking objective without integration into the stability analysis. In [1], a sub-task control signal was introduced and can be seen in equation (2.211) as $h(t)$. In the stability analysis of [1], this sub-task signal is inconsequential to the tracking control objective as long as $h(t)$ and $\dot{h}(t)$ remain bounded. This work will exploit the

property of self-motion for redundant robot manipulators by designing a general sub-task controller that meets the above conditions while controlling the joint motion in the null-space of the Jacobian matrix to alleviate potential problems in the physical system or select configurations that are better suited for a particular application. Specific sub-task controllers will be designed for singularity avoidance, joint limit avoidance, bounding the impact forces and bounding the potential energy.

Dynamic and Kinematic Models

The dynamic model for an n-joint ($n \geq 6$), revolute, direct drive robot manipulator is described by the following expression

$$M(\theta)\ddot{\theta} + V_m(\theta, \dot{\theta})\dot{\theta} + G(\theta) + F_d\dot{\theta} = \tau \tag{1.1}$$

where $\theta(t), \dot{\theta}(t), \ddot{\theta}(t) \in \mathbb{R}^n$ denote the joint position, velocity, and acceleration in the joint-space, respectively. In (1.1), $M(\theta) \in \mathbb{R}^{n\times n}$ represents the inertia effects, $V_m(\theta, \dot{\theta}) \in \mathbb{R}^{n\times n}$ represents centripetal-Coriolis effects, $G(\theta) \in \mathbb{R}^n$ represents the gravity effects, $F_d \in \mathbb{R}^{n\times n}$ represents the constant positive definite diagonal dynamic frictional effects, $\tau(t) \in \mathbb{R}^n$ represents the control input torque vector. The subsequent development is based on the following properties [15].

Property 1 *The inertia matrix $M(\theta)$ is symmetric and positive-definite, and satisfies the following inequalities*

$$m_1 \|\xi\|^2 \leq \xi^T M(\theta)\xi \leq m_2 \|\xi\|^2 \qquad \forall \xi \in \mathbb{R}^n \tag{1.2}$$

where m_1, $m_2 \in \mathbb{R}$ are positive constants, and $\|\cdot\|$ denotes the standard Euclidean norm.

Property 2 *The inertia and centripetal-Coriolis matrices satisfy the following skew symmetric relationship*

$$\xi^T \left(\frac{1}{2} \dot{M}(\theta, \dot{\theta}) - V_m(\theta, \dot{\theta}) \right) \xi = 0 \qquad \forall \xi \in \mathbb{R}^n \tag{1.3}$$

where $\dot{M}(\theta, \dot{\theta})$ denotes the time derivative of the inertia matrix.

Property 3 *The left-hand side of (1.1) can be linearly parameterized as shown below*

$$M(\theta)\ddot{\theta} + V_m(\theta,\dot{\theta})\dot{\theta} + G(\theta) + F_d\dot{\theta} = Y_g\left(\theta,\dot{\theta},\ddot{\theta}\right)\phi \tag{1.4}$$

where $\phi \in \mathbb{R}^p$ *contains the constant system parameters, and the regression matrix* $Y_g(\cdot) \in \mathbb{R}^{n\times p}$ *contains known functions dependent on the signals* $\theta(t)$, $\dot{\theta}(t)$, *and* $\ddot{\theta}(t)$.

Let $\mathcal{E}$ and $\mathcal{B}$ be orthogonal coordinate frames attached to the end-effector of a redundant robot manipulator and its inertial frame, respectively. The position and orientation of $\mathcal{E}$ relative to $\mathcal{B}$ are commonly represented by a homogeneous transformation matrix, $T(\theta) \in \mathbb{R}^{4\times 4}$ which is defined as [15]

$$T(\theta) \triangleq \begin{bmatrix} R(\theta) & p(\theta) \\ 0_{1\times 3} & 1 \end{bmatrix} \tag{1.5}$$

where $0_{1\times 3} \triangleq \begin{bmatrix} 0 & 0 & 0 \end{bmatrix}$, the vector $p(\theta) \in \mathbb{R}^3$ and the rotation matrix $R(\theta) \in \mathbb{R}^{3\times 3}$ represent the position and orientation of the end-effector coordinate frame, respectively. From this homogeneous transformation matrix, the constrained four-parameter unit quaternion representation can be used to develop the kinematic model. From (1.5), a relationship between the position and orientation of $\mathcal{E}$ relative to $\mathcal{B}$ can be developed as follows [16]

$$\begin{bmatrix} p \\ q \end{bmatrix} \triangleq \begin{bmatrix} f_p(\theta) \\ f_q(\theta) \end{bmatrix} \tag{1.6}$$

where $f_p(\theta) \in \mathbb{R}^3$ and $f_q(\theta) \in \mathbb{R}^4$ are kinematic functions, $q(t) \triangleq \begin{bmatrix} q_o(t) & q_v^T(t) \end{bmatrix}^T \in \mathbb{R}^4$ with $q_o(t) \in \mathbb{R}$ and $q_v(t) \in \mathbb{R}^3$. The variable $q(t)$, as given in (1.6), denotes the unit quaternion [17]. The unit quaternion represents a *global nonsingular* parameterization of the end-effector orientation, and is subject to the constraint $q^Tq = 1$. Note that, while $f_p(\theta)$ is directly obtained from (1.5), several algorithms exist to determine $f_q(\theta)$ from $R(\theta)$ ([17] and [18]). Conversely, $R(q)$ can be determined given the unit quaternion parameterization [17]

$$R(q) \triangleq \left(q_o^2 - q_v^Tq_v\right) I_3 + 2q_vq_v^T + 2q_oq_v^\times \tag{1.7}$$

where $I_3 \in \mathbb{R}^{3\times 3}$ is the standard identity matrix, and the notation $a^{\times} \in \mathbb{R}^{3\times 3}$ $\forall a = [a_1 \ a_2 \ a_3]^T$, denotes the following skew-symmetric matrix

$$a^{\times} \triangleq \begin{bmatrix} 0 & -a_3 & a_2 \\ a_3 & 0 & -a_1 \\ -a_2 & a_1 & 0 \end{bmatrix}. \tag{1.8}$$

Velocity relationships can be formulated by differentiating (1.6) which can be written as

$$\begin{bmatrix} \dot{p} \\ \dot{q} \end{bmatrix} = \begin{bmatrix} J_p(\theta) \\ J_q(\theta) \end{bmatrix} \dot{\theta} \tag{1.9}$$

where $\dot{\theta}(t) \in \mathbb{R}^n$ denotes the velocity of $\mathcal{E}$ in a generalized coordinate system, and $J_p(\theta) \in \mathbb{R}^{3\times n}$, $J_q(\theta) \in \mathbb{R}^{4\times n}$ denotes the position and orientation Jacobian matrices, respectively. To facilitate the subsequent control development and stability analysis, the fact that $q(t)$ is related to the angular velocity of $\mathcal{E}$ relative to $\mathcal{B}$, denoted by $\omega(t) \in \mathbb{R}^3$ with coordinates expressed in $\mathcal{B}$, via the following differential equation ([16] and [19])

$$\dot{q} \triangleq B(q)\omega \tag{1.10}$$

where the Jacobian-type matrix $B(q) \in \mathbb{R}^{4\times 3}$ is defined as follows

$$B(q) \triangleq \frac{1}{2} \begin{bmatrix} -q_v^T \\ q_o I_3 - q_v^{\times} \end{bmatrix} \tag{1.11}$$

where $B(q)$ satisfies the following useful property

$$B^T(q)B(q) = I_3. \tag{1.12}$$

The final kinematic expression that relates the generalized Cartesian velocity to the generalized coordinate system is developed as follows

$$\begin{bmatrix} \dot{p} \\ \omega \end{bmatrix} = J(\theta)\dot{\theta} \tag{1.13}$$

where (1.9), (1.10) and (1.12) were utilized, and $J(\theta) \in \mathbb{R}^{6\times n}$ is defined as follows

$$J(\theta) \triangleq \begin{bmatrix} J_p(\theta) \\ B^T(q)J_q(\theta) \end{bmatrix}. \tag{1.14}$$

To facilitate the control development, the pseudo-inverse of $J(\theta)$ is denoted by $J^+(\theta) \in \mathbb{R}^{n\times 6}$, which is defined as follows

$$J^+ \triangleq J^T \left(JJ^T\right)^{-1} \tag{1.15}$$

where $J^+(\theta)$ satisfies the following equality

$$JJ^+ = I_6 \tag{1.16}$$

where $I_6 \in \mathbb{R}^{6\times 6}$ is the standard identity matrix. As shown in [6], the pseudo-inverse defined by (1.15) satisfies the Moore-Penrose Conditions given below

$$\begin{array}{ll} JJ^+J = J & J^+J\,J^+ = J^+ \\ (J^+J)^T = J^+J & (JJ^+)^T = JJ^+. \end{array} \tag{1.17}$$

In addition to the above properties, the matrix $(I_n - J^+J)$ satisfies the following useful properties

$$\begin{array}{l} (I_n - J^+J)\,(I_n - J^+J) = I_n - J^+J \\ (I_n - J^+J)^T = (I_n - J^+J) \\ J\,(I_n - J^+J) = 0 \\ (I_n - J^+J)\,J^+ = 0 \end{array} \tag{1.18}$$

where $I_n \in \mathbb{R}^{n\times n}$ is the standard identity matrix.

Remark 1 *During the control development, the assumption that the minimum singular value of the manipulator Jacobian, denoted by σ_m is greater than a known small positive constant $\delta > 0$, such that $\max\{\|J^+(\theta)\|\}$ is known a priori and all kinematic singularities are always avoided.*

Remark 2 *The dynamic and kinematic terms for a general revolute robot manipulator, denoted by $M(\theta)$, $V_m(\theta,\dot{\theta})$, $G(\theta)$, $J(\theta)$, and $J^+(\theta)$, are assumed to depend on $\theta(t)$ only as arguments of trigonometric functions, and hence, remain bounded for all possible $\theta(t)$. During the control development, the assumption will be made that if $p(t) \in \mathcal{L}_\infty$ then $\theta(t) \in \mathcal{L}_\infty$ (Note that $q(t)$ is always bounded since $q(t)^Tq(t) = 1$).*

Task-Space Tracking

The objective for the redundant robotic system is to design a control input that ensures the position and orientation of $\mathcal{E}$ tracks the position and orientation of a desired orthogonal coordinate frame $\mathcal{E}_d$ where $p_d(t) \in \mathbb{R}^3$ denotes the position of the origin of $\mathcal{E}_d$, relative to the origin of $\mathcal{B}$ and the rotation matrix from $\mathcal{E}_d$ to $\mathcal{B}$ is denoted by $R_d(\cdot) \in \mathbb{R}^{3\times 3}$. The standard assumption that $p_d(t)$, $\dot{p}_d(t)$, $\ddot{p}_d(t)$, $R_d(\cdot)$, $\dot{R}_d(\cdot)$, and $\ddot{R}_d(\cdot) \in \mathcal{L}_\infty$ will be utilized in the subsequent stability analysis. The position tracking error $e_p(t) \in \mathbb{R}^3$ can be defined as follows

$$e_p \triangleq p_d - p \tag{1.19}$$

where $p(t)$ was defined in (1.5). If the orientation of $\mathcal{E}_d$ relative to $\mathcal{B}$ is described by the desired unit quaternion, $q_d(t) \triangleq \begin{bmatrix} q_{od}(t) & q_{vd}^T(t) \end{bmatrix}^T \in \mathbb{R}^4$, then similar to (1.7), the desired rotation matrix can be described as follows

$$R_d(q_d) = \left(q_{od}^2 - q_{vd}^T q_{vd}\right) I_3 + 2q_{vd}q_{vd}^T + 2q_{od}q_{vd}^\times. \tag{1.20}$$

As in (1.10), $q_d(t)$ is related to the desired angular velocity of $\mathcal{E}_d$ relative to $\mathcal{B}$, denoted by $\omega_d(t) \in \mathbb{R}^3$, through the kinematic equation

$$\dot{q}_d \triangleq B(q_d)\,\omega_d. \tag{1.21}$$

To quantify the difference between the actual and desired end-effector orientations, a rotation matrix $\tilde{R}(\cdot) \in \mathbb{R}^{3\times 3}$ of $\mathcal{E}$ with respect to $\mathcal{E}_d$ is defined as follows

$$\tilde{R} \triangleq R_d^T R = \left(e_o^2 - e_v^T e_v\right) I_3 + 2e_v e_v^T + 2e_o e_v^\times \tag{1.22}$$

where the unit quaternion tracking error, $e_q(t) \triangleq \begin{bmatrix} e_o(t) & e_v^T(t) \end{bmatrix}^T \in \mathbb{R}^4$ can be derived as follows (see [5] and Theorem 5.3 of [20])

$$e_q \triangleq \begin{bmatrix} e_o \\ e_v \end{bmatrix} = \begin{bmatrix} q_o q_{od} + q_v^T q_{vd} \\ q_{od} q_v - q_o q_{vd} + q_v^\times q_{vd} \end{bmatrix} \tag{1.23}$$

where $e_q(t)$ satisfies the constraint

$$e_q^T e_q = e_0^2 + e_v^T e_v = 1, \tag{1.24}$$

which indicates that

$$0 \leq \|e_v(t)\| \leq 1 \qquad 0 \leq |e_0(t)| \leq 1 \tag{1.25}$$

for all time.

Based on the above definitions, the end-effector position and orientation tracking objectives can be stated as follows

$$\|e_p(t)\| \to 0 \text{ and } \tilde{R}(e_q) \to I_3 \text{ as } t \to \infty, \tag{1.26}$$

respectively. The orientation tracking objective given in (1.26) can also be stated in terms of the unit quaternion error of (1.23). Specifically, it is easy to see from (1.24) that

$$\text{if } \|e_v(t)\| \to 0 \text{ as } t \to \infty, \text{ then } |e_0(t)| \to 1 \text{ as } t \to \infty; \tag{1.27}$$

hence, it can be stated from (1.22) and (1.27) that

$$\text{if } \|e_v(t)\| \to 0 \text{ as } t \to \infty, \text{ then } \tilde{R}(e_q) \to I_3 \text{ as } t \to \infty. \tag{1.28}$$

Task-Space Control Development

Based on the open-loop kinematic tracking error system given in [1] and the subsequent stability analysis, the control input is designed as follows

$$\tau \triangleq Y\hat{\phi} + K_r r + (\Lambda J)^T \begin{bmatrix} e_p \\ e_v \end{bmatrix} \tag{1.29}$$

where $K_r \in \mathbb{R}^{n \times n}$ is a positive-definite, diagonal, control gain matrix, and $\hat{\phi}(t) \in \mathbb{R}^p$ denotes the parameter estimate vector which is updated according to

$$\dot{\hat{\phi}} \triangleq \Gamma Y^T r \tag{1.30}$$

with $\Gamma \in \mathbb{R}^{p \times p}$ being a positive-definite, diagonal, adaptation gain matrix. The auxiliary signal $r(t) \in \mathbb{R}^n$ can be defined as follows

$$r \triangleq u_d - \dot{\theta} \tag{1.31}$$

where $u_d(t) \in \mathbb{R}^n$ is an auxiliary control input defined as follows

$$u_d \triangleq J^+ \Lambda^{-1} \begin{bmatrix} \dot{p}_d + K_1 e_p \\ -R_d^T \omega_d + K_2 e_v \end{bmatrix} + \left(I_n - J^+ J \right) h \tag{1.32}$$

where K_1, $K_2 \in \mathbb{R}^{3\times 3}$ are positive-definite, diagonal, control gain matrices, the matrix $\Lambda(t) \in \mathbb{R}^{6\times 6}$ is defined as follows

$$\Lambda \triangleq \begin{bmatrix} -I_3 & 0_{3\times 3} \\ 0_{3\times 3} & R_d^T \end{bmatrix} \tag{1.33}$$

where $0_{3\times 3} \in \mathbb{R}^{3\times 3}$ denotes a matrix of zeros, and $h(\theta) \in \mathbb{R}^n$ is the subsequently designed sub-task controller signal. The linear parameterization introduced in (1.29) is defined as follows

$$Y\phi \triangleq M\dot{u}_d + V_m u_d + G(\theta) + F_d \dot{\theta} \tag{1.34}$$

where $Y(p_d, \dot{p}_d, \ddot{p}_d, e_q, \theta, \dot{\theta}, h, \dot{h}) \in \mathbb{R}^{n\times p}$ denotes the measurable regression matrix, and $\phi \in \mathbb{R}^p$ represents the constant parameter vector (*e.g.*, mass, inertia, and friction coefficients). To obtain the closed-loop dynamics for $r(t)$, the time derivative of (1.31) is taken, pre-multiply the resulting equation by $M(\theta)$, and substitute (1.1) to obtain the following

$$M\dot{r} = -V_m r + Y\tilde{\phi} - K_r r - (\Lambda J)^T \begin{bmatrix} e_p \\ e_v \end{bmatrix} \tag{1.35}$$

where the parameter estimation error signal $\tilde{\phi}(t) \in \mathbb{R}^p$ is defined as follows

$$\tilde{\phi} \triangleq \phi - \hat{\phi}. \tag{1.36}$$

Remark 3 *A benchmark adaptive controller was utilized to compensate for the parametric uncertainties present in the dynamic model (e.g., mass, inertia, and friction coefficients). Alternatively, a robust or sliding mode controller could also be used to compensate for modeling uncertainties not restricted to parametric uncertainties (e.g. see [21]).*

The following theorem can be stated regarding the stability of the closed loop system.

Theorem 1 *The control law described by (1.29) guarantees global asymptotic end-effector position and orientation tracking in the sense that*

$$\|e_p(t)\| \to 0 \ as \ t \to \infty \tag{1.37}$$

and

$$\tilde{R}(e_q(t)) \to I_3 \ as \ t \to \infty, \tag{1.38}$$

as well as that all signals are bounded provided $h(\theta) \in \mathcal{L}_\infty$ *and* $\frac{\partial h(\theta)}{\partial \theta} \in \mathcal{L}_\infty$. *(Note the assumption given in Remark 2 has been utilized.)*

Proof. See [1] for proof.

Sub-Task Control Objective

In addition to the tracking control objective, there can be sub-task objectives that are required for a particular redundant robot application. To this end, the auxiliary control signal $h(\theta)$, as introduced in (1.32), allows for sub-task objectives to be integrated into the controller. This sub-task integration is completed by designing a framework that places preferences on desirable configurations where an infinite number of choices are available when dealing with the *self-motion* of the redundant robot. These sub-tasks are integrated through the joint motion in the null-space of the standard Jacobian matrix by designing $h(\theta)$. Theorem 1 requires that $h(\theta)$, $\frac{\partial h(\theta)}{\partial \theta} \in \mathcal{L}_\infty$, provided $\theta(t) \in \mathcal{L}_\infty$. Based on Remark 2, and the proof of Theorem 1 it is clear that $\theta(t) \in \mathcal{L}_\infty$. In the subsequent section, $h(\theta)$ will be designed to meet these conditions. In the event that a subsequently defined Jacobian-related matrix loses rank, the sub-task objective is not guaranteed. More specifically, if the Jacobian-related matrix maintains full rank, then the sub-task objective is met as proven in the subsequent stability analysis.

Sub-Task Closed-Loop Error System

In this section, a general sub-task closed-loop error system is developed. To this end, an auxiliary signal $y_a(t) \in \mathbb{R}^+$ is defined as follows

$$y_a \triangleq \exp\left(-\alpha\beta(\theta)\right) \tag{1.39}$$

where $\alpha \in \mathbb{R}^+$ is a constant, $\beta(\theta) \in \mathbb{R}^+$ is selected for each sub-task, and $\exp(\cdot)$ is the standard logarithmic exponential function. To determine the dynamics of $y_a(t)$, the time derivative of (1.39) is taken and can be written as follows

$$\dot{y}_a = J_s\dot{\theta} \tag{1.40}$$

where a Jacobian-type vector $J_s(t) \in \mathbb{R}^{1\times n}$ is defined as follows

$$J_s = \frac{\partial y_a}{\partial \theta}. \tag{1.41}$$

From (1.40), a substitution can be made for $\dot{\theta}(t)$ and the following expression for $\dot{y}_a(t)$ can be written as follows

$$\dot{y}_a = J_s J^+\Lambda^{-1}\begin{bmatrix} \dot{p}_d + K_1 e_p \\ -R_d^T\omega_d + K_2 e_v \end{bmatrix} + J_s\left(I_n - J^+J\right)h - J_s r \tag{1.42}$$

where (1.31) and (1.32) were both utilized. Based on the dynamics of (1.42) and the subsequent stability analysis, the sub-task control input can be designed as follows

$$h \triangleq -k_{s1}\left[J_s\left(I_n - J^+J\right)\right]^T y_a \tag{1.43}$$

where $k_{s1} \in \mathbb{R}^+$ is a constant gain. After substituting (1.43) into (1.42), the following expression can be obtained

$$\dot{y}_a = J_s J^+\Lambda^{-1}\begin{bmatrix} \dot{p}_d + K_1 e_p \\ -R_d^T\omega_d + K_2 e_v \end{bmatrix} - J_s r - k_{s1}\left\|J_s\left(I_n - J^+J\right)\right\|^2 y_a. \tag{1.44}$$

Remark 4 *The auxiliary signal $y_a(t)$ in (1.39) was selected because of the useful properties of the logarithmic exponential function. From (1.39) it is clear that $0 < y_a(t) \leq 1$, and that as $\beta(\theta)$ increases, $y_a(t)$ decreases. This definition of $y_a(t)$ is arbitrary and many different positive functions could also be utilized.*

The following theorem can now be stated regarding the performance of the sub-task closed-loop error system.

Theorem 2 *The control law described by (1.43) guarantees that $y_a(t)$ is practically regulated (i.e., ultimately bounded) in the following sense*

$$|y_a(t)| \leq \sqrt{|y_a^2(t_0)| \exp\left(-2\gamma t\right) + \frac{\varepsilon}{\gamma}} \tag{1.45}$$

provided the following sufficient conditions hold

$$\left\| J_s \left(I_n - J^+ J \right) \right\|^2 > \bar{\delta} \tag{1.46}$$

and

$$k_{s1} > \frac{1}{\bar{\delta} \delta_2} \tag{1.47}$$

where ε, γ, $\bar{\delta}$, $\delta_2 \in \mathbb{R}^+$ are constants.

Proof. See Appendix A.

Remark 5 *In the subsequent sub-sections, specific $\beta(\theta)$ functions will be designed for different sub-task objectives. Each $\beta(\theta)$ is designed specifically to only depend on $\theta(t)$. For most of the sub-task objectives, the problem is set up to require that $\beta(\theta) > 0$ which is achieved by keeping $y_a(t) < 1$. From (1.45), it is clear that $y_a(t) < 1$ if the following inequality holds*

$$\sqrt{|y_a^2(t_0)| + \frac{\varepsilon}{\gamma}} < 1 \tag{1.48}$$

which can be achieved through the selection of the robot manipulator's initial condition, control gains k_{s1}, α, and bounding constants. For other sub-task objectives, the problem is to maximize $\beta(\theta)$ as $t \to \infty$ (minimize $y_a(t)$ as $t \to \infty$). From the result of Theorem 2 as seen in (1.45), a true maximization of $\beta(\theta)$ (minimization of $y_a(t)$) is not achieved. However, an increasing lower bound for $\beta(\theta)$ (an exponentially decreasing upper bound for $y_a(t)$) is achieved from (1.45).

Remark 6 *The four sub-task objectives as described in the subsequent sub-sections are met only if the sufficient conditions as described by (1.46) and (1.47) are met. These sub-task objectives are secondary to the tracking objective which is always guaranteed by Theorem 1. In the event that the sub-task controller attempts to force the robot manipulator's end-effector to take a path not allowed by the tracking controller, the condition in (1.46) will not be met; hence, the result of Theorem 2 will not hold. With this fact in mind, the formulation of the desired task-space trajectory and the sub-task objectives require careful consideration to meet both the tracking and sub-task objectives simultaneously.*

Sub-Task 1: Singularity Avoidance

The objective for this sub-task is to keep the robot manipulator away from configurations that result in singularities, and hence, decrease the manipulability of the robot manipulator. For this sub-task, let $\beta(\theta)$ be defined as the manipulability measure of a robot manipulator given by the following definition [22]

$$\beta = \sqrt{\det\left[JJ^T\right]} \tag{1.49}$$

where $\det[\cdot]$ is the determinant of the 6×6 matrix $J(\theta) J^T(\theta)$ and $\beta(\theta) = 0$ when the robot is in a singular configuration. From (1.39), (1.45), (1.48), and (1.49), it is clear that $\beta(\theta) > 0 \; \forall t$, provided the sufficient conditions are met, hence meeting this sub-task objective.

Sub-Task 2: Joint Limits

Joint limits are a mechanical constraint for almost all robot manipulators. In (1.1), the joint angles represented by $\theta_i(t) \in \mathbb{R}^+ \; \forall i = 1..n$ operate in the range of $\theta_i \in \left[\begin{array}{cc} \theta_i^{\min} & \theta_i^{\max} \end{array} \right]$, where $\theta_i^{\min}$, $\theta_i^{\max} \in \mathbb{R}^+$ are the minimum and maximum joint limits for each joint, respectively. The objective for this sub-task is to keep each

joint angle away from its respective joint limits, while executing the tracking control objective. For this sub-task, the auxiliary signal $\beta(\theta)$ is defined as follows

$$\beta \triangleq \prod_{i=1}^{n} \left[\left(1 - \frac{\theta_i}{\theta_i^{\max}} \right) \left(\frac{\theta_i}{\theta_i^{\min}} - 1 \right) \right]. \tag{1.50}$$

From (1.50), it is clear that $\beta(\theta) > 0$ as long as all joints are not at the joint limits. From (1.39), (1.45), (1.48), and (1.50), it is clear that $\beta(\theta) > 0 \ \forall t$, provided the sufficient conditions are met, hence meeting this sub-task objective.

Sub-Task 3: Impact Force Configurations

For collision applications of robotic manipulators, the user often requires the ability to specify the impact force the end-effector makes with the environment. For hammering, or chiseling applications, the user may want to maximize the impact force, while in a medical application, the desire to have reduced collision force may be necessary. To study these concepts, an impact force measure is defined as, $F(t) \in \mathbb{R}$, which can be written as follows [23]

$$F \triangleq \frac{-(1+\kappa)\,\vartheta^T \eta}{\eta^T J M^{-1} J^T \eta} \tag{1.51}$$

where $\kappa \in \mathbb{R}$ denotes the type of collision (κ is either zero or one), $\vartheta(t) \in \mathbb{R}^3$ is the velocity vector for the two colliding bodies, and $\eta(t) \in \mathbb{R}^3$ is a vector normal to the plane of contact for the two colliding bodies, $M(\theta) \in \mathbb{R}^{n \times n}$ is the inertia matrix as found in (1.1). Utilizing (1.51), impact force sub-task objectives can be defined to either upper or lower bound the impact force with the environment.

Upper Bounding the Impact Force

The objective for this sub-task is to keep the robot manipulator away from postures that are "best" suited for impact with the environment for a given end-effector velocity and point of contact, hence $\vartheta(t)$ and $\eta(t)$ are predetermined and fixed. To this end, $\beta(\theta)$, is defined as the denominator of (1.51), and can be written as follows [23]

$$\beta = \eta^T J M^{-1} J^T \eta. \tag{1.52}$$

Large values of $\beta(\theta)$ indicate postures with small impact forces at the end-effector [23]; therefore, the goal of this sub-task is to force the manipulator into postures that results in larger values of $\beta(\theta)$. From (1.39), (1.45), (1.48), and (1.52), it is clear that $\beta(\theta(t)) > 0 \ \forall t$, provided the sufficient conditions are met.

Withstanding Impacts

An alternate impact sub-task is to push the robot manipulator into postures that are "best" suited to withstand impacts with the environment. For this case, let $\beta(\theta)$ be defined as the *dynamic impact measure* given by the following definition [23]

$$\beta \triangleq \sqrt{\det\left[(J^{+})^{T} M^{2} J^{+}\right]}. \tag{1.53}$$

Large values of $\beta(\theta)$ indicate postures with high impact forces at the end-effector [23]; therefore, the goal of this sub-task is to force the manipulator into postures that results in larger values of $\beta(\theta)$. From (1.39), (1.45), (1.48), and (1.53), it is clear that $\beta(\theta(t)) > 0 \ \forall t$, provided the sufficient conditions are met.

Remark 7 *For the adaptive control paradigm, the constant parameters for the inertia matrix $M(\theta)$ are not precisely known; therefore, estimates of these parameters must be utilized in (1.52) and (1.53) in lieu of the actual values. The matrix inverse of the estimate of $M(\theta)$ (i.e., $\hat{M}(\theta)$) can be guaranteed through the use of a projection as described in [24].*

Sub-Task 4: Upper Bounding the Potential Energy

The objective for this sub-task is to keep the robot manipulator away from postures that result in an unnecessarily high level of potential energy. With the flexibility inherent to redundant robots, a posture with less potential energy is more desirable, thus providing an increase in system efficiency. The potential energy, $\mu(t) \in \mathbb{R}$, stored in the manipulator can be defined as follows [22]

$$\mu \triangleq -\sum_{i=1}^{n} \left[m_{li} g_o^T P_{li} + m_{mi} g_o^T P_{mi}\right] \tag{1.54}$$

where $m_{li}, m_{mi}\ \forall i = 1..n$ are the joint and rotor masses, respectively, $P_{mi}(\theta) \in \mathbb{R}^3$ is a vector from the origin of the base frame $\mathcal{B}$ to the center position of the rotor, $g_o \triangleq \begin{bmatrix} 0 & 0 & -g \end{bmatrix}^T$ is the gravitational acceleration vector in the base frame where g is the gravitational constant, and $P_{li}(\theta) \in \mathbb{R}^3$ is a vector described as follows [22]

$$P_{li} \triangleq \frac{1}{m_{li}} \int_{V_{li}} P_i^* \rho dV \tag{1.55}$$

where $\rho \in \mathbb{R}$ is the density of the elementary particle of volume dV, $P_i^*(\theta) \in \mathbb{R}^3$ is a vector from the origin of $\mathcal{B}$ to the center joint position. From (1.54) and (1.55), it is clear that $\mu(t)$ is a function of $\theta(t)$ and by convention is always positive. For this sub-task, the auxiliary signal $y_a(t) \in \mathbb{R}$ is defined as follows

$$y_a \triangleq \mu(\theta). \tag{1.56}$$

The goal is to force the manipulator to take postures with less potential energy. From (1.45), (1.48), and (1.56), provided the sufficient conditions are met, it is clear that by making the control gain k_{s1} large, γ is made large (See Appendix A), and by examining (1.45), it is clear that the potential energy will have an exponentially decreasing upper bounded.

Remark 8 *For the adaptive control paradigm, the constant parameters for the rotor and joint masses are not precisely known; therefore, estimates of these parameters must be utilized in (1.54) and (1.55) in lieu of the actual values as discussed in Remark 7.*

Simulation Results

To illustrate the performance of the tracking and sub-task controller presented above, a simplified kinematic simulation was completed for a planar 3-joint revolute robot. This robot is redundant because there are 3 joints in a 2 dimensional task-space. For the simulation, a feedback linearization controller was utilized, and hence

the adaptation mechanism was not required[1]. Specifically, the following dynamic model was utilized

$$M(\theta)\ddot{\theta} + N\left(\theta, \dot{\theta}\right) = \tau \tag{1.57}$$

where $\ddot{\theta}(t)$, $\tau(t) \in \mathbb{R}^3$, the inertia matrix $M(\theta) \in \mathbb{R}^{3\times 3}$ is defined as follows

$$M(\theta) = \begin{bmatrix} M_{11} & M_{12} & M_{13} \\ M_{12} & M_{22} & M_{23} \\ M_{13} & M_{23} & M_{33} \end{bmatrix}$$

where

$$\begin{array}{ll} M_{11} = p_1 + 2p_4c2 + 2p_5c23 + 2p_6c3 & M_{22} = p_2 + 2p_6c3 \\ M_{12} = p_2 + p_4c2 + p_5c23 + 2p_6c3 & M_{23} = p_2 + p_6c3 \\ M_{13} = p_2 + p_5c23 + p_6c3 & M_{33} = p_3 \end{array}$$

where $p_1 = 1.2746$ [kg·m^2], $p_2 = 0.3946$ [kg·m^2], $p_3 = 0.0512$ [kg·m^2], $p_4 = 0.4752$ [kg·m^2], $p_5 = 0.128$ [kg·m^2], $p_6 = 0.1152$ [kg·m^2] and $c2 \triangleq \cos(\theta_2)$, $c3 \triangleq \cos(\theta_3)$, and $c23 \triangleq \cos(\theta_2 + \theta_3)$, $N\left(\theta, \dot{\theta}\right) \in \mathbb{R}^3$ represents the centripetal-Coriolis, gravitational and frictional effects. For the potential energy simulations given below, the gravitational effects $G(\theta) = \begin{bmatrix} G_1(\theta) & G_2(\theta) & G_3(\theta) \end{bmatrix}^T$where $G_1(\theta), G_2(\theta), G_3(\theta) \in \mathbb{R}$ are defined as follows

$$G_1(\theta) = \frac{1}{2}m_{l1}gl_1c1 + m_{l2}g(l_1c1 + \frac{1}{2}l_2c12) + m_{l3}g(l_1c1 + l_2c12 + \frac{1}{2}l_3c123)$$

$$G_2(\theta) = \frac{1}{2}m_{l2}gl_2c12 + m_{l3}g(l_2c12 + \frac{1}{2}l_3c123)$$

$$G_3(\theta) = \frac{1}{2}m_{l3}gl_3c123$$

where the center of mass is at the midpoint of each joint, and was selected as follows: $m_{l1} = 3.6$ [kg], $m_{l2} = 2.6$ [kg], and $m_{l3} = 2$ [kg], the joint lengths were selected as follows: $\ell_1 = 0.40$ [m], $\ell_2 = 0.36$ [m], and $\ell_3 = 0.32$ [m], the gravitational constant

[1] A feedback linearization controller was utilized, as opposed to an adaptive controller, to more clearly illustrate the performance of the sub-task objective.

was selected as follows: $g = 9.8\ [\frac{\text{m}}{\text{sec}^2}]$, and $c1 \triangleq \cos(\theta_1)$, $c12 \triangleq \cos(\theta_1 + \theta_2)$, $c123 \triangleq \cos(\theta_1 + \theta_2 + \theta_3)$, $s1 \triangleq \sin(\theta_1)$, $s12 \triangleq \sin(\theta_1 + \theta_2)$, and $s123 \triangleq \sin(\theta_1 + \theta_2 + \theta_3)$. Feedback linearization can be used to linearize (1.57) as follows

$$M(\theta) U_c + N\left(\theta, \dot{\theta}\right) = \tau \tag{1.58}$$

where $U_c(t) \in \mathbb{R}^3$ is the inner loop control input. After substituting (1.58) into (1.57), we have

$$\ddot{\theta} = U_c. \tag{1.59}$$

The task-space is defined by $x(t) \in \mathbb{R}^2$, where $x(t) \triangleq \begin{bmatrix} x_1(t) & x_2(t) \end{bmatrix}^T$, and $x_1(t)$, $x_2(t) \in \mathbb{R}$ are scalar euclidean coordinates. The planar 3-joint robot has the following forward kinematics for the end-effector

$$\begin{bmatrix} x_1 \\ x_2 \end{bmatrix} \triangleq \begin{bmatrix} \ell_1 c1 + \ell_2 c12 + \ell_3 c123 \\ \ell_1 s1 + \ell_2 s12 + \ell_3 s123 \end{bmatrix} \tag{1.60}$$

and the manipulator Jacobian

$$J(q) \triangleq \begin{bmatrix} -\ell_1 s1 - \ell_2 s12 - \ell_3 s123 & -\ell_2 s12 - \ell_3 s123 & -\ell_3 s123 \\ \ell_1 c1 + \ell_2 c12 + \ell_3 c123 & \ell_2 c12 + \ell_3 c123 & \ell_3 c123 \end{bmatrix} \tag{1.61}$$

The elimination of the dynamics and rotational tracking requirement simplifies the control problem, therefore it is necessary to redefine some key terms to establish a simplified closed-loop error system. The position tracking error signal $e(t) \in \mathbb{R}^2$ can now be defined as follows

$$e \triangleq x_d - x \tag{1.62}$$

where the desired trajectory $x_d(t) \in \mathbb{R}^2$ is generated by the following bounded dynamic system

$$\begin{bmatrix} \dot{x}_{d1} \\ \dot{x}_{d2} \end{bmatrix} \triangleq \begin{bmatrix} -0.05 \sin(0.1t) \\ 0.004 \left(\cos(0.1t)\right)^2 - 0.004 \left(\sin(0.1t)\right)^2 \end{bmatrix} \tag{1.63}$$

and can be seen in Figure 1.1.

The auxiliary control input $u_d(t)$ as defined in (1.32) can be simplified as follows

$$u_d \triangleq J^+ \left(K_s e + \dot{x}_d\right) + \left(I_3 - J^+ J\right) h \in \mathbb{R}^3 \tag{1.64}$$

where $K_s \in \mathbb{R}^{2\times 2}$ is a positive-definite, diagonal, control gain matrix. The inner loop control input is defined as follows

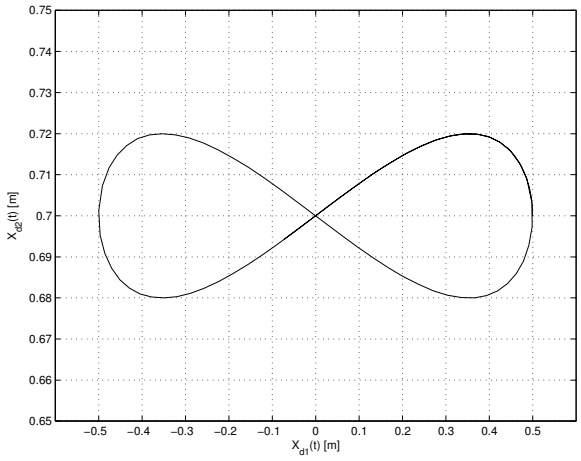

Figure 1.1 Desired task-space trajectory.

$$U_c \triangleq k_o r + \dot{u}_d + J^T e \tag{1.65}$$

where $k_o \in \mathbb{R}^+$is a positive control gain. The simplified closed-loop error system can now be written as follows

$$\dot{r} = -k_o r - J^T e. \tag{1.66}$$

To demonstrate the performance of all the sub-task controllers, a different simulation was completed for each sub-task. The initial conditions for the robot manipulator in each sub-task were intentionally selected to make $\beta\left(\theta(t_0)\right) \approx 0$ (i.e. maximize $y_a(t_0)$) to demonstrate that (1.45) holds for each simulation run. In the case of the potential energy sub-task, the initial conditions for the robot manipulator was selected to maximize $\mu(t_0)$.

Singularity Avoidance

To demonstrate the sub-task controller's performance for singularity avoidance as described by (1.39), (1.43) and (1.49), the robot manipulator was initially at rest at

the following joint positions (i.e. $\beta(\theta(t_0)) \approx 0$):

$$\theta(t_0) = \begin{bmatrix} 0.45[rad] & 0.0[rad] & 3.1[rad] \end{bmatrix}^T$$

with the gains selected as follows

$$K_s = diag\{2, 2\},\ k_0 = 2,\ k_{s1} = 1 \text{ and } \alpha = 4$$

where $diag\{\cdot\}$ denotes a diagonal matrix with arguments along the diagonal. Both the tracking and singularity avoidance sub-task were successfully demonstrated, and can be seen by the following figures: the manipulability measure $\beta(\theta)$ and the tracking error can be seen in Figures 1.2 and 1.3, respectively.

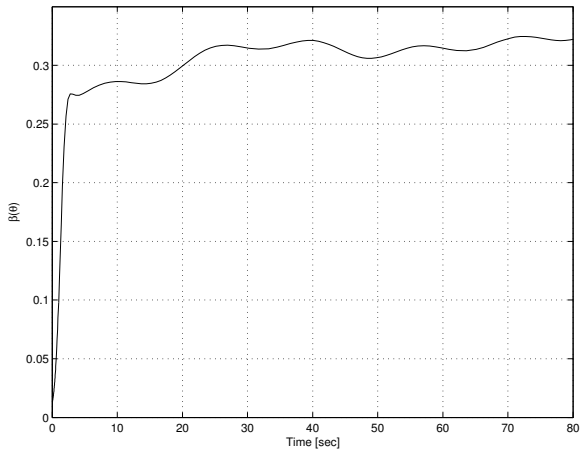

Figure 1.2 Manipulability Measure

Joint Limits

To demonstrate the sub-task controller's performance for joint limit avoidance as described by (1.39), (1.43), and (1.50), the robot manipulator was initially at rest at the following joint positions (i.e. $\beta(\theta(t_0)) = 0$):

$$\theta(t_0) = \begin{bmatrix} 0.5[rad] & 1.5[rad] & 3.5[rad] \end{bmatrix}^T$$

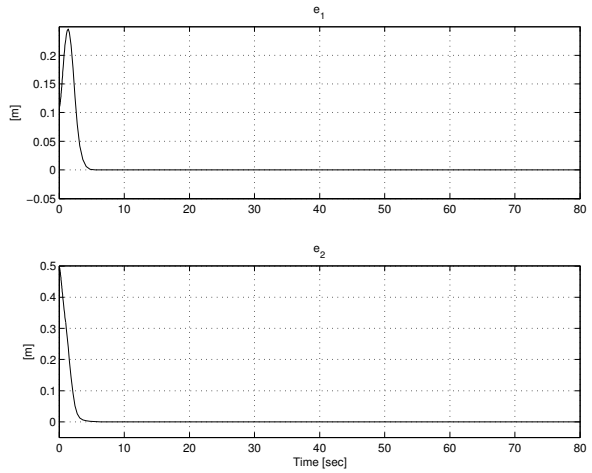

Figure 1.3 Tracking Error (Manipulability sub-task)

with the gains selected as follows

$$K_s = diag\{1, 4\},\ k_0 = 8,\ k_{s1} = 1 \text{ and } \alpha = 1.$$

The joint limits were set to the following values

$$\begin{aligned} \theta_1^{\min} &= \theta_2^{\min} = 0.5[rad] \text{ and } \theta_3^{\min} = 0.1[rad] \\ \theta_1^{\max} &= \theta_2^{\max} = 2[rad] \text{ and } \theta_3^{\max} = 6[rad]. \end{aligned}$$

Both the tracking and joint limits sub-task were successfully demonstrated and can be seen by the following figures: the auxiliary signal $\beta(\theta)$ and the tracking error can be seen in Figures 1.4 and 1.5, respectively.

Impact Force Configurations

Upper Bounding the Impact Force

To demonstrate the sub-task controller's performance for upper bounding the impact force as described by (1.39), (1.43) and (1.52), the robot manipulator was initially at rest at the following joint positions:

$$\theta(t_0) = \begin{bmatrix} 0.45[rad] & 0.0[rad] & 2.9[rad] \end{bmatrix}^T \tag{1.67}$$

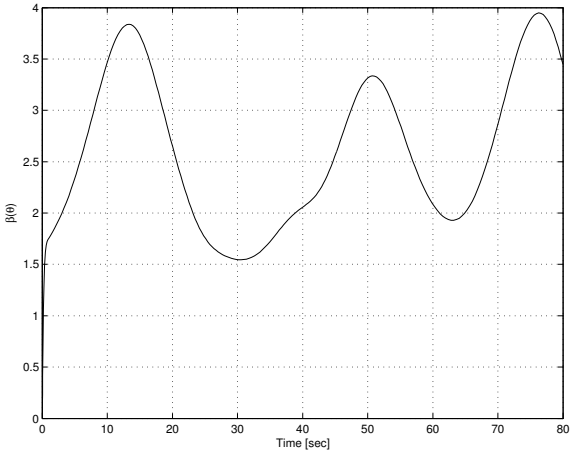

Figure 1.4 $\beta(\theta)$ for Joint Limits Avoidance Sub-Task

with the gains selected as follows

$$K_s = diag\{4, 4\}, k_0 = 3, k_{s1} = 1 \text{ and } \alpha = 8.$$

The initial conditions as described in (1.67) places the robot in a configuration resulting in $\beta(\theta(t_0)) \approx 0$, (i.e. a configuration with a high impact force potential). For this simulation, a plane of contact that is always perpendicular to $x_1 axis$ is assumed, so $\eta(t) = \begin{bmatrix} 1 & 0 \end{bmatrix}^T$ and is fixed. Although contact is never made, the sub-task controller works to place the robot in a configuration with less impact force potential (i.e. $\beta(\theta(t)) > \beta(\theta(t_0))$). Both the tracking and upper bounding the impact force sub-task were successfully demonstrated and can be seen by the following figures: the denominator of (1.51) which was defined as $\beta(\theta)$ and the tracking error can be seen in Figures 1.6 and 1.7, respectively.

Withstanding Impacts

To demonstrate the sub-task controller's performance for withstanding impacts as described by (1.39), (1.43) and (1.53), the robot manipulator was initially at rest at

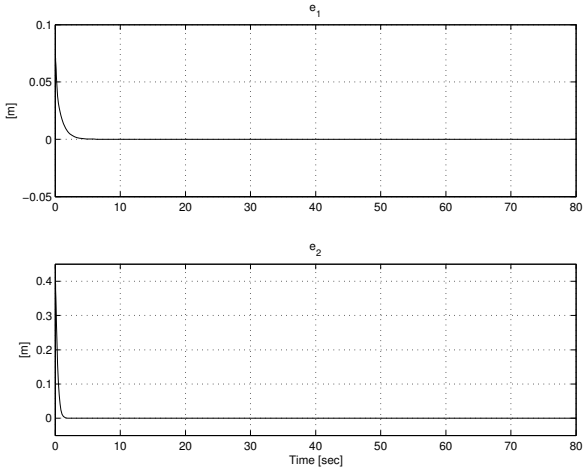

Figure 1.5 Tracking Error (Joint Limits Avoidance Sub-Task)

the following joint positions:

$$\theta(t_0) = \begin{bmatrix} 0.1[rad] & 1.7[rad] & 4.5[rad] \end{bmatrix}^T \tag{1.68}$$

with the gains selected as follows

$$K_s = diag\{1, 1\},\ k_0 = 4,\ k_{s1} = 1 \text{ and } \alpha = 1.$$

The initial conditions as described in (1.68) places the robot in a configuration with a high impact force potential. For this simulation, a plane of contact that is always perpendicular to desired trajectory is assumed. Although contact is never made, the sub-task controller works to place the robot in a configuration with greater impact force potential (i.e. $\beta(\theta(t)) > \beta(\theta(t_0))$). Both the tracking and withstanding impacts sub-task were successfully demonstrated and can be seen by the following figures: the withstanding impacts measure $\beta(\theta)$ and the tracking error can be seen in Figures 1.8 and 1.9, respectively.

Upper Bounding the Potential Energy

To demonstrate the sub-task controller's performance for upper bounding the potential energy as described by (1.43) and (1.56), the robot manipulator was initially

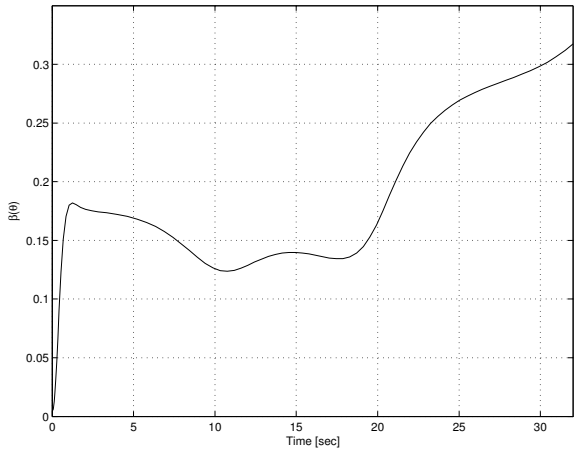

Figure 1.6 $\beta(\theta)$ for Upper Bounding the Impact Force Sub-Task

at rest at the following joint positions:

$$\theta(t_0) = \begin{bmatrix} 1.57[rad] & 0.1[rad] & 0.48[rad] \end{bmatrix}^T$$

with the gains selected as follows

$$K_s = diag\{1, 1\},\ k_0 = 2 \text{ and } k_{s1} = 1.$$

Both the tracking and upper bounding the potential energy sub-task were successfully demonstrated and can be seen by the following figures: the potential energy measure $\mu(\theta)$ and the tracking error can be seen in Figures 1.10 and 1.11, respectively.

Conclusion

This work utilized an adaptive full-state feedback quaternion based controller developed in [1] and focused on the design of a general sub-task controller. This general sub-task controller was developed as to not affect the tracking control objective, and allows for the design of specific sub-task objectives. Four specific sub-tasks were designed as follows: singularity avoidance, joint-limit avoidance, bounding the impact forces, and bounding the potential energy. Simulation results are presented that demonstrates both the tracking and sub-task objectives were met simultaneously.

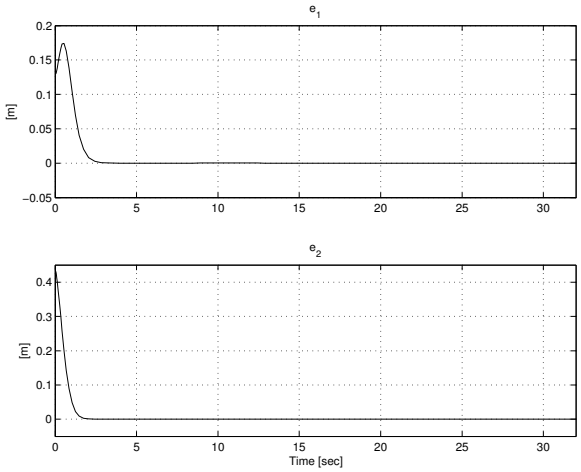

Figure 1.7 Tracking Error (Upper Bounding the Impact Force Sub-Task)

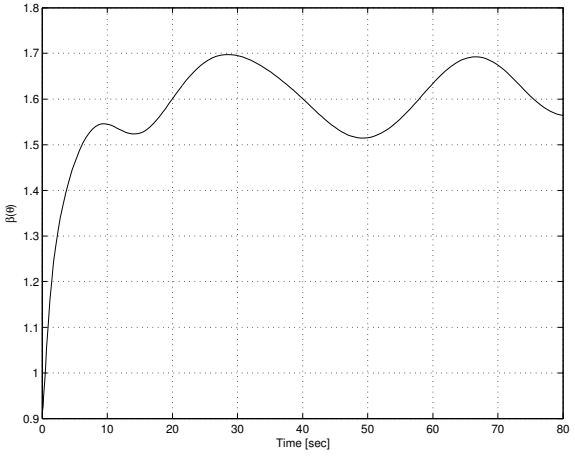

Figure 1.8 $\beta(\theta)$ for Withstanding Impacts Sub-Task

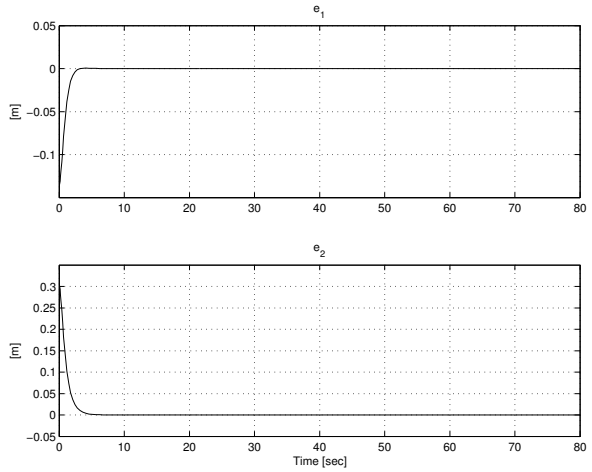

Figure 1.9 Tracking Error (Withstanding Impacts Sub-Task)

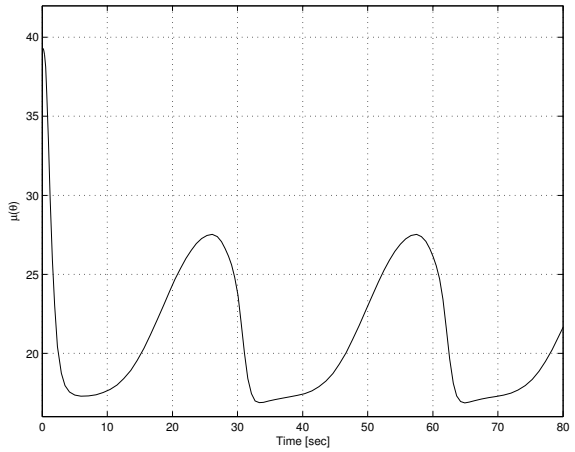

Figure 1.10 $\mu(\theta)$ for Upper Bounding the Potential Energy Sub-Task

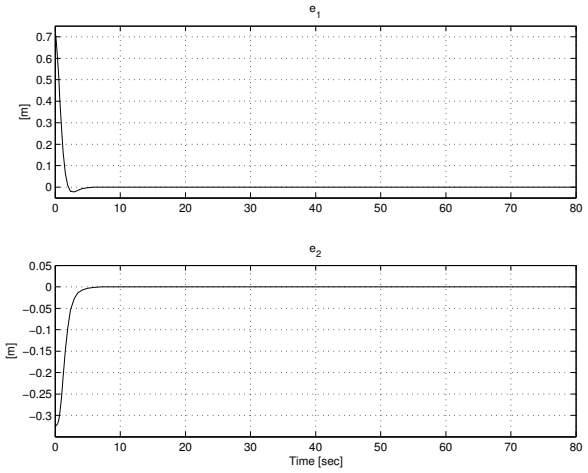

Figure 1.11 Tracking Error (Upper Bounding the Potential Energy Sub-Task)

CHAPTER 2
COORDINATION CONTROL
FOR HAPTIC AND TELEOPERATOR SYSTEMS

Introduction

For the purposes of this research, the following definitions are made. A teleoperator system enables a user to execute a remote task with an output system (i.e., a slave system) operating in a physical environment by manipulating an input system (i.e., a joystick or a master system) while providing feedback on the input system. A haptic system is similar to a teleoperator system with the exception that the slave system operates in a virtual environment. Some common application areas for teleoperator and haptic systems include handling hazardous materials, maneuvering mobile robots, underwater vehicles, and microsurgery in either a physical or a virtual environment. The operator's ability to accurately complete these tasks is affected by the transparency of the teleoperator or haptic system. Tactile and force feedback from the system controller along with assistive mechanisms greatly increase the user's performance in completing the desired task [25]. Tactile and force feedback provides the user of the system with a sense of feel or sense of *telepresence* [26] of what the slave system is experiencing in either a physical or a virtual environment. Assistive mechanisms can be integrated into the system controller in various ways. One example, which will be discussed further in subsequent sections of this chapter, is the encoding of a tracking objective in the master system that assists the user in completing a predefined task (i.e., consider a teleoperator grinding application where the remote user controls the slave system to track a repeated circular path to complete the desired task).

Both the teleoperator and/or haptic problem are theoretically challenging due to issues that impact the user's ability to impart a desired motion on the remote environment while maintaining a sense of feel through the system controller. This

problem is further complicated due to the fact that master system apparent inertia is normally very different than that of the slave system that is operating in the remote environment, be it physical or virtual. If the apparent inertia of the master system could be adjusted by the system controller to appear like that of the slave systems, the operator's sense of *telepresence* would be achieved, hence, increasing the user's ability to operate the slave system. To address the above control objective, commercially available haptic systems come in two distinct classes: impedance controlled devices, and admittance controlled devices [27]. Both classes have advantages/disadvantages depending on the application, see [25] and [27] for more details.

The focus of some of the previous teleoperator system research has been to achieve ideal transparency between the environment and the user. In [28], Hannaford modeled the teleoperator system as a two-port network where an estimate of the impedance of the slave system is required to achieve transparency. In [29], *a priori* knowledge of the environmental inputs to the slave system is required to achieve the transparency control objective. Controllers aiming at low-frequency transparency were suggested in [30], [31], and [32]. Frequency-based control designs given in [28], [29], [30], [31], and [32] are for linear teleoperator systems. The concept of the four-channel architecture, which assumes knowledge of system impedances was introduced by the authors of [31] and [33]. To overcome parametric uncertainties, common in teleoperator systems, adaptive controllers were developed in [34], [35], [36], [37], [38], and [39].

Other research has focused on maintaining safe and stable operation of the teleoperator system through passivity concepts. In [40], Anderson and Spong transformed the time delay problem of the teleoperator system into a transmission line problem and presented a controller for the communication circuit that guarantees passivity of the teleoperator system independent of time delay present in the communication block. In [41], Niemeyer and Slotine extended the results in [40], and introduced wave-variables formulation to represent transmission delays, which results in a new configuration for force-reflecting teleoperation. These results were then extended to

solve the position tracking problem where [42] and [43] provided a solution when the time delay is constant and [44] provided a solution when the time delay is time-varying. In [45], a passive decomposition for linear dynamically similar systems is introduced. In [46], Lee and Li extended these results to define a nonlinear decomposition which achieves passivity of the master and the slave robots by decomposing the closed-loop teleoperator system into two sub-systems. The reader is referred to [47], [48], and [49] for improvements of passive decomposition. In [50] and [51], Lee suggested a controller for a master and multiple cooperative slave robots over a communication network in the presence of a time delay. In [52], Hannaford and Ryu proposed a passivity based model-insensitive approach that measures the total energy of the system and damps excess energy by injecting a variable damping, which was then extended in [53].

In this chapter, the work in [54] is extended so that it is applicable for the control of both teleoperator and haptic systems. Two controllers are developed for nonlinear haptic and teleoperator systems that target coordination of the master and slave. The first controller is proven to yield a semi-global asymptotic result in the presence of parametric uncertainty in the master and slave dynamic models provided the user and environmental input forces are measurable; henceforth, referred to as the MIF, (measurable input force) controller. The second controller yields a global asymptotic result despite unmeasurable user and environmental input forces (UMIF) provided the dynamic models of the master and slave systems are known. This development differs from [54], in that the transformation and target system development are both modified to allow the master system's impedance, felt by the user, to be adjusted so that it closely matches that of a desired target system operating in a remote environment. This work also provides the encoding of a velocity field assist mechanism to provide the user help in controlling the slave system in completing a pre-defined contour following task. To achieve these control objectives, a continuous nonlinear integral feedback controller/observer (see [55] and [56]) is exploited to compensate for the lack of master

and slave dynamics information or user and environmental force measurements. For each controller, Lyapunov-based techniques are used to prove that the controller development implements a stable coordinated haptic/teleoperator system with the optional assist mechanism enabled. When this mechanism is disabled, the subsequent analysis proves the controller development implements a stable passively coordinated haptic/teleoperator system. The passivity objective is motivated to ensure the safety of the user and the environment when in contact with the haptic/teleoperator system. Simulation results are presented for proof of concept for both controllers.

System Model

The mathematical model for a $2n$-DOF nonlinear haptic/teleoperator system consisting of a revolute n-DOF master and a revolute n-DOF slave system are assumed to have the following forms

$$M_1(x_m)\ddot{x}_m + N_1(x_m, \dot{x}_m) = T_1 + F_H \tag{2.1}$$

$$M_2(x_s)\ddot{x}_s + N_2(x_s, \dot{x}_s) = T_2 + F_E. \tag{2.2}$$

In (2.1) and (2.2), $x_m(t)$, $\dot{x}_m(t)$, $\ddot{x}_m(t) \in \mathbb{R}^n$ denote the task-space position, velocity, and acceleration for the master system and $x_s(t)$, $\dot{x}_s(t)$, $\ddot{x}_s(t)$ denote the task-space position, velocity, and acceleration for the slave system, $M_1(x_m)$, $M_2(x_s) \in \mathbb{R}^{n\times n}$ represent the inertia effects, $N_1(x_m, \dot{x}_m)$, $N_2(x_s, \dot{x}_s) \in \mathbb{R}^n$ represent other dynamic effects, $T_1(t)$, $T_2(t) \in \mathbb{R}^n$ represent the control input vectors, $F_H(t) \in \mathbb{R}^n$ represents the user input force, and $F_E(t) \in \mathbb{R}^n$ represents the input force from the physical or virtual environment. End-effector positions $x_m(t)$ and $x_s(t)$ can be decomposed as follows

$$x_m \triangleq \begin{bmatrix} x_{mp}^T & x_{mr}^T \end{bmatrix}^T \qquad x_s \triangleq \begin{bmatrix} x_{sp}^T & x_{sr}^T \end{bmatrix}^T$$

where $x_{mp}(t)$, $x_{sp}(t) \in \mathbb{R}^p$ represent position vectors and $x_{mr}(t)$, $x_{sr}(t) \in \mathbb{R}^r$ represent orientation angle vectors, where the integers p and r satisfy $p + r = n$. The

subsequent development utilizes the property that the master and slave inertia matrices are positive definite, symmetric and satisfies the following inequalities [15]

$$m_{1i} \left\| \xi \right\|^2 \leq \xi^T M_i \left(\cdot \right) \xi \leq m_{2i} \left\| \xi \right\|^2 \tag{2.3}$$

$\forall \xi \in \mathbb{R}^n$ and $i = 1, 2$ where m_{1i}, $m_{2i} \in \mathbb{R}$ are positive constants, and $\left\| \cdot \right\|$ denotes the Euclidean norm. To achieve the control objectives, the subsequent development is derived based on the assumption that $x_m \left(t \right)$, $x_s \left(t \right)$, $\dot{x}_m \left(t \right)$, $\dot{x}_s \left(t \right)$ are measurable, and $M_i \left(\cdot \right)$, $N_i \left(\cdot \right)$ are second order differentiable for $i = 1, 2$.

Assumption 1 *The user input force and the environmental force along with their first and second time derivatives,* $F_H \left(t \right)$, $\dot{F}_H \left(t \right)$, $\ddot{F}_H \left(t \right)$, $F_E \left(t \right)$, $\dot{F}_E \left(t \right)$, *and* $\ddot{F}_E \left(t \right)$ *are bounded (see [45] and [46] for the precedence of this type of assumption).*

Measurable Input Forces (MIF) Control Development

For the MIF controller development, the following analysis will prove a semi-global asymptotic result despite parametric uncertainty in the master and slave system dynamic models provided the user and the physical or virtual environmental input forces are measurable. It should be noted that for many types of virtual slave systems, the dynamic model of the virtual slave is known *a priori*; however; unstructured uncertainties in the dynamic model are common for teleoperator slave systems.

Control Objective and Model Transformation

A control objective for haptic and teleoperator systems is to ensure the coordination between the master and the slave systems and to meet the tracking objective in the following sense

$$x_s \left(t \right) \rightarrow x_m \left(t \right) \text{ as } t \rightarrow \infty \tag{2.4}$$

$$x_m \left(t \right) \rightarrow \xi_d \left(t \right) \text{ as } t \rightarrow \infty \tag{2.5}$$

where $\xi_d(t) \in \mathbb{R}^n$ is a subsequently designed desired trajectory. Another sub-control objective is to guarantee that the closed-loop system remains passive with respect to the user and the physical/virtual environmental power in the following sense [46]

$$\int_{t_0}^{t} \left(\dot{x}_m^T(\tau) F_H(\tau) + \dot{x}_s^T(\tau) F_E(\tau) \right) d\tau \geq -c_1^2 \tag{2.6}$$

where $c_1 \in \mathbb{R}$ is a bounding constant. The passivity objective is motivated to ensure the safety of the user and the physical environment [46]. The final objective is that all signals are required to remain bounded within the closed-loop system. It should be noted that, the passivity objective is not met when the subsequently presented user assist mechanism is enabled.

To facilitate the subsequent development, an invertible transformation is defined that encodes the control objectives as follows

$$x \triangleq S \begin{bmatrix} x_m^T & x_s^T \end{bmatrix}^T \tag{2.7}$$

where $x(t) \in \mathbb{R}^{2n}$ and $S \in \mathbb{R}^{2n \times 2n}$ is defined as follows

$$S \triangleq \begin{bmatrix} I_n & 0_{nxn} \\ I_n & -I_n \end{bmatrix} \tag{2.8}$$

where $I_n \in \mathbb{R}^{n \times n}$ denotes the identity matrix, $0_{nxn} \in \mathbb{R}^{n \times n}$ denotes a matrix of zeros, and it is noted that $S^{-1} = S$. After utilizing the transformation defined in (2.7), the dynamic models of the haptic/teleoperator systems given in (2.1) and (2.2) can be combined as follows

$$\bar{M}\ddot{x} + \bar{N} = \bar{T} + \bar{F} \tag{2.9}$$

where $\bar{N}(x, \dot{x})$, $\bar{T}(t)$, $\bar{F}(t) \in \mathbb{R}^{2n}$ and $\bar{M}(x) \in \mathbb{R}^{2n \times 2n}$ are defined as follows

$$\bar{M} \triangleq S^{-T} \begin{bmatrix} M_1 & 0_{nxn} \\ 0_{nxn} & M_2 \end{bmatrix} S^{-1} \tag{2.10}$$

$$\bar{N} \triangleq S^{-T} \begin{bmatrix} N_1^T & N_2^T \end{bmatrix}^T \tag{2.11}$$

$$\bar{T} \triangleq S^{-T} \begin{bmatrix} T_1^T & T_2^T \end{bmatrix}^T \tag{2.12}$$

$$\bar{F} \triangleq S^{-T} \begin{bmatrix} F_H^T & F_E^T \end{bmatrix}^T. \tag{2.13}$$

The subsequent development utilizes the property that $\bar{M}(x)$ is positive definite, symmetric and satisfies the following inequalities [15]

$$\bar{m}_1 \|\xi\|^2 \leq \xi^T \bar{M}(x) \xi \leq \bar{m}_2 \|\xi\|^2 \tag{2.14}$$

$\forall \xi \in \mathbb{R}^{2n}$ where $\bar{m}_1$, $\bar{m}_2 \in \mathbb{R}$ are positive constants. By utilizing the assumption that $M_i(\cdot)$, $N_i(\cdot)$ are second order differentiable for $i = 1, 2$, it is clear that $\bar{M}(\cdot)$ and $\bar{N}(\cdot)$ are also second order differentiable.

To facilitate the development of the error system, the filtered tracking error signal, denoted by $r(t) \in \mathbb{R}^{2n}$, is defined as follows

$$r \triangleq \dot{e}_2 + \alpha_1 e_2 \tag{2.15}$$

where $e_2(t) \in \mathbb{R}^{2n}$ is defined as follows

$$e_2 \triangleq \dot{e}_1 + \alpha_2 e_1 \tag{2.16}$$

where α_1, $\alpha_2 \in \mathbb{R}$ are positive control gains, and $e_1(t) \in \mathbb{R}^{2n}$ is defined as follows

$$e_1 \triangleq x_d - x. \tag{2.17}$$

The error signal $e_1(t)$ can be decomposed as follows

$$e_1 \triangleq \begin{bmatrix} e_{11}^T & e_{12}^T \end{bmatrix}^T \tag{2.18}$$

where $e_{11}(t) \in \mathbb{R}^n$ represents the master system tracking error, and $e_{12}(t) \in \mathbb{R}^n$ represents the coordination error. In (2.17), $x_d(t) \in \mathbb{R}^{2n}$ is defined as follows

$$x_d \triangleq \begin{bmatrix} \xi_d^T & 0_n^T \end{bmatrix}^T \tag{2.19}$$

where $0_n \in \mathbb{R}^n$ denotes a vector of zeros. Based on the definition of $x(t)$ in (2.7) and $e_1(t)$ in (2.17), it is clear that if $\|e_1(t)\| \to 0$ then $x_s(t) \to x_m(t)$ and $x_m(t) \to \xi_d(t)$.

The desired trajectory $\xi_d(t)$ introduced in (2.5) is generated by the following second-order coupled dynamic target system

$$\dot{\xi}_d = \gamma \begin{bmatrix} \varphi^T(\xi_p) & 0_r^T \end{bmatrix}^T + \eta_d \tag{2.20}$$

$$M_T\dot{\eta}_d + B_T\eta_d + K_T\lambda_d = F \tag{2.21}$$

where $\eta_d(t) \in \mathbb{R}^n$ is an auxiliary filter signal, M_T, B_T, $K_T \in \mathbb{R}^{n\times n}$ are constant positive definite, diagonal matrices, $\varphi(\cdot) \in \mathbb{R}^p$ is a velocity field function [57] that encodes the user assist mechanism, $0_r \in \mathbb{R}^r$ denotes a vector of zeros, γ is a constant gain that is either 0 or 1. It should be noted that, when $\gamma = 0$, the user assist mechanism is disabled, and when $\gamma = 1$, then the user assist mechanism is enabled. In (2.21), $F(t) \in \mathbb{R}^n$ is defined as follows

$$F \triangleq F_H + F_E. \tag{2.22}$$

Also, in (2.21) the term $\lambda_d(t) \in \mathbb{R}^n$ is defined as follows

$$\lambda_d \triangleq \xi_d - \gamma \left[\int_{t_0}^{t} \varphi^T\left(\xi_p(\tau)\right) d\tau \quad 0_r^T \right]^T \tag{2.23}$$

where $\xi_d(t)$ is generated by the differential equation of (2.20), and can be decomposed as follows

$$\xi_d \triangleq \left[\xi_p^T \quad \xi_r^T \right]^T \tag{2.24}$$

where $\xi_p(t) \in \mathbb{R}^p$ represents a position vector, and $\xi_r(t) \in \mathbb{R}^r$ represents an orientation angle vector.

Remark 1 *Velocity fields have been utilized in previous control literature, see [57] and [58] for their definition and application. The velocity field function in (2.20) is integrated to assist the user in executing a remote task (i.e., tracking a circular contour). It is assumed that the velocity field function is designed such that* $\varphi(\cdot)$, $\dot{\varphi}(\cdot)$, $\ddot{\varphi}(\cdot)$ *and* $\dddot{\varphi}(\cdot)$ *are bounded provided that their arguments are bounded.*

Remark 2 *The velocity field function* $\varphi(\cdot)$ *is assumed to be designed such that, from (2.20), if* $\eta_d(t) \in \mathcal{L}_\infty$ *then* $\xi_d(t)$, $\dot{\xi}_d(t) \in \mathcal{L}_\infty$. *Based on this assumption and the analysis in Appendix B, it is easy to show that all signals in dynamic target system given in (2.20) and (2.21) are bounded, and that the higher order derivatives are also bounded.*

Remark 3 *It should be noted that, when the user assist mechanism is disabled, (i.e., $\gamma = 0$) the target system defined by (2.20) and (2.21), becomes a standard impedance model as follows*

$$M_T\ddot{\xi}_d + B_T\dot{\xi}_d + K_T\xi_d = F. \tag{2.25}$$

Closed-Loop Error System

Based on the assumption that the user forces $F_H(t)$, and the physical/virtual environmental forces $F_E(t)$, are measurable, the control input $\bar{T}(t)$ of (2.9) is designed as follows

$$\bar{T} \triangleq \bar{u} - \bar{F} \tag{2.26}$$

where $\bar{u}(t) \in \mathbb{R}^{2n}$ is a subsequently designed auxiliary control input. Substituting (2.26) into (2.9) results in the following simplified dynamic system

$$\bar{M}\ddot{x} + \bar{N} = \bar{u}. \tag{2.27}$$

After taking the time derivative of (2.15) and premultiplying by $\bar{M}(x)$, the following expression can be derived

$$\bar{M}\dot{r} = \bar{M}\,\ddot{x}_d + \dot{\bar{M}}\ddot{x} + \dot{\bar{N}} - \dot{\bar{u}} + \alpha_2\bar{M}\ddot{e}_1 + \alpha_1\bar{M}\dot{e}_2 \tag{2.28}$$

where (2.16), (2.17), and the time derivative of (2.27) were utilized. To facilitate the subsequent analysis, the expression in (2.28) can be arranged as follows

$$\bar{M}\dot{r} = \tilde{N} + N_d - e_2 - \dot{\bar{u}} - \frac{1}{2}\,\dot{\bar{M}}\,r \tag{2.29}$$

where $\tilde{N}(x, \dot{x}, \ddot{x}, t) \in \mathbb{R}^{2n}$ is defined as follows

$$\tilde{N} \triangleq N - N_d \tag{2.30}$$

where $N(x, \dot{x}, \ddot{x}, t) \in \mathbb{R}^{2n}$ is defined as follows

$$N \triangleq \bar{M}\,\ddot{x}_d + \dot{\bar{M}}\,\ddot{x} + \alpha_2\bar{M}\ddot{e}_1 + \alpha_1\bar{M}\dot{e}_2 + e_2 + \dot{\bar{N}} + \frac{1}{2}\,\dot{\bar{M}}\,r \tag{2.31}$$

and $N_d(t) \in \mathbb{R}^{2n}$ is defined as follows

$$\begin{aligned} N_d &\triangleq N|_{x=x_d,\, \dot{x}=\dot{x}_d,\, \ddot{x}=\ddot{x}_d} \\ &= \bar{M}(x_d)\dddot{x}_d + \dot{\bar{M}}(x_d)\ddot{x}_d + \dot{\bar{N}}(x_d, \dot{x}_d). \end{aligned} \tag{2.32}$$

Remark 4 *After utilizing (2.19), (2.32) and the fact that we show in Appendix B, then* $\|N_d(t)\|$ *and* $\left\|\dot{N}_d(t)\right\|$ *can be upper bounded as follows*

$$\|N_d(t)\| \leq \varsigma_1 \qquad \left\|\dot{N}_d(t)\right\| \leq \varsigma_2 \tag{2.33}$$

where ς_1, $\varsigma_2 \in \mathbb{R}$ *are known positive constants.*

To achieve the stated control objectives, the auxiliary control input $\bar{u}(t)$ introduced in (2.26) is designed as follows

$$\begin{aligned} \bar{u} &\triangleq (k_s+1)\left[e_2(t) - e_2(t_0) + \alpha_1 \int_{t_0}^{t} e_2(\tau)\, d\tau\right] \\ &\quad + (\beta_1+\beta_2)\int_{t_0}^{t} sgn(e_2(\tau))\, d\tau \end{aligned} \tag{2.34}$$

where k_s, β_1, $\beta_2 \in \mathbb{R}$ are positive control gains, and $sgn(\cdot)$ denotes the vector signum function. The term $e_2(t_0)$ in (2.34) is used to ensure that $\bar{u}(t_0) = 0_{2n}$ where $0_{2n} \in \mathbb{R}^{2n}$ denotes a vector of zeros. The time derivative of (2.34) is obtained as follows

$$\dot{\bar{u}} = (k_s+1)\, r + (\beta_1+\beta_2)\, sgn(e_2) \tag{2.35}$$

where (2.15) was utilized. Substituting (2.35) into (2.29) results in the following closed-loop error system

$$\bar{M}\dot{r} = -(k_s+1)\, r - (\beta_1+\beta_2)\, sgn(e_2) + \tilde{N} + N_d - e_2 - \frac{1}{2}\dot{\bar{M}}\, r. \tag{2.36}$$

Stability Analysis

Theorem 3 *The controller given in (2.26) and (2.34) guarantees that all the system signals are bounded under the closed-loop operation and that coordination between the master and the slave systems, and the tracking objective are met in the sense that*

$$x_s(t) \rightarrow x_m(t) \text{ as } t \rightarrow \infty \tag{2.37}$$

$$x_m(t) \rightarrow \xi_d(t) \text{ as } t \rightarrow \infty \tag{2.38}$$

provided the control gain β_1 introduced in (2.34) is selected to satisfy the following sufficient condition

$$\beta_1 > \varsigma_1 + \frac{1}{\alpha_1}\varsigma_2 \tag{2.39}$$

where ς_1 and ς_2 were introduced in (2.33), the control gains α_1 and α_2 are selected greater than 2, and k_s is selected sufficiently large relative to the system's initial conditions.

Proof. See Appendix C.

Theorem 4 *The controller given in (2.26) and (2.34) guarantees the closed-loop system is passive with respect to the user and the physical/virtual environmental power when the user assist mechanism is disabled (i.e., $\gamma = 0$).*

Proof. See Appendix D.

MIF Controller Simulation Results

A numerical simulation was performed to demonstrate the performance of the MIF controller given in (2.26) and (2.34). A 2-link, revolute robot dynamic model was utilized for both the master and slave systems [59] where $M_i(\cdot)$ and $N_i(\cdot)$ are defined as follows

$$\begin{aligned} M_i &= \begin{bmatrix} 3.12 + 2\sin(q_{i2}) & 0.75 + \sin(q_{i2}) \\ 0.75 + \sin(q_{i2}) & 0.75 \end{bmatrix} \\ N_i &= \begin{bmatrix} \sin(q_{i2})\,\dot{q}_{i2} & \sin(q_{i2})\,(\dot{q}_{i1} + \dot{q}_{i2}) \\ -\sin(q_{i2})\,\dot{q}_{i1} & 0 \end{bmatrix} \begin{bmatrix} \dot{q}_{i1} \\ \dot{q}_{i2} \end{bmatrix} \end{aligned} \tag{2.40}$$

where $i = 1$ denotes the master system and $i = 2$ denotes the slave system. By utilizing the forward kinematics [59], the task-space dynamic model is used in the simulation. The task-space user and environmental input forces were set equal to the following time-varying signals

$$F_H = \begin{bmatrix} -\sin(t) \\ -\cos(t) \end{bmatrix} \; F_E = \begin{bmatrix} -0.18\dot{x}_{s1} - 0.3x_{s1} \\ -0.18\dot{x}_{s2} - 0.3x_{s2} \end{bmatrix}. \tag{2.41}$$

The target system, described by (2.20) and (2.21), is defined as follows

$$\dot{\xi}_p = \gamma\varphi\left(\xi_p\right) + \eta_d \tag{2.42}$$

$$M_T \begin{bmatrix} \dot{\eta}_{dx} \\ \dot{\eta}_{dy} \end{bmatrix} = F_H + F_E \tag{2.43}$$

where $M_T = I_2$ where $I_2 \in \mathbb{R}^{2\times 2}$ denotes the identity matrix and the terms B_T, and K_T are selected to be zero. The following planar task-space velocity field was utilized [58]

$$\varphi\left(\xi_p\right) \triangleq -2K\left(\xi_p\right) f\left(\xi_p\right) \xi_p + 2c\left(\xi_p\right) \begin{bmatrix} -\xi_{py} \\ \xi_{px} \end{bmatrix} \tag{2.44}$$

where $\xi_p = \begin{bmatrix} \xi_{px} & \xi_{py} \end{bmatrix}^T$ is the desired end-effector position, and $f\left(\cdot\right), K\left(\cdot\right), c\left(\cdot\right) \in \mathbb{R}$ are defined as follows

$$\begin{aligned} f\left(\xi_p\right) &\triangleq \xi_{px}^2 + \xi_{py}^2 - r_o^2 \\ K\left(\xi_p\right) &\triangleq k_o \left(\sqrt{f^2\left(\xi_p\right)} \left\| \frac{\partial f\left(\xi_p\right)}{\partial \xi_p} \right\| + \epsilon \right)^{-1} \\ c\left(\xi_p\right) &\triangleq \frac{c_o \exp\left(-\mu\sqrt{f^2\left(\xi_p\right)}\right)}{\left\| \frac{\partial f\left(\xi_p\right)}{\partial \xi_p} \right\|}. \end{aligned} \tag{2.45}$$

In (2.45), $r_o = 1$ [m] denotes the circle radius, $k_o = 3$ [ms^{-1}], $\epsilon = 0.005$ [m^3], $c_o = 0.25$ [ms^{-1}], and $\mu = 20$ [m^{-1}] were selected for the simulation. For the simulation, the user assist mechanism is enabled, hence, $\gamma = 1$. The controller gains are selected as $k_s = 100$, $\beta_1 + \beta_2 = 100$, and $\alpha_1 = \alpha_2 = 2$.

In Figure 2.1, the desired end-effector position $\xi_p\left(t\right)$ is presented when the user assist mechanism is disabled (i.e., $\gamma = 0$) where the environmental force vector $F_E\left(t\right)$

is assumed to be zero. From Figure 2.1, it is clear that the user can create a circular desired trajectory. For the remaining simulation runs, environmental force vector $F_E(t)$ is set to be a spring-like input force vector, as defined in (2.41). The desired end-effector position $\xi_p(t)$, when the user assist mechanism is disabled (i.e., $\gamma = 0$) and when the user assist mechanism is enabled (i.e., $\gamma = 1$) are presented Figure 2.2. From Figure 2.2, it is clear that the user can not create a circular desired trajectory in the presence of the environmental input force. When the user assist mechanism is enabled (i.e., $\gamma = 1$), then the user can create a circular desired trajectory even in the presence of environmental force. The end-effector positions for the master and the slave systems are given in Figures 2.3 and 2.4, respectively. The master system tracking error $e_{11}(t)$ and coordination error $e_{12}(t)$ are presented in Figures 2.5 and 2.6, respectively. From Figures 2.5 and 2.6, it is clear that tracking and coordination control objectives defined in (2.4) and (2.5), are met. The control inputs for the master system $T_1(t)$ and the slave system $T_2(t)$ are provided in Figures 2.7 and 2.8, respectively.

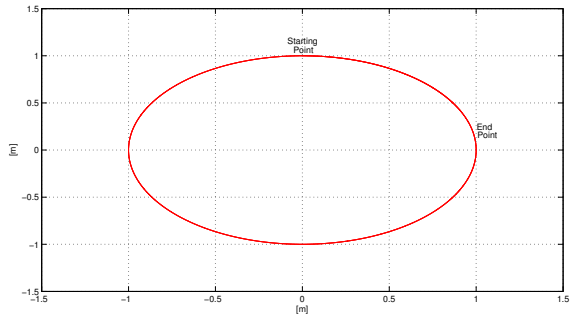

Figure 2.1 The desired end-effector position $\xi_p(t)$ when the user assist mechanism is disabled (i.e., $\gamma = 0$) and the environmental input force $F_E(t)$ is assumed to be zero

Un-measurable Input Forces (UMIF) Control Development

For the UMIF controller development, the following analysis will prove a global asymptotic result despite unmeasurable user and environmental input forces provided

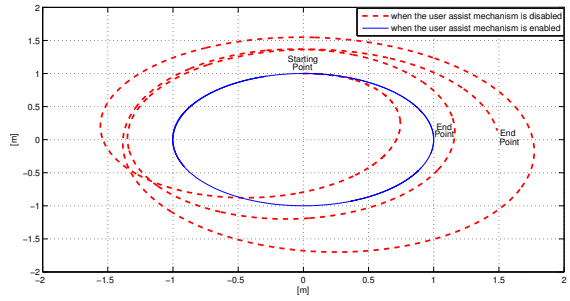

Figure 2.2 Desired End-Effector Position $\xi_p(t)$

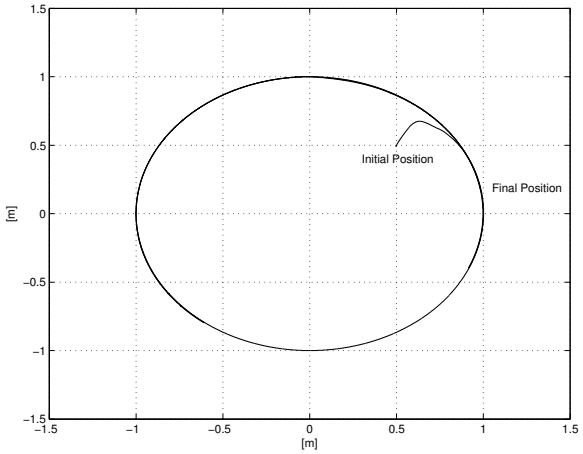

Figure 2.3 Master System End-Effector Position $x_m(t)$ when the user assist mechanism is enabled (i.e., $\gamma = 1$)

the dynamic models of the master and slave systems are known. Assumption 1 is also utilized for the subsequent development. It should be noted that, for many types of virtual slave systems, the virtual environmental forces are measurable; however, the user input force may not be measurable.

Control Objective and Model Transformation

A control objective for haptic and teleoperator systems is to guarantee coordination between the master and the slave systems and to meet the tracking objective in

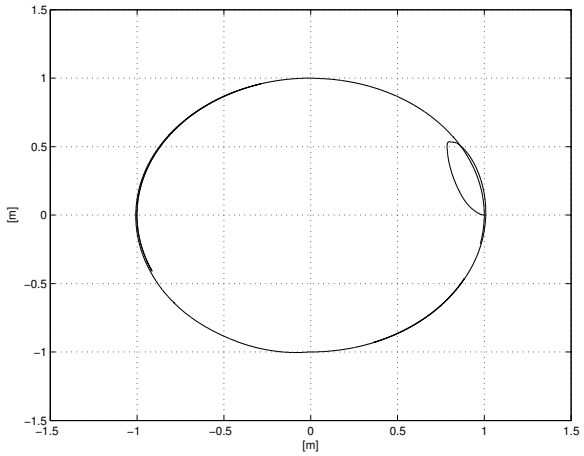

Figure 2.4 Slave System End-Effector Position $x_s(t)$ when the user assist mechanism is enabled (i.e., $\gamma = 1$)

the following sense

$$x_s(t) \rightarrow x_m(t) \text{ as } t \rightarrow \infty \tag{2.46}$$

$$x_m(t) \rightarrow \xi_1(t) \text{ as } t \rightarrow \infty \tag{2.47}$$

where $\xi_1(t) \in \mathbb{R}^n$ is a subsequently designed desired trajectory. Another sub-control objective is to guarantee that the system remains passive with respect to the user and the environmental power as in (2.6). It should be noted that the passivity objective is not met when the user assist mechanism is enabled. The final objective is that all signals are required to remain bounded within the closed-loop system.

To facilitate the subsequent development, an invertible transformation is defined that encodes the control objectives as follows

$$x \triangleq S \begin{bmatrix} x_m \\ x_s \end{bmatrix} + \begin{bmatrix} 0_n \\ \xi_2 \end{bmatrix} \tag{2.48}$$

where $x(t) \in \mathbb{R}^{2n}$ and $\xi_2(t) \in \mathbb{R}^n$ is a subsequently defined desired trajectory, and $S \in \mathbb{R}^{2n \times 2n}$ was defined in (2.8). After utilizing the transformation defined in (2.48), the dynamic models of the haptic/teleoperator system given in (2.1) and (2.2) can be

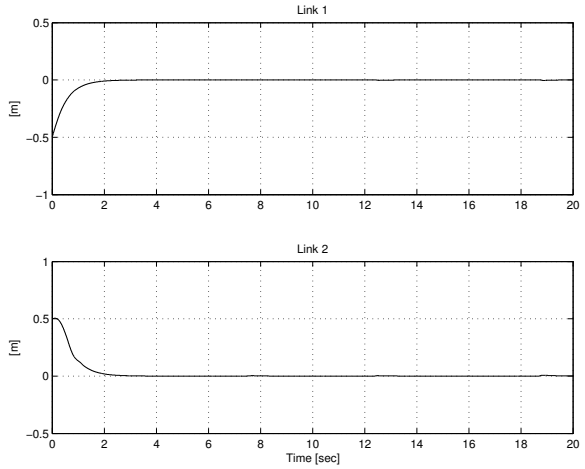

Figure 2.5 Master System Tracking Error $e_{11}(t)$ when the user assist mechanism is enabled (i.e., $\gamma = 1$)

combined as follows

$$\bar{M}\ddot{x} - \bar{M}\begin{bmatrix} 0_n \\ \ddot{\xi}_2 \end{bmatrix} + \bar{N} = \bar{T} + \bar{F} \tag{2.49}$$

where $\bar{M}(x)$, $\bar{N}(x, \dot{x})$, $\bar{T}(t)$, and $\bar{F}(t)$ were defined in (2.10)-(2.13).

The filtered tracking error signal denoted by $r(t) \in \mathbb{R}^{2n}$ is defined as follows

$$r \triangleq \dot{e}_2 + e_2 \tag{2.50}$$

where $e_2(t) \in \mathbb{R}^{2n}$ is defined as follows

$$e_2 \triangleq \bar{M}(\dot{e}_1 + \alpha e_1) \tag{2.51}$$

where $\alpha \in \mathbb{R}$ is a positive control gain, and $e_1(t) \in \mathbb{R}^{2n}$ is defined as follows

$$e_1 \triangleq \xi_d - x \tag{2.52}$$

where $\xi_d(t)$ is a subsequently defined desired trajectory. The error signal $e_1(t)$ can be decomposed as follows

$$e_1 \triangleq \begin{bmatrix} e_{11}^T & e_{12}^T \end{bmatrix}^T \tag{2.53}$$

where $e_{11}(t) \in \mathbb{R}^n$ represents the master system tracking error, and $e_{12}(t) \in \mathbb{R}^n$ represents the coordination error.

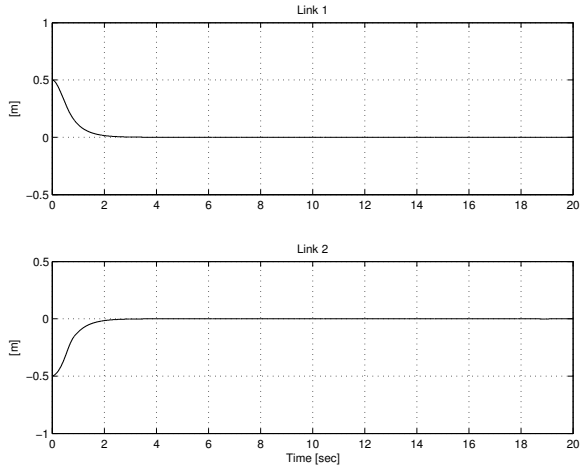

Figure 2.6 Coordination Error $e_{12}(t)$ when the user assist mechanism is enabled (i.e., $\gamma = 1$)

To compensate for the unmeasurable user and physical/virtual environmental forces, a nonlinear force observer is designed subsequently. This nonlinear observer is utilized in driving the target system, thus requiring a $2n$-dimensional system. As a result of this fact, the desired trajectory, defined as $\xi_d(t) \in \mathbb{R}^{2n}$, is generated by the following second order coupled dynamic target system[2]

$$\dot{\xi}_d = \gamma \left[\begin{array}{cc} \varphi^T(\xi_{1p}) & 0_s^T \end{array} \right]^T + \eta_d \tag{2.54}$$

$$M_T \dot{\eta}_d + B_T \eta_d + K_T \lambda_d = \left(\bar{M} M_T^{-1}\right)^{-1} \hat{F} \tag{2.55}$$

where $\eta_d(t) \in \mathbb{R}^{2n}$ is an auxiliary filter signal, $\bar{M}(x)$ was defined in (2.10), M_T, B_T and $K_T \in \mathbb{R}^{2n \times 2n}$ represent constant, positive definite, diagonal matrices, $\hat{F}(t) \in \mathbb{R}^{2n}$ is a subsequently designed nonlinear observer, $\varphi(\cdot) \in \mathbb{R}^p$ was introduced (2.20), $0_s \in \mathbb{R}^s$ denotes a vector of zeros where $s + p = 2n$, and γ is a constant gain that is either 0 or 1. It should be noted that, when $\gamma = 0$, the user assist mechanism is disabled, and when $\gamma = 1$, then the user assist mechanism is enabled. In (2.55), the

[2]For the existence of $\left(\bar{M} M_T^{-1}\right)^{-1}$ see Appendix H.

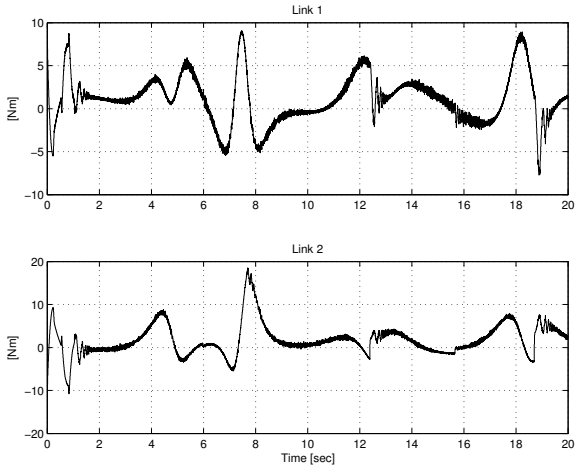

Figure 2.7 Control Input for Master System $T_1(t)$ when the user assist mechanism is enabled (i.e., $\gamma = 1$)

term $\lambda_d(t) \in \mathbb{R}^{2n}$ is defined as follows

$$\lambda_d \triangleq \xi_d - \gamma \left[\begin{array}{cc} \int_{t_0}^{t} \varphi^T \left(\xi_{1p}(\tau) \right) d\tau & 0_s^T \end{array} \right]^T \tag{2.56}$$

where $\xi_d(t) \triangleq \left[\begin{array}{cc} \xi_1^T & \xi_2^T \end{array} \right]^T$ is generated by the differential equation given in (2.54) where $\xi_1(t), \xi_2(t) \in \mathbb{R}^n$. The desired trajectory for the master system denoted by $\xi_1(t)$, can be decomposed as follows

$$\xi_1 \triangleq \left[\begin{array}{cc} \xi_{1p}^T & \xi_{1r}^T \end{array} \right]^T \tag{2.57}$$

where $\xi_{1p}(t) \in \mathbb{R}^p$ represents a position vector, and $\xi_{1r}(t) \in \mathbb{R}^r$ represents an orientation angle vector.

Remark 5 *The velocity field function $\varphi(\cdot)$ is assumed to be designed such that, from (2.54), if $\eta_d(t) \in \mathcal{L}_\infty$ then $\xi_d(t)$, $\dot{\xi}_d(t) \in \mathcal{L}_\infty$. Subsequent analysis will prove that $\hat{F}(t) \in \mathcal{L}_\infty$. After utilizing these facts along with (2.14), the analysis in Appendix G proves that all signals in the dynamic target system given in (2.54) and (2.55) are bounded.*

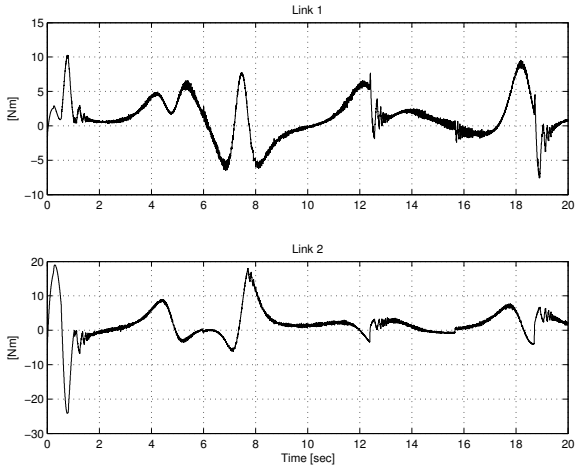

Figure 2.8 Control Input for Slave System $T_2(t)$ when the user assist mechanism is enabled (i.e., $\gamma = 1$)

Remark 6 *Although the desired trajectory dynamics defined in (2.54) and (2.55) generated a $2n$-dimensional signal, it should be noted that the master system tracks an n-dimensional signal, denoted as $\xi_1(t)$. The use of a $2n$-dimensional desired trajectory generator is a consequence of the fact that both the user input force and the physical/virtual environmental force are unmeasurable, and hence, a $2n$-dimensional nonlinear force observer must be utilized to drive the target system as defined in (2.55). From the definition of the transformation and the error signal $e_1(t)$ (see (2.48) and (2.52)), it is clear that additional set of desired trajectory dynamics, denoted by $\xi_2(t)$, are eliminated in the error system development.*

Remark 7 *It should be noted that, when the user assist mechanism is disabled (i.e., $\gamma = 0$), then the target system defined by (2.54) and (2.55), becomes an impedance model described as follows*

$$M_T \ddot{\xi}_d + B_T \dot{\xi}_d + K_T \xi_d = \left(\bar{M} M_T^{-1}\right)^{-1} \hat{F}. \tag{2.58}$$

Closed-Loop Error System

To develop the closed-loop error system for $r(t)$, error system dynamics for $e_1(t)$ and $e_2(t)$ are derived first. After taking the second time derivative of (2.52) and

premultiplying by $\bar{M}(x)$, the following expression can be derived

$$\begin{aligned}\bar{M}\ddot{e}_1 &= \hat{F} - \left(\bar{M}M_T^{-1}\right)\left(B_T\eta_d + K_T\lambda_d\right) - \bar{M}\begin{bmatrix} 0_n \\ \ddot{\xi}_2 \end{bmatrix} + \bar{N} \\ &\quad -\bar{T} - \bar{F} + \gamma\bar{M}\frac{d}{dt}\left(\begin{bmatrix} \varphi^T\left(\xi_{1p}\right) & 0_s^T \end{bmatrix}^T\right) \end{aligned} \tag{2.59}$$

where (2.49), (2.54) and (2.55) were utilized. Based on the assumption of exact model knowledge, the control input $\bar{T}(t)$ is designed as follows

$$\begin{aligned}\bar{T} &\triangleq \bar{T}_1 - \left(\bar{M}M_T^{-1}\right)\left(B_T\eta_d + K_T\lambda_d\right) - \bar{M}\begin{bmatrix} 0_n \\ \ddot{\xi}_2 \end{bmatrix} \\ &\quad +\bar{N} + \gamma\bar{M}\frac{d}{dt}\left(\begin{bmatrix} \varphi^T\left(\xi_{1p}\right) & 0_s^T \end{bmatrix}^T\right) \end{aligned} \tag{2.60}$$

where $\bar{T}_1(t) \in \mathbb{R}^{2n}$ is a subsequently designed auxiliary control input. Substituting (2.60) into (2.59) results in the following simplified expression

$$\bar{M}\ddot{e}_1 = \hat{F} - \bar{F} - \bar{T}_1. \tag{2.61}$$

The time derivative of $e_2(t)$ in (2.51) can be obtained as follows

$$\dot{e}_2 = \dot{\bar{M}}\ \dot{e}_1 + \alpha\ \dot{\bar{M}}\ e_1 + \alpha\bar{M}\dot{e}_1 + \hat{F} - \bar{F} - \bar{T}_1 \tag{2.62}$$

where (2.61) was utilized. Based on (2.62), the auxiliary control input $\bar{T}_1(t)$ is designed as follows

$$\bar{T}_1 \triangleq \dot{\bar{M}}\ \dot{e}_1 + \alpha\ \ \dot{\bar{M}}\ e_1 + \alpha\bar{M}\dot{e}_1. \tag{2.63}$$

After substituting (2.63) into (2.62), the following simplified expression is obtained

$$\dot{e}_2 = \hat{F} - \bar{F}. \tag{2.64}$$

Taking the time derivative of (2.64) results in the following expression

$$\ddot{e}_2 = \dot{\hat{F}} - \dot{\bar{F}}\ . \tag{2.65}$$

The error system dynamics for $r(t)$ can be derived by taking the time derivative of (2.50)

$$\dot{r} = r - e_2 + \dot{\hat{F}} - \dot{\bar{F}} \tag{2.66}$$

where (2.50) and (2.65) were both utilized. To achieve the stated control objectives, the proportional-integral like nonlinear observer $\hat{F}(t)$ introduced in (2.55) is designed as follows

$$\begin{aligned} \hat{F} &\triangleq -(k_s+1)\left[e_2(t) - e_2(t_0) + \int_{t_0}^{t} e_2(\tau)\, d\tau\right] \\ &\quad -(\beta_1+\beta_2)\int_{t_0}^{t} sgn(e_2(\tau))\, d\tau \end{aligned} \tag{2.67}$$

where k_s, β_1, and $\beta_2 \in \mathbb{R}$ are positive control gains. The term $e_2(t_0)$ is used to ensure that $\hat{F}(t_0) = 0_{2n}$. The time derivative of (2.67) is obtained as follows

$$\dot{\hat{F}} = -(k_s+1)\, r - (\beta_1+\beta_2)\, sgn(e_2) \tag{2.68}$$

where (2.50) was utilized. Substituting (2.68) into (2.66) results in the following closed-loop error system

$$\dot{r} = -e_2 - \dot{\bar{F}} - k_s r - (\beta_1+\beta_2)\, sgn(e_2). \tag{2.69}$$

Remark 8 *After utilizing (2.13) and Assumption 1, then* $\left\|\dot{\bar{F}}(t)\right\|$ *and* $\left\|\ddot{\bar{F}}(t)\right\|$ *can be upper bounded as follows*

$$\left\|\dot{\bar{F}}(t)\right\| \leq \varsigma_3 \qquad \left\|\ddot{\bar{F}}(t)\right\| \leq \varsigma_4 \tag{2.70}$$

where ς_3, $\varsigma_4 \in \mathbb{R}$ *denote positive bounding constants.*

Stability Analysis

Theorem 5 *The controller given in (2.60) and (2.63) guarantees that all signals are bounded under closed-loop operation and that coordination between the master and the slave systems, and the tracking objective are met in the sense that*

$$x_s(t) \rightarrow x_m(t) \quad as\ t \rightarrow \infty \tag{2.71}$$

$$x_m(t) \rightarrow \xi_1(t) \quad as\ t \rightarrow \infty \tag{2.72}$$

provided the control gain β_1, introduced in (2.67) is selected to satisfy the sufficient condition

$$\beta_1 > \varsigma_3 + \varsigma_4, \tag{2.73}$$

where ς_3 and ς_4 were introduced in (2.70).

Proof. See Appendix E.

Theorem 6 *The controller given in (2.60) and (2.63) guarantees that the haptic/tele-operator system is passive with respect to the user and the physical/virtual environmental power when the user assist mechanism is disabled (i.e., $\gamma = 0$).*

Proof. See Appendix F.

UMIF Controller Simulation Results

A numerical simulation was performed for the UMIF controller given in (2.60) and (2.63). The 2-link, revolute robot dynamic model introduced in (2.40) was utilized for both the master and slave systems. By utilizing the exact model knowledge of the simulated system, $\bar{F}(t)$ introduced in (2.13) is defined as follows

$$\bar{F} = \bar{M} M_T^{-1} \begin{bmatrix} F_H + F_E \\ -F_E \end{bmatrix} \tag{2.74}$$

where $F_H(t)$ and $F_E(t)$ were defined in (2.41). The planar task-space velocity field defined in (2.44) was utilized with the same parameters. The constants for the target system, described by (2.55), are set to $M_T = I_4$, where $I_4 \in \mathbb{R}^{4\times 4}$ denotes the identity matrix and the terms B_T and K_T are selected to be zero. The controller gains are selected as $k_s = 100$, $\beta_1 + \beta_2 = 100$, and $\alpha = 1$.

The desired end-effector position $\xi_{1p}(t)$, when the user assist mechanism is disabled (i.e., $\gamma = 0$) and when the user assist mechanism is enabled (i.e., $\gamma = 1$) are presented Figure 2.9. From Figure 2.9, it is clear that the proposed user assist mechanism provides a major improvement to the desired end-effector position. The end-effector positions for the master and the slave systems are given in Figures 2.10

and 2.11, respectively. The master system tracking error $e_{11}(t)$ and the coordination error $e_{12}(t)$ are presented in Figures 2.12 and 2.13, respectively. From Figures 2.12 and 2.13, it is clear that tracking and coordination control objectives defined in (2.46) and (2.47), are met. The control inputs for the master system $T_1(t)$ and the slave system $T_2(t)$ are provided in Figures 2.14 and 2.15, respectively. The output of the nonlinear force observer $\hat{F}(t)$ is presented in Figure 2.16.

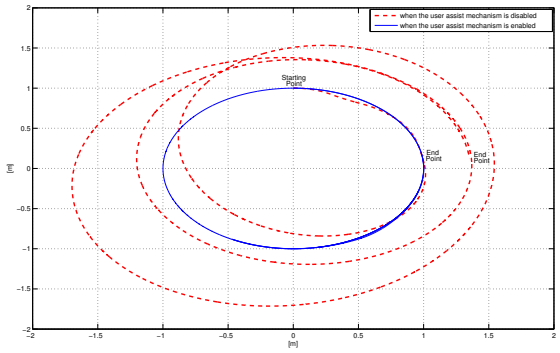

Figure 2.9 Desired End-Effector Position $\xi_{d1p}(t)$

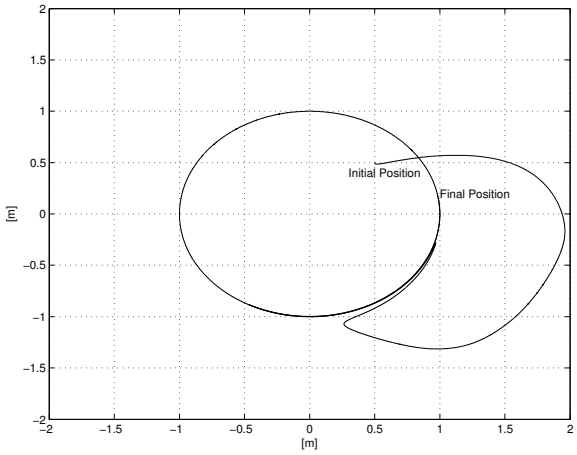

Figure 2.10 Master System End-Effector Position $x_m(t)$ when the user assist mechanism is enabled (i.e., $\gamma = 1$)

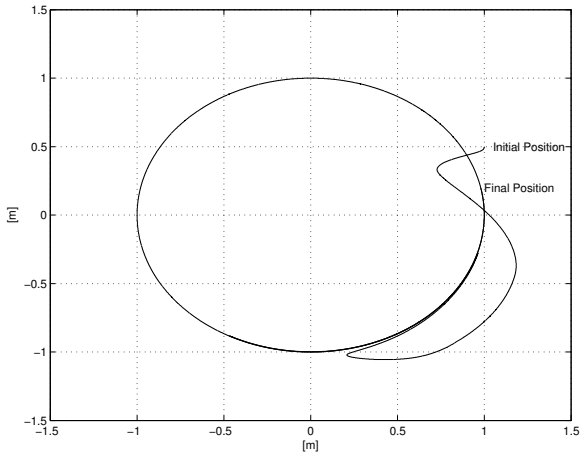

Figure 2.11 Slave System End-Effector Position $x_s(t)$ when the user assist mechanism is enabled (i.e., $\gamma = 1$)

Conclusion

Two controllers were developed for nonlinear haptic and teleoperator systems that target coordination of the master and slave. The first controller was proven to yield a semi-global asymptotic result in the presence of parametric uncertainty in the master and slave dynamic models provided the user and environmental input forces are measurable. The second controller was proven to yield a global asymptotic result despite unmeasurable user and environmental input forces provided the dynamic models of the master and slave are known. A transformation along with an adjustable target system were utilized that allows the master system's impedance to be adjusted so that matches a desired target system operating in a remote physical/virtual environment. This work also presented an optional strategy to encode a velocity field assist mechanism that provides the user of the system help in controlling the slave system in completing a pre-defined contour following task. For each controller, Lyapunov-based techniques were used to prove the control development implements a stable coordinated teleoperator/haptic system with a user assist mechanism. When the optional velocity field assist mechanism is disabled, the analysis proved the control development implements a stable passively coordinated teleoperator/haptic system.

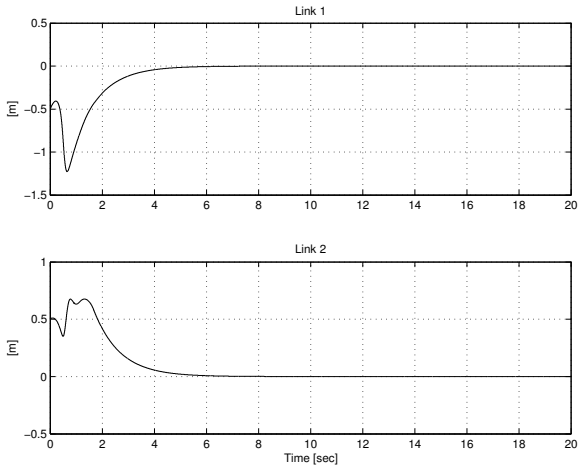

Figure 2.12 Master System Tracking Error $e_{11}(t)$ when the user assist mechanism is enabled (i.e., $\gamma = 1$)

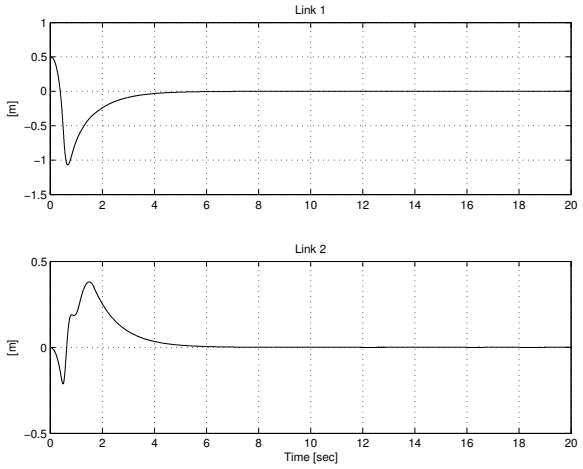

Figure 2.13 Coordination Error $e_{12}(t)$ when the user assist mechanism is enabled (i.e., $\gamma = 1$)

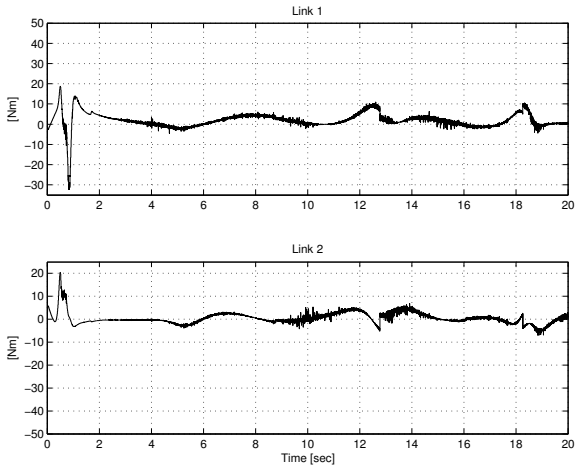

Figure 2.14 Torque Input for Master System $T_1(t)$ when the user assist mechanism is enabled (i.e., $\gamma = 1$)

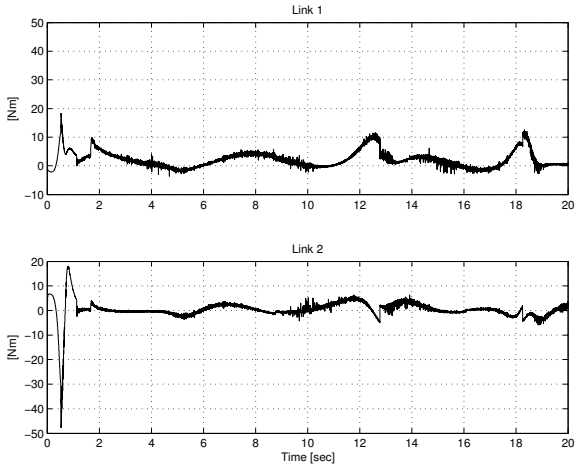

Figure 2.15 Torque Input for Slave System $T_2(t)$ when the user assist mechanism is enabled (i.e., $\gamma = 1$)

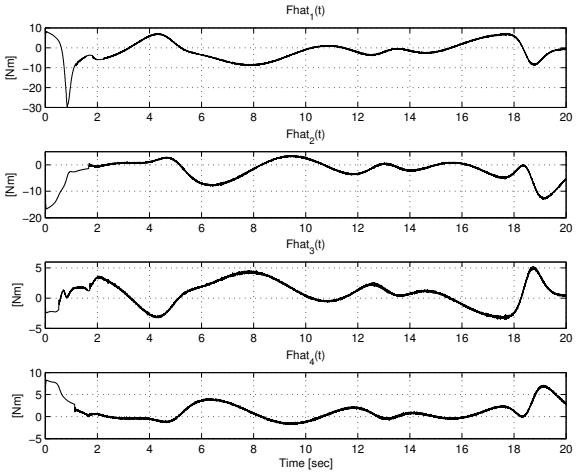

Figure 2.16 The Output of the Nonlinear Force Observer $\hat{F}(t)$ when the user assist mechanism is enabled (i.e., $\gamma = 1$)

CHAPTER 3
ADAPTIVE CONTROL OF FLAT MULTI-INPUT MULTI-OUTPUT NONLINEAR SYSTEMS WITH ADDITIVE DISTURBANCE

Introduction

Arguably, an interesting control problem is one that is both challenging from a theoretical perspective and applicable to real systems – the family of "flat" nonlinear systems appears to embody both of these properties. A flat system is characterized by a dynamic model where there exists a set of special outputs (equal to the number of inputs) such that the states and the inputs can be expressed in terms of outputs and a finite number of its derivatives [60]. A surprising number of practical machines match this form including mobile robots and cars, cars with multiple trailers, underwater vehicles, crane systems, induction motors, and planar satellite/manipulator systems [61], [62]. The reader is referred to [61] and [62] for a more detailed explanation of flatness and its applications to physical systems. It is the case of multi-input multi-output (MIMO) flat systems with parametric uncertainty and bounded disturbances that is considered here. Review of the basic control problem suggests and disqualifies certain solutions. It is probably wise at the outset to discard an exact model-based control approach for this problem given that any parameter estimation error and disturbances are not directly addressed, and hence, the system performance and stability cannot be predicted *a priori*. Given the parametric uncertainty in the proposed class of systems to be studied, an adaptive control solution may be warranted. However, an adaptive controller designed for a disturbance free system model may not compensate for the disturbances and may even go unstable under certain conditions. Enhancing the adaptive control approach with a robust component to form a robust adaptive controller can generally guarantee closed-loop signal boundedness in the presence of the additive disturbances. Unfortunately, while a robust

adaptive controller can potentially guarantee the convergence of the tracking error to a bounded set (i.e., the tracking error can't necessarily be driven to zero) the asymptotic tracking result (where the tracking error is driven to zero) that would be shown for an adaptive controller applied to the disturbance free model will be lost. These trade-offs in performance and robustness have framed the last ten years of research in robust adaptive control.

Review of relevant work highlights some of the different tacks used to approach this problem. An adaptive backstepping controller was shown by Zhang and Ioannou in [63] for a class of single-input/single-output (SISO) linear systems with both input and output disturbances. The proposed controller demonstrates the use of a projection algorithm to bound the parameter estimates and guarantees an ultimately bounded tracking error. In an alternate approach, the work of Polycarpou and Ioannou [64] demonstrate a leakage-based adaptation law to compensate for parametric uncertainties. The proposed robust adaptive backstepping controller is applicable to a class of higher-order SISO systems with unknown nonlinearities. The suggested control law guarantees global uniform ultimate boundedness of the system state (with some restrictions on the bounding functions of the nonlinearities). Robust adaptive control laws were developed in [65], utilizing the modular design introduced in [66] and a tuning function design, for a class of systems similar to that studied in [64]. These authors show estimates on the effect of the bounded uncertainties and external disturbances on the tracking error. In [67], an adaptive backstepping controller for linear systems in the presence of output and multiplicative disturbances is designed. Ikhouane and Krstic, added a switching σ-modification to the tuning functions to obtain a tracking error proportional to the size of the perturbations. Marino and Tomei [68] proposed a robust adaptive tracking controller that achieves boundedness of all signals. The result is based on a class of SISO nonlinear systems that have additive disturbances but also unknown time-varying bounded parameters. It is significant that the result shows arbitrary disturbance attenuation. In [69], Pan

and Basar proposed a robust adaptive controller for a similar class of systems in [68], where the tracking error is proven to be $\mathcal{L}_2-$bounded. In [70], Ge and Wang proposed a robust adaptive controller for SISO nonlinear systems with unknown parameters in the presence of disturbances, which ensure the global uniform boundedness of the tracking error.

Most of the research in adaptive control discussed above has focused on the convergence of the error signals and boundedness of the closed-loop system signals. As the sophistication in adaptive control techniques has evolved, additional questions about system performance have arisen. Notably, the final disposition of the parameters estimates in the closed-loop system has been examined. It is well established that without persistent excitation at the input, it is not typically possible to show the convergence of the parameter estimates to the corresponding system values (with an exception being a least-squares algorithm). In fact, for gradient and Lyapunov-type algorithms, convergence to a constant value, is typically not even guaranteed. Krstic summarizes this question well in [71] and also begins to provide some answers. In [71], it is shown that for the proposed adaptive controller; the parameter estimates will reach constant values after a sufficient amount of time. It is shown that the adaptation mechanism can be "turned off" after sufficient time and that the learned parameters can be used in a non-adaptive controller of the same structure to stabilize a restart of the system from new initial conditions. An important goal of the present work is to include a statement on parameter estimate limits for a controller proposed for the flat systems.

A recent paper by Cai *et al.* [72] presented a robust adaptive controller for MIMO nonlinear systems with parametric uncertainty and additive disturbances. With some restrictions placed on the disturbances, it was assumed that the disturbance is twice continuously differentiable and has bounded time derivatives up to second order, the proposed controller was proven to yield an asymptotic output tracking result. However, no mention of the convergence of the parameter estimates was made. Thinking

out loud for a moment, it *might* stand to reason that if the robust part of the controller is compensating for the disturbances and an asymptotic tracking result is obtained then perhaps something special is happening to the parameter estimates. Exploring this vague notion with mathematical rigor, we will show that with a minor modification to the control in [72] and with some additional analysis of the stability result, we are able to formulate a new conclusion about the parameter estimates. What is shown is that this robust adaptive controller will yield constant parameter estimates even in the presence of the disturbance. The stability analysis parallels that presented in [72] but with the extended analysis the convergence of the parameter estimates is demonstrated. The main contribution of this research is to add to the small number of results where parameter convergence has been shown. In the second part of the chapter, a learning controller for the same class of flat systems is designed under the assumption that the reference trajectory is periodic (for past research related to the design of learning controllers, reader is referred to [73], [74], [75] and the references therein). This controller is proven to yield a semi-global asymptotic result in the presence of additive disturbances. In the design of both controllers, a continuous nonlinear integral feedback controller (see [76]) is utilized and Lyapunov-based techniques are used to guarantee that the tracking error is asymptotically driven to zero. Numerical simulation results are presented for both controllers to demonstrate their viability.

Adaptive Control Development

Problem Statement

A system model for the flat nonlinear systems is considered to be of the following form

$$x^{(n)} = f + G\left(u + d_1\right) + d_2 \tag{3.1}$$

where $x^{(i)}\left(t\right) \in \mathbb{R}^m$, $i = 0, ..., (n-1)$, are the system states, $f\left(x, \dot{x}, ..., x^{(n-1)}, \theta\right) \in \mathbb{R}^m$ and $G\left(x, \dot{x}, ..., x^{(n-1)}, \theta\right) \in \mathbb{R}^{m \times m}$ are nonlinear functions, $\theta \in \mathbb{R}^p$ is an unknown

constant parameter vector, $d_1(t), d_2(t) \in \mathbb{R}^m$ are unknown additive nonlinear disturbances, and $u(t) \in \mathbb{R}^m$ is the control input. The system model is assumed to satisfy the following assumptions.

Assumption 1 *The nonlinear function $G(\cdot)$ is symmetric, positive definite and satisfies the following inequalities*

$$\underline{m} \|\xi\|^2 \leq \xi^T M(\cdot) \xi \leq \bar{m}(\cdot) \|\xi\|^2 \quad \forall \xi \in \mathbb{R}^m \tag{3.2}$$

where $M\left(x, \dot{x}, ..., x^{(n-1)}, \theta\right) \in \mathbb{R}^{m \times m}$ is defined as

$$M \triangleq G^{-1} \tag{3.3}$$

and $\underline{m} \in \mathbb{R}$ is a positive bounding constant, $\bar{m}\left(x, \dot{x}, ..., x^{(n-1)}\right) \in \mathbb{R}$ is a positive, globally invertible, nondecreasing function of each variable, and $\|\cdot\|$ denotes the Euclidean norm.

Assumption 2 *The nonlinear functions, $f(\cdot)$ and $G(\cdot)$, are continuously differentiable up to their second derivatives (i.e., $f(\cdot), G(\cdot) \in \mathcal{C}^2$).*

Assumption 3 *The nonlinear functions, $f(\cdot)$ and $M(\cdot)$, are affine in θ.*

Assumption 4 *The additive disturbances, $d_1(t)$ and $d_2(t)$, are assumed to be continuously differentiable and bounded up to their second derivatives (i.e., $d_i(t) \in \mathcal{C}^2$ and $d_i(t), \dot{d}_i(t), \ddot{d}_i(t) \in \mathcal{L}_\infty$, $i = 1, 2$).*

The output tracking error $e_1(t) \in \mathbb{R}^m$ is defined as follows

$$e_1 \triangleq x_r - x \tag{3.4}$$

where $x_r(t) \in \mathbb{R}^m$ is the reference trajectory satisfying the following property

$$x_r(t) \in \mathcal{C}^n \ , \ x_r^{(i)}(t) \in \mathcal{L}_\infty \ , \ i = 0, 1, ..., (n+2). \tag{3.5}$$

The control design objective is to develop an adaptive control law that ensures $\left\|e_1^{(i)}(t)\right\| \to 0$ as $t \to \infty$, $i = 1, ..., n$, and that all signals remain bounded within the closed-loop system. To achieve the control objectives, the subsequent development is derived based on the assumption that the system states $x^{(i)}(t)$, $i = 0, ..., (n-1)$ are measurable.

Development of Robust Adaptive Control Law

The filtered tracking error signals, $e_i(t) \in \mathbb{R}^m$, $i = 2, 3, ..., n$ are defined as follows

$$e_2 \triangleq \dot{e}_1 + e_1 \tag{3.6a}$$

$$e_3 \triangleq \dot{e}_2 + e_2 + e_1 \tag{3.6b}$$

$$\vdots$$

$$e_n \triangleq \dot{e}_{n-1} + e_{n-1} + e_{n-2}. \tag{3.6c}$$

A general expression for e_i, $i = 2, 3, ..., n$ in terms of e_1 and its time derivatives is given as follows [76]

$$e_i = \sum_{j=0}^{i-1} a_{i,j} e_1^{(j)} \tag{3.7}$$

where the constants $a_{i,j}$ are defined as follows

$$\begin{aligned} a_{i,0} &= B(i) = \frac{1}{\sqrt{5}}\left[\left(\frac{1+\sqrt{5}}{2}\right)^i - \left(\frac{1-\sqrt{5}}{2}\right)^i\right] \\ i &= 2, 3, ..., n \end{aligned} \tag{3.8}$$

$$\begin{aligned} a_{i,j} &= \sum_{k=1}^{i-1} B(i-k-j+1)\, a_{k+j-1,j-1} \\ i &= 3, 4, ..., n \ , \ j = 1, 2, ..., (i-2) \end{aligned} \tag{3.9}$$

$$a_{i,i-1} = 1 \ , \ i = 1, 2, ..., n. \tag{3.10}$$

After utilizing (3.3), the system model can be rewritten as follows

$$Mx^{(n)} = h + u + d_1 + Md_2 \tag{3.11}$$

where $h(t) \in \mathbb{R}^m$ is defined as follows

$$h \triangleq Mf. \tag{3.12}$$

To facilitate the control development, the filtered tracking error signal, denoted by $r(t) \in \mathbb{R}^m$, is defined as follows

$$r \triangleq \dot{e}_n + \Lambda e_n \tag{3.13}$$

where $\Lambda \in \mathbb{R}^{m \times m}$ is a constant, diagonal, positive definite, gain matrix. After differentiating (3.13) and premultiplying by $M(\cdot)$, the following expression can be derived

$$\begin{aligned} M\dot{r} &= M\left(x_r^{(n+1)} + \sum_{j=0}^{n-2} a_{nj} e_1^{(j+2)} + \Lambda \dot{e}_n\right) \\ &\quad + \dot{M}x^{(n)} - \dot{h} - \dot{u} - \dot{d}_1 - M\dot{d}_2 - \dot{M}d_2 \end{aligned} \tag{3.14}$$

where (3.4), (3.7) and the first time derivative of (3.11) were utilized. The dynamics of $\dot{r}(t)$ in (3.14) can be arranged as follows

$$M\dot{r} = -\frac{1}{2}\dot{M}r - e_n - \dot{u} + N - \dot{d}_1 - M\dot{d}_2 - \dot{M}d_2 \tag{3.15}$$

where the auxiliary function $N\left(x, \dot{x}, ..., x^{(n)}, t\right) \in \mathbb{R}^m$ is defined as follows

$$N \triangleq M\left(x_r^{(n+1)} + \sum_{j=0}^{n-2} a_{nj} e_1^{(j+2)} + \Lambda \dot{e}_n\right) + \dot{M}\left(x^{(n)} + \frac{1}{2}r\right) + e_n - \dot{h}. \tag{3.16}$$

To facilitate the subsequent analysis, (3.15) can be rearranged as follows

$$M\dot{r} = -\frac{1}{2}\dot{M}r - e_n - \dot{u} + \tilde{N} + N_r + \psi \tag{3.17}$$

where $\tilde{N}\left(x, \dot{x}, ..., x^{(n)}, t\right), N_r(t), \psi(t) \in \mathbb{R}^m$ are defined as follows

$$\tilde{N} \triangleq \left(N - M\dot{d}_2 - \dot{M}d_2\right) - \left(N_r - M_r\dot{d}_2 - \dot{M}_r d_2\right) \tag{3.18}$$

$$N_r \triangleq N|_{x=x_r,\ \dot{x}=\dot{x}_r,\ldots,\ x^{(n)}=x_r^{(n)}} \tag{3.19}$$

$$\psi \triangleq -\dot{d}_1 - M_r\dot{d}_2 - \dot{M}_r d_2 \tag{3.20}$$

and $M_r(t) \in \mathbb{R}^{m \times m}$ is defined as follows

$$M_r \triangleq M|_{x=x_r,\ \dot{x}=\dot{x}_r,\ldots,\ x^{(n-1)}=x_r^{(n-1)}}. \tag{3.21}$$

Remark 1 *By utilizing the Mean Value Theorem along with Assumptions 2 and 4, the following upper bound can be developed*

$$\left\| \tilde{N}(\cdot) \right\| \leq \rho(\|z\|)\|z\| \tag{3.22}$$

where $z(t) \in \mathbb{R}^{(n+1)m\times 1}$ *is defined as follows*

$$z \triangleq \left[\begin{array}{cccc} e_1^T & e_2^T & ... & e_n^T \end{array} \right. \left. \begin{array}{c} r^T \end{array} \right]^T \tag{3.23}$$

and $\rho(\cdot) \in \mathbb{R}_{\geq 0}$ *is some globally invertible, nondecreasing function.*

Remark 2 *After utilizing (3.5) and Assumption 4 along with (3.20) and its time derivative, then it is clear that* $\psi(t), \dot{\psi}(t) \in \mathcal{L}_\infty$.

Remark 3 *After utilizing (3.5) and (3.16) along with (3.19) and its time derivative, then it is clear that* $N_r(t), \dot{N}_r(t) \in \mathcal{L}_\infty$.

Remark 4 *In view of Assumption 3,* $N_r(\cdot)$ *defined in (3.19), can be linearly parameterized in the sense that*

$$N_r \triangleq W_r\theta \tag{3.24}$$

where $W_r(t) \in \mathbb{R}^{m\times p}$ *is the known regressor matrix and is a function of only* $x_r(t)$ *and its time derivatives.*

Based on (3.17) and (3.24), the control input is designed as follows

$$\begin{aligned} u &\triangleq (K+I_m)\left[e_n(t) - e_n(t_0) + \Lambda\int_{t_0}^{t} e_n(\tau)\,d\tau\right] \\ &\quad + \int_{t_0}^{t}\left[W_r(\tau)\hat{\theta}(\tau) + (C_1+C_2)\,\mathrm{Sgn}(e_n(\tau))\right]d\tau \end{aligned} \tag{3.25}$$

where $\hat{\theta}(t) \in \mathbb{R}^p$ is generated via

$$\begin{aligned} \hat{\theta} &\triangleq \Gamma\int_{t_0}^{t} W_r^T(\tau)\Lambda e_n(\tau)\,d\tau - \Gamma\int_{t_0}^{t}\dot{W}_r^T(\tau)e_n(\tau)\,d\tau \\ &\quad + \Gamma W_r^T(t)e_n(t) - \Gamma W_r^T(t_0)e_n(t_0) \end{aligned} \tag{3.26}$$

with $K, C_1, C_2 \in \mathbb{R}^{m\times m}$ and $\Gamma \in \mathbb{R}^{p\times p}$ being constant, diagonal, positive definite, gain matrices, $I_m \in \mathbb{R}^{m\times m}$ being the standard identity matrix, and $\text{Sgn}(\cdot)$ being the vector signum function defined as follows

$$\begin{aligned} \text{Sgn}(\xi) &\triangleq \left[\begin{array}{cccc} \text{sgn}(\xi_1) & \text{sgn}(\xi_2) & ... & \text{sgn}(\xi_m) \end{array} \right]^T \\ \forall \xi &= \left[\begin{array}{cccc} \xi_1 & \xi_2 & ... & \xi_m \end{array} \right]^T. \end{aligned} \tag{3.27}$$

It should be noted that $\hat{\theta}(t_0) = 0_{p\times 1}$ and $u(t_0) = 0_{m\times 1}$ where $0_{p\times 1} \in \mathbb{R}^p$ and $0_{m\times 1} \in \mathbb{R}^m$ are vectors of zeros. Based on the structure of (3.25) and (3.26), the following are obtained

$$\dot{u} \triangleq (K + I_m) r + (C_1 + C_2) \text{Sgn}(e_n) + W_r \hat{\theta} \tag{3.28}$$

$$\dot{\hat{\theta}} \triangleq \Gamma W_r^T r. \tag{3.29}$$

Finally, after substituting (3.28) into (3.17), the following closed-loop error system for $r(t)$ is obtained

$$M\dot{r} = -\frac{1}{2}\dot{M}r - e_n - (K + I_m) r + W_r \tilde{\theta} - (C_1 + C_2) \text{Sgn}(e_n) + \tilde{N} + \psi \tag{3.30}$$

where the parameter estimation error signal $\tilde{\theta}(t) \in \mathbb{R}^p$ is defined as follows

$$\tilde{\theta} \triangleq \theta - \hat{\theta}. \tag{3.31}$$

Stability Analysis

Theorem 7 *The control law (3.25) and the update law (3.26) ensure the boundedness of all closed-loop system signals and* $\left\| e_1^{(i)}(t) \right\| \to 0$ *as* $t \to \infty$, $i = 0, ..., n$, *provided*

$$\lambda_{\min}(\Lambda) > \frac{1}{2}, \tag{3.32}$$

$$C_{1i} > \|\psi_i(t)\|_{\mathcal{L}_\infty} + \frac{1}{\Lambda_i} \left\| \dot{\psi}_i(t) \right\|_{\mathcal{L}_\infty} \tag{3.33}$$

where the subscript $i = 1, ..., m$ *denotes the ith element of the vector or diagonal matrix and the elements of* K *are selected sufficiently large relative to the system initial conditions.*

Proof. See Appendix J.

Theorem 8 *There exists a constant vector* $\hat{\theta}_\infty \in \mathbb{R}^p$ *such that*

$$\lim_{t\to\infty} \hat{\theta}(t) = \hat{\theta}_\infty. \tag{3.34}$$

Proof. See Appendix K.

Numerical Simulation Results

A numerical simulation was performed to demonstrate the performance of the adaptive controller given in (3.25) and (3.26). A first-order flat system with following modelling functions is utilized [72]

$$\begin{aligned} f &= \begin{bmatrix} x_1 x_2 \\ x_2^2 \end{bmatrix}, \quad G = \begin{bmatrix} \dfrac{2+\cos x_1}{\theta_1} & 0 \\ 0 & \dfrac{3+\sin x_2}{\theta_2} \end{bmatrix}, \\ \theta &= \begin{bmatrix} \theta_1 \\ \theta_2 \end{bmatrix} = \begin{bmatrix} 2 \\ 1 \end{bmatrix}, \end{aligned} \tag{3.35}$$

$$d_1 = \begin{bmatrix} \cos(2t) + \exp(-0.5t) \\ \sin(3t) + \exp(-0.5t) \end{bmatrix}, d_2 = \begin{bmatrix} \sin(2t) + \exp(-0.5t) \\ \cos(3t) + \exp(-0.5t) \end{bmatrix} \tag{3.36}$$

where $x = \begin{bmatrix} x_1 & x_2 \end{bmatrix}^T$. The nonlinear disturbances defined in (3.36), are chosen to show the validity of the proposed controller for nonrepeating disturbances. The reference trajectory was selected as

$$x_r = \begin{bmatrix} x_{r1} \\ x_{r2} \end{bmatrix} = \begin{bmatrix} \sin t \left(1 - \exp\left(-\dfrac{t^3}{5}\right)\right) \\ 2\sin t \left(1 - \exp\left(-\dfrac{t^3}{2}\right)\right) \end{bmatrix}. \tag{3.37}$$

The initial conditions of the system were set to $x(t_0) = \begin{bmatrix} 0.1 & 0.2 \end{bmatrix}^T$ and $\hat{\theta}(t_0) = \begin{bmatrix} 0 & 0 \end{bmatrix}^T$, while the controller parameters were chosen as $\Lambda = I_2$, $K = 20I_2$, $C_1 = 10I_2$, $C_2 = 5I_2$, and $\Gamma = 20I_2$ where $I_2 \in \mathbb{R}^{2\times 2}$ is the standard identity matrix. In Figures 3.1 and 3.2, the reference trajectory $x_r(t)$ and the tracking error $e_1(t)$ are presented, respectively. From Figure 3.2, it is clear that the tracking objective is

satisfied. In Figures 3.3 and 3.4, the parameter estimate $\hat{\theta}(t)$ and the control input $u(t)$ are presented, respectively. From Figure 3.3, it is clear that the parameter estimate vector is driven to a constant vector. In Figures 3.5 and 3.6, the additive disturbances $d_1(t)$ and $d_2(t)$ are presented, respectively.

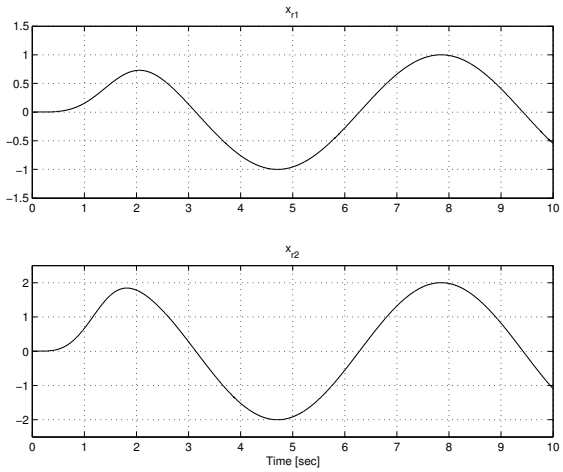

Figure 3.1 Reference Trajectory $x_r(t)$(Adaptive Controller)

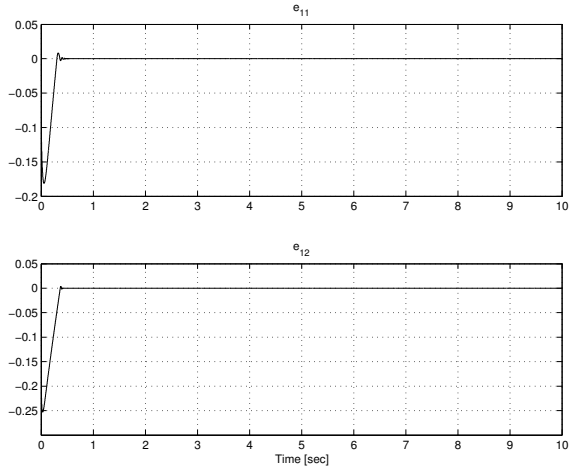

Figure 3.2 Tracking Error $e_1(t)$ (Adaptive Controller)

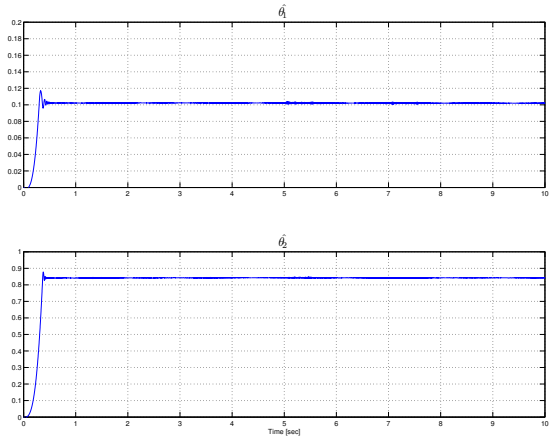

Figure 3.3 Parameter Estimate $\hat{\theta}(t)$ (Adaptive Controller)

Learning Control Development

Problem Statement

A system model for the flat nonlinear systems is considered to be of the following form

$$x^{(n)} = f + G(u + d_1) + d_2 \tag{3.38}$$

where $x^{(i)}(t) \in \mathbb{R}^m$, $i = 0, ..., (n-1)$ are the system states, $f(x, \dot{x}, ..., x^{(n-1)}) \in \mathbb{R}^m$ and $G(x, \dot{x}, ..., x^{(n-1)}) \in \mathbb{R}^{m \times m}$ are nonlinear functions, $d_1(t), d_2(t) \in \mathbb{R}^m$ are unknown additive disturbances, and $u(t) \in \mathbb{R}^m$ is the control input. The system model is assumed to satisfy Assumptions 1, 2, and 4.

The output tracking error $e_1(t)$ is defined in (3.4) and in this case the reference trajectory satisfies the following property

$$x_r^{(i)}(t + T) = x_r^{(i)}(t) \ , \ x_r^{(i)}(t) \in \mathcal{L}_\infty \ i = 0, 1, ..., (n+2) \tag{3.39}$$

where $T \in \mathbb{R}^+$ is the period of the reference trajectory.

The control objective is to develop a nonlinear control that ensures $\|e_1(t)\| \to 0$ as $t \to \infty$. To achieve the control objective, the subsequent development is derived based on the assumption that the system states $x^{(i)}(t)$, $i = 0, ..., (n-1)$ are measurable.

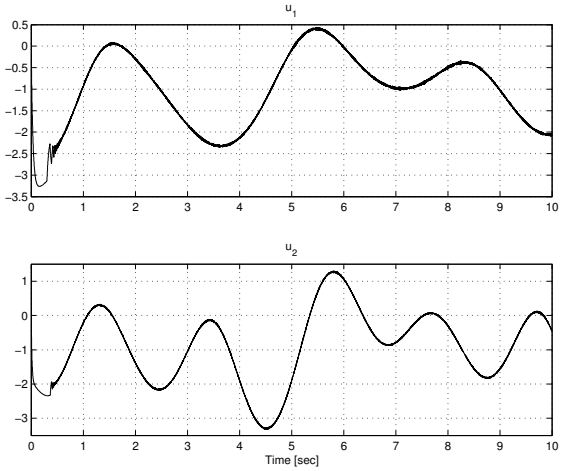

Figure 3.4 Control Input $u(t)$ (Adaptive Controller)

Development of Learning Control Law

The open-loop error system development for the learning control law is exactly the same as the open-loop error system development for the adaptive control law. The control design is assumed to continue after Remark 1 of Adaptive Control Development.

Remark 5 *After utilizing (3.39) and Assumption 4 along with (3.20) and its time derivative, then it is clear that* $\psi(t), \dot{\psi}(t) \in \mathcal{L}_\infty$.

Remark 6 *After utilizing (3.16) and (3.39) along with (3.19) and its time derivative, then it is clear that* $N_r(t), \dot{N}_r(t) \in \mathcal{L}_\infty$.

Remark 7 *After utilizing (3.39), it is clear that* $N_r(t)$ *satisfies the following equation*

$$N_r(t+T) = N_r(t). \tag{3.40}$$

Based on (3.17), the control input is designed as follows

$$\begin{aligned} u(t) &\triangleq (K+I_m)\left[e_n(t) - e_n(t_0) + \Lambda \int_{t_0}^{t} e_n(\tau)\, d\tau\right] \\ &\quad + C_1 \int_{t_0}^{t} \mathrm{Sgn}(e_n(\tau))\, d\tau + \hat{W}_r(t) \end{aligned} \tag{3.41}$$

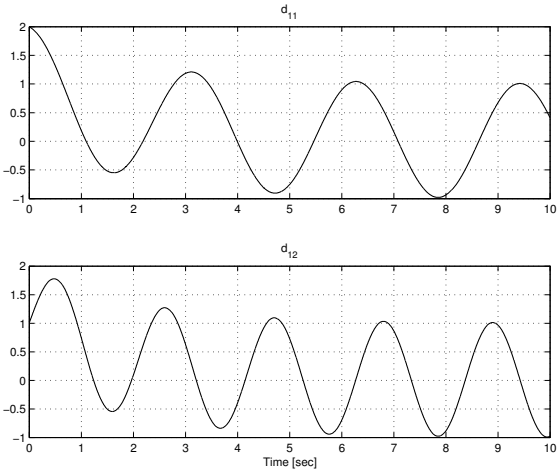

Figure 3.5 Additive Disturbance $d_1(t)$

where $K, C_1, \Lambda \in \mathbb{R}^{m\times m}$ are constant, diagonal, positive definite, gain matrices, $\mathrm{Sgn}(\cdot)$ is defined in (3.27), and $\hat{W}_r(t) \in \mathbb{R}^m$ is defined as follows

$$\hat{W}_r(t) \triangleq \hat{W}_r(t-T) + k_L\Lambda \int_{t_0}^{t} e_n(\tau)\, d\tau + k_L e_n(t) - k_L e_n(t_0) \tag{3.42}$$

where $k_L \in \mathbb{R}$ is a positive gain. It should be noted that since $\hat{W}_r(t_0) = 0_{m\times 1}$ it follows that $u(t_0) = 0_{m\times 1}$. The auxiliary function $\hat{N}_r(t) \in \mathbb{R}^m$ is defined as

$$\hat{N}_r \triangleq \dot{\hat{W}}_r\,. \tag{3.43}$$

By utilizing (3.43) along with (3.42), the following can be obtained

$$\hat{N}_r(t) = \hat{N}_r(t-T) + k_L r(t)\,. \tag{3.44}$$

Taking the time derivative of (3.41) along (3.42) and (3.43) generates

$$\dot{u} = (K + I_m)\, r + C_1 \mathrm{Sgn}(e_n) + \hat{N}_r(t)\,. \tag{3.45}$$

Finally, after substituting (3.45) into (3.17), the closed-loop error system for $r(t)$ is obtained as follows

$$M\dot{r} = -\frac{1}{2}\dot{M}r - e_n - (K + I_m)\, r - C_1 \mathrm{Sgn}(e_n) + \tilde{N} + \tilde{N}_r + \psi \tag{3.46}$$

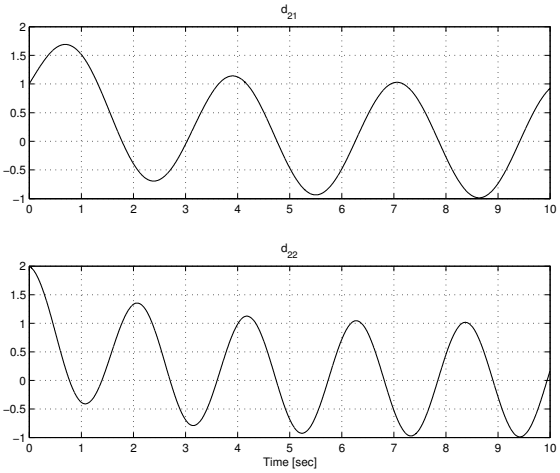

Figure 3.6 Additive Disturbance $d_2(t)$

where $\tilde{N}_r(t) \in \mathbb{R}^m$ is defined as follows

$$\tilde{N}_r \triangleq N_r - \hat{N}_r. \tag{3.47}$$

By utilizing (3.40) and (3.44), $\tilde{N}_r(t)$ can be rewritten as follows

$$\tilde{N}_r(t) = \tilde{N}_r(t - T) - k_L r. \tag{3.48}$$

Stability Analysis

Theorem 9 *The control law (3.41) and (3.42) ensures that* $\|e_1(t)\| \to 0$ *as* $t \to \infty$*, provided that (3.32) and (3.33) are satisfied and the elements of* K *are selected sufficiently large relative to the system initial conditions.*

Proof. See Appendix L.

Numerical Simulation Results

A numerical simulation was performed to demonstrate the performance of the learning controller given in (3.41) and (3.42). The flat system model in (3.35), (3.36) with the following reference trajectory is utilized

$$x_r = \begin{bmatrix} x_{r1} \\ x_{r2} \end{bmatrix} = \begin{bmatrix} \sin(\pi t) \\ \cos(\pi t) \end{bmatrix}. \tag{3.49}$$

The initial conditions of the system were set to $x(t_0) = \begin{bmatrix} 0.1 & 0.2 \end{bmatrix}^T$, while the controller parameters were chosen as $\Lambda = 20I_2$, $K = 20I_2$, $C_1 = 10I_2$, and $k_L = 1$. In Figures 3.7 and 3.8, the reference trajectory and the tracking error are presented, respectively. From Figure 3.8, it is clear that the tracking objective is satisfied. In Figures 3.9 and 3.10, the control input $u(t)$and $\hat{W}_r(t)$ are presented, respectively.

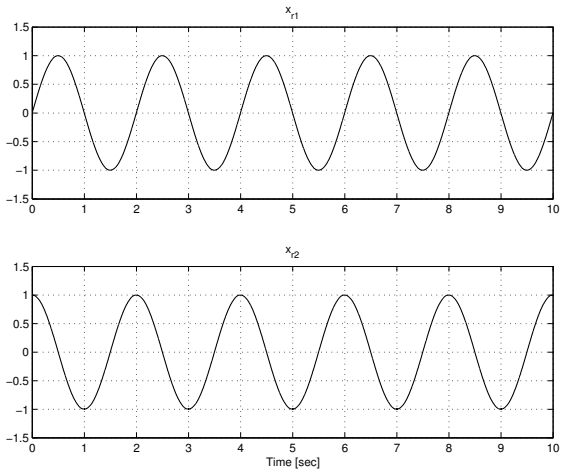

Figure 3.7 Reference Trajectory $x_r(t)$ (Learning Controller)

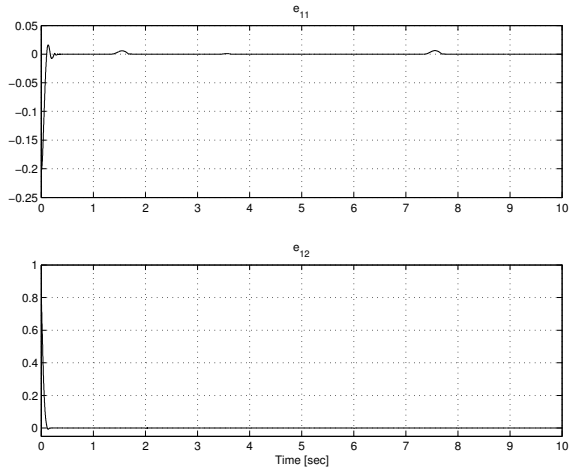

Figure 3.8 Tracking Error $e_1(t)$ (Learning Controller)

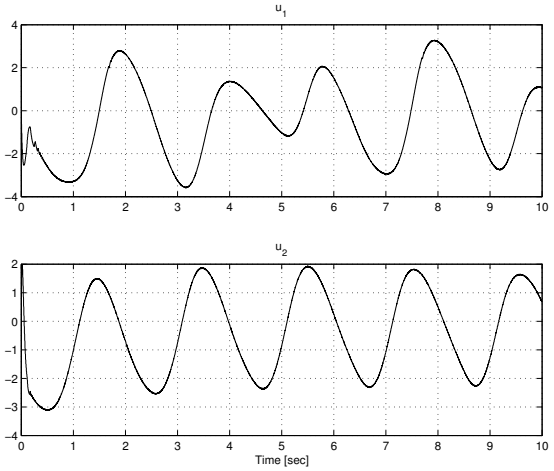

Figure 3.9 Control Input $u(t)$ (Learning Controller)

Conclusion

Two controllers were developed for flat MIMO nonlinear systems in the presence of additive disturbances. The robust adaptive controller was proven to yield a semi-global asymptotic tracking result in the presence of parametric uncertainty along with additive disturbances. The adaptive controller and the adaptation law were designed such that, the parameter estimate vector is proven to go to a constant vector. In the second part of the chapter, the learning controller was proven to yield a semi-global asymptotic result in the presence of additive disturbances and when the desired trajectory is periodic. In the development of both controllers, the bounded additive disturbances were assumed to be twice continuously differentiable and have bounded time derivatives up to second order. Since no assumptions were made regarding the periodicity of the disturbances, it is clear that the suggested controllers compensated for both repeating and nonrepeating disturbances. For each controller, Lyapunov-based techniques were used to guarantee that the tracking error is asymptotically driven to zero. Numerical simulation results were presented for both controllers where nonrepeating disturbances were utilized.

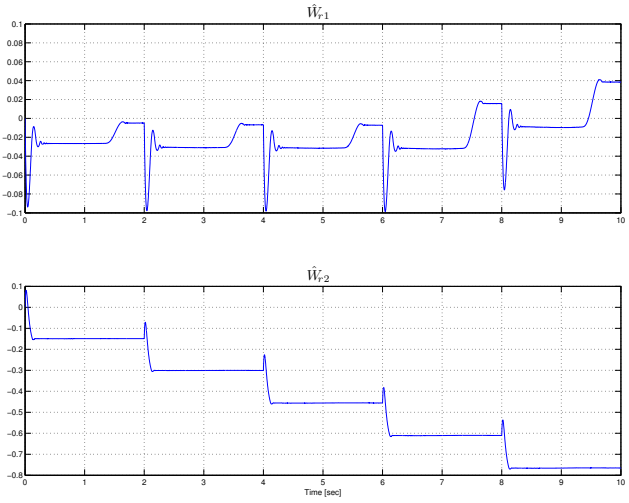

Figure 3.10 $\hat{W}_r(t)$ (Learning Controller)

CHAPTER 4
NEW DYNAMIC MODELS FOR PLANAR EXTENSIBLE CONTINUUM ROBOT MANIPULATORS

Introduction

In most engineered systems, the behaviour of the system is required to be accurately modelled to improve the performance of the system. In many applications, design simulation and proposed control algorithms require more than just a simple kinematic or dynamic model [77]. Not only an accurate model but a real-time calculation of the dynamic model is also needed for control algorithms or simulations.

The desire to enhance the performance of robot manipulators resulted in a renewed interest in continuum robots [78]. To our best knowledge, the concept of continuum robot was first introduced in the 1960's [79]. Numerous designs of continuum robots were presented in [80], [81], [82], [83], and [84]. Recently, there has been an increasing interest in designing 'biologically inspired' continuum robots. Some of these designs are mimicking trunks [85], [86], tentacles [87], [88], [89] and snakes [82]. Several commercial implementations have appeared (i.e., [90] and [91]).

The results in this chapter are motivated by and are applicable to the OCTARM continuum manipulator. The OCTARM manipulator is a biologically inspired soft robot manipulator resembling an elephant trunk or an octopus arm [92]. The OCTARM, shown in Figure 4.1, is a three-section robot with nine degrees of freedom. Aside from two axis bending with constant curvature, each section is also capable of extension. The bending and extension capabilities of OCTARM makes it suitable for a wide variety of physical applications ranging from whole arm grasping of various shapes of payloads to navigation of unstructured environments [87] and provides an increased workspace compared to its inextensible counterparts [93]. In a recent work, Jones and Walker [94] discussed the limiting-case analysis for a general class of continuum manipulators. In [95], Jones and Walker presented a kinematic model for

a general class of continuum robots which has been applied to OCTARM. However, kinematic control of continuum robot hardware remains the state of the art due to the current lack of appropriate dynamic models.

There has been previous research in dynamic modelling of biologically inspired robot manipulators. In two recent papers [96] and [97], the authors presented dynamic models for snake-like robots. However, in both cases, hyper-redundant serial rigid-link systems are considered. This does not model the continuous nature of continuum robots. In [98], researchers presented a 2-D dynamic model for the octopus arm. However, while allowing extensibility, the model is based on an approximation (by a finite number of linear models) to the true continuum case. In [81], Chirikjian and Burdick considered extensibility of hyper-redundant manipulators and a kinematic model was presented based on the modal approach introduced in [99]. The papers presented by Chirikjian [100], Ivanescu [101], [102], and Mochiyama [2], [103], [104] considered dynamic modeling of continuum robot manipulators. However, the dynamic model proposed in [100] for 3-D case remains in integral differential form, which makes it problematic for real-time control, and the dynamic model in [102] was derived based on the restrictive assumption that the manipulator does not bend past a small-strain region. In [2], [103], and [104], Mochiyama and Suzuki presented a three-dimensional dynamic model for an inextensible (constant length) continuum manipulator, considering the continuum robot as a combination of slices where each slice is a rigid link. To derive the dynamic model, limit of a serial rigid chain model is obtained as the kinematic degrees of freedom goes to infinity. However, the dynamic model was for inextensible robot manipulators and did not include elastic potential energy terms due to bending effects. In [101], Ivanescu *et al.* considered both gravitational and elastic potential energy effects when deriving their model. However, the elastic potential energy due to bending was calculated as a summation of all the elements of the manipulator and while deriving the elastic potential energy due to bending and extension the spring constants were considered to be the same along the backbone

curve of the manipulator. This approach results in an approximation of the elastic potential energy and does not reflect the characteristics of different sections of the physical manipulators.

In this chapter, first, the work in [2] is modified and extended in order to include the important class of extensible continuum robot manipulators. A geometric model of a 3-section extensible continuum robot manipulator with a circular cross-section is considered (see Figure 4.2). For simplicity, the geometric model is assumed to have no torsional effects. After presenting the system model and properties, the kinetic energy of a slice of the continuum robot is evaluated. The total kinetic energy of the manipulator is obtained by utilizing a limit operation (i.e., sum of the kinetic energy of the slices). Then, the potential energy terms are considered. For this, first, based on the definition presented in [2], the gravitational potential energy of one backbone slice is derived. After integrating the gravitational potential energy of one slice along the backbone curve the total gravitational potential energy of the robot manipulator is calculated. Then, the elastic potential energy of the manipulator is considered. First, the elastic potential energy due to the effects of bending is derived for one slice of the manipulator. After integrating the elastic potential energy of one slice along the backbone curve the total elastic potential energy due to bending is calculated. Next, elastic potential energy reflecting the extensibility of the robot is considered. The elastic potential energy caused by extension is calculated by modeling each section of the manipulator as a spring. The total elastic potential energy of the manipulator due to extension effects is found by adding the corresponding energy terms of each section. While deriving the elastic potential energy, separate spring constants are assigned for each section of the robot manipulator to reflect the different characteristics of different sections of the physical manipulator. This approach provides an improvement over a similar definition introduced in [101] where the spring constant was assumed to be the same along the backbone curve. By utilizing the Lagrangian representation, the dynamic model of a planar 3-section extensible continuum robot manipulator

is obtained. It is also proved that the skew-symmetry property is satisfied for the presented dynamic model (i.e., $(\dot{M}(q) - 2V(q,\dot{q}))$ is skew-symmetric). Numerical simulation results are presented for a planar 3-section extensible continuum robot manipulator.

System Model and Definitions

In this section, system model, properties, and definitions are presented. The geometric model of a 3-section extensible continuum robot manipulator utilized in this chapter is presented in Figure 4.2. This geometric model is a good approximation of the OCTARM which is shown in Figure 4.1.

The following convention, which is adopted from [2], will be adhered throughout the following development[3]. The matrix, ${}^{0}\Phi(0) \in SO(3)$ represents the orientation matrix of the base frame, and ${}^{0}p(0) \in \mathbb{R}^3$ represents the position vector of the origin. The matrices, ${}^{0}\Phi(\sigma,t)$, ${}^{\xi}\Phi(\sigma,t) \in SO(3)$ represent the orientation matrices of the extended Frenet frame at σ relative to the base frame and ${}^{\xi}\Phi(\xi,t) \in SO(3)$, respectively. The vectors, ${}^{0}p(\sigma,t)$, ${}^{\xi}p(\sigma,t) \in \mathbb{R}^3$ represent the position vectors of the point σ relative to the origin as viewed from the base frame and ${}^{\xi}\Phi(\xi,t)$, respectively. For simplicity, the notation of $\Phi(\sigma,t)$ and $p(\sigma,t)$ will be preferred instead of ${}^{\sigma}\Phi(\sigma,t)$ and ${}^{\sigma}p(\sigma,t)$ throughout the rest of the chapter. The section lengths of the manipulator are denoted as $d_i(t) \in \mathbb{R}_+$, $i = 1,2,3$, and $\kappa(\sigma,t) \in \mathbb{R}$ represents the curvature of the point σ. The total length of the robot manipulator, denoted as $d(t) \in \mathbb{R}_+$, is equal to the following

$$d(t) \triangleq d_1(t) + d_2(t) + d_3(t). \tag{4.1}$$

The system model is assumed to satisfy the following properties.

Property 4 *The curvature κ at each point σ of the manipulator is a function of both time and σ. In the following analysis, consistent with the OCTARM, it is assumed*

[3]To set a basis for our future work three-dimensional space is preferred for representing the orientation and velocity instead of their two-dimensional counterparts.

that the curvature of a section is only function of time (i.e., $\kappa(\sigma,t) = \kappa_i(t)$ *if* σ *is a point on Section* i*,* $i = 1,2,3$*). In the subsequent analysis, it is assumed that the curvature is always non-zero (i.e.,* $\kappa(\sigma,t) \neq 0 \ \forall(\sigma,t)$*). The reader is referred to [94] for a detailed limiting-case analysis for a general class of continuum robot manipulators.*

Property 5 *In Figure 4.2,* $p(\xi,t) \in \mathbb{R}^3$ *is the position vector of point* ξ *of the backbone curve and* $p_c(\xi,t) \in \mathbb{R}^3$ *is the position vector of the center of mass of the slice at* ξ*. In the analysis, again consistent with the OCTARM, it is assumed that* $p(\xi,t)$ *and* $p_c(\xi,t)$ *coincide (i.e.,* $\Delta p(\xi) = \begin{bmatrix} 0 & 0 & 0 \end{bmatrix}^T$*).*

Property 6 *The robot manipulator is assumed to have uniform mass density. The line mass density of the slice, denoted as* $m(\sigma,t) \in \mathbb{R}$*, is defined as follows*

$$m(\sigma,t) = \frac{m}{d(t)} \tag{4.2}$$

where $m \in \mathbb{R}$ *is the total mass of the manipulator.*

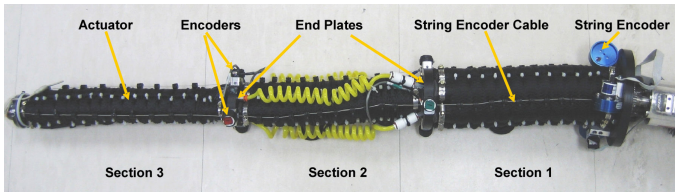

Figure 4.1 OCTARM (ver. 5.2)

The orientation matrix of the extended Frenet frame at σ with respect to the base frame, denoted as ${}^0\Phi(\sigma,t)$, is given as follows

$${}^0\Phi(\sigma,t) = \begin{bmatrix} \cos(\sigma\kappa(\sigma,t)) & 0 & -\sin(\sigma\kappa(\sigma,t)) \\ 0 & 1 & 0 \\ \sin(\sigma\kappa(\sigma,t)) & 0 & \cos(\sigma\kappa(\sigma,t)) \end{bmatrix} \tag{4.3}$$

The orientation matrix given in (4.3) is equal to the orientation matrix provided in Equation (8) of [95] with the angle of curvature is equal to zero (i.e., $\phi(\sigma,t) = 0$).

The change of the orientation matrix along the manipulator is characterized by the following equation

$$\frac{\partial\ {}^{0}\Phi(\sigma,t)}{\partial\sigma} = {}^{0}\Phi(\sigma,t)\, a^{\times}(\sigma,t) \tag{4.4}$$

where $a^{\times}(\sigma,t) \in \mathbb{R}^{3\times3}$ is the skew-symmetric matrix of the frame rate vector $a(\sigma,t) \in \mathbb{R}^{3}$. After utilizing (4.3) and (4.4), $a(\sigma,t)$ and $a^{\times}(\sigma,t)$ can be defined as follows

$$a(\sigma,t) = \begin{bmatrix} 0 \\ -\kappa(\sigma,t) \\ 0 \end{bmatrix},\ a^{\times}(\sigma,t) = \begin{bmatrix} 0 & 0 & -\kappa(\sigma,t) \\ 0 & 0 & 0 \\ \kappa(\sigma,t) & 0 & 0 \end{bmatrix}. \tag{4.5}$$

The position vector of the point σ from the origin $p(0)$ with respect to the base frame, denoted as ${}^{0}p(\sigma,t)$, is evaluated as follows

$${}^{0}p(\sigma,t) = \int_{0}^{\sigma} {}^{0}\Phi(\eta,t)\, e_{\times} d\eta \tag{4.6}$$

where $e_{\times} \triangleq \begin{bmatrix} 1 & 0 & 0 \end{bmatrix}^{T}$. The orientation matrix of the extended Frenet frame at σ relative to $\Phi(\xi,t)$, denoted as ${}^{\xi}\Phi(\sigma,t)$, is calculated as follows

$${}^{\xi}\Phi(\sigma,t) \triangleq {}^{0}\Phi^{T}(\xi,t)\ {}^{0}\Phi(\sigma,t). \tag{4.7}$$

The position vector of the point σ relative to the origin as viewed from $\Phi(\xi,t)$, denoted as ${}^{\xi}p(\sigma,t)$, is evaluated as follows

$${}^{\xi}p(\sigma,t) \triangleq {}^{0}\Phi^{T}(\xi,t)\ {}^{0}p(\sigma,t). \tag{4.8}$$

The internal variable vector at σ which is denoted as $\theta(\sigma,t) \in \mathbb{R}^{2}$ is defined as follows

$$\theta(\sigma,t) \triangleq \begin{bmatrix} l(\sigma,t) \\ \kappa(\sigma,t) \end{bmatrix} \tag{4.9}$$

where $l(\sigma,t)$ and $\kappa(\sigma,t)$ reflect the extension and curvature of the model. The extended axis matrix $\overline{A}(\theta(\sigma,t)) \in \mathbb{R}^{6\times2}$ is defined as follows

$$\overline{A}(\theta(\sigma,t)) \triangleq \begin{bmatrix} 1 & 0 & 0 & 0 & 0 & 0 \\ 0 & 0 & 0 & 0 & -1 & 0 \end{bmatrix}^{T}. \tag{4.10}$$

So far, the main extension of this development over [2] is the definition of the internal variable vector. The extensibility of our model is reflected by designing $\theta(\sigma,t)$ to

include $l(\sigma,t)$. This design allows the model to extend in each section, which results in a variable total length, while the geometric model presented in [2] had a constant total length. As a consequence of this new design for the internal variable vector, the extended axis matrix is modified accordingly. The adjoint matrix $Ad_{g(\sigma,\eta,t)} \in \mathbb{R}^{6\times 6}$ in terms of the rigid body transformation $g(\sigma,\eta,t) \in SE(3)$ is defined as follows

$$Ad_{g(\sigma,\eta,t)} \triangleq \begin{bmatrix} {}^{\sigma}\Phi(\eta,t) & ({}^{\sigma}p^{\times}(\eta,t) - {}^{\sigma}p^{\times}(\sigma,t)) \; {}^{\sigma}\Phi(\eta,t) \\ 0_{3\times 3} & {}^{\sigma}\Phi(\eta,t) \end{bmatrix} \tag{4.11}$$

where $0_{3\times 3} \in \mathbb{R}^{3\times 3}$ is a matrix of zeros.

Kinetic Energy

The kinetic energy of the slice at σ (see Figure 4.2) is given as follows [2]

$$\begin{aligned} K(\sigma,t) \triangleq \frac{1}{2}\int_0^{\sigma}\int_0^{\sigma} & \frac{\partial\theta^T(\eta,t)}{\partial t}\overline{A}^T(\eta,t)\, Ad^T_{g(\sigma,\eta,t)} \\ & M(\sigma,t)\, Ad_{g(\sigma,\xi,t)}\overline{A}(\xi,t)\frac{\partial\theta(\xi,t)}{\partial t} d\eta d\xi \end{aligned} \tag{4.12}$$

where $M(\sigma,t) \in \mathbb{R}^{6\times 6}$ is the inertia matrix of the slice at σ which is defined as follows

$$M(\sigma,t) \triangleq \begin{bmatrix} m(\sigma,t)\, I_3 & -m(\sigma,t)\,\Delta p^{\times}(\sigma) \\ m(\sigma,t)\,\Delta p^{\times}(\sigma) & I(\sigma) \end{bmatrix} \tag{4.13}$$

where $m(\sigma,t)\,\Delta p(\sigma) \in \mathbb{R}^3$ is the first moment of inertia of the slice, $I(\sigma) \in \mathbb{R}^{3\times 3}$ is the inertia tensor of the slice, and $I_3 \in \mathbb{R}^{3\times 3}$ is the standard identity matrix. The inertia tensor of the slice is assumed to be of the following form

$$I(\sigma) \triangleq \frac{mr^2}{2d}\begin{bmatrix} 1 & 0 & 0 \\ 0 & 0 & 0 \\ 0 & 0 & 0 \end{bmatrix} \tag{4.14}$$

where r is the radius of the circular cross-section of the robot manipulator. After utilizing Properties 1 and 2, the inertia matrix of the slice at σ can be evaluated as follows

$$M(\sigma,t) = diag\left\{\frac{m}{d},\, \frac{m}{d},\, \frac{m}{d},\, \frac{mr^2}{2d},\, 0,\, 0\right\}. \tag{4.15}$$

Due to the piecewise definition of the curvature (see Property 1), the kinetic energy of the slice at σ which is formulated by (4.12) will not be evaluated explicitly. However, by sliding the slice at σ over every section of the manipulator, the kinetic energy of every slice at σ can be calculated. The expression in (4.12) can be rewritten as follows

$$K(\sigma,t)=\int_0^{\sigma}\int_0^{\sigma} I(\sigma,\eta,\xi,t)\,d\eta d\xi \tag{4.16}$$

where $I(\sigma,\eta,\xi,t)$ is the integrand defined as follows

$$\begin{aligned}
I \triangleq \frac{m}{2d}\Big\{ & \dot{l}(\xi,t)\,\dot{l}(\eta,t)\cos(\xi\kappa(\xi,t)-\eta\kappa(\eta,t)) \\
& +\dot{l}(\xi,t)\,\dot{\kappa}(\eta,t)\left[\left(\frac{1}{\kappa(\eta,t)}-\frac{1}{\kappa(\sigma,t)}\right)\cos(\xi\kappa(\xi,t))\right. \\
& +\frac{1}{\kappa(\sigma,t)}\cos(\xi\kappa(\xi,t)-\sigma\kappa(\sigma,t)) \\
& \left.-\frac{1}{\kappa(\eta,t)}\cos(\xi\kappa(\xi,t)-\eta\kappa(\eta,t))\right] \\
& +\dot{\kappa}(\xi,t)\,\dot{l}(\eta,t)\left[\left(\frac{1}{\kappa(\xi,t)}-\frac{1}{\kappa(\sigma,t)}\right)\cos(\eta\kappa(\eta,t))\right. \\
& \left.+\frac{1}{\kappa(\sigma,t)}\cos(\sigma\kappa(\sigma,t)-\eta\kappa(\eta,t))-\frac{1}{\kappa(\xi,t)}\cos(\xi\kappa(\xi,t)-\eta\kappa(\eta,t))\right] \\
& +\dot{\kappa}(\xi,t)\,\dot{\kappa}(\eta,t)\left[\frac{1}{\kappa(\sigma,t)}\left(\frac{1}{\kappa(\xi,t)}+\frac{1}{\kappa(\eta,t)}-\frac{2}{\kappa(\sigma,t)}\right)\cos(\sigma\kappa(\sigma,t))\right. \\
& +\frac{1}{\kappa(\xi,t)}\left(\frac{1}{\kappa(\sigma,t)}-\frac{1}{\kappa(\eta,t)}\right)\cos(\xi\kappa(\xi,t)) \\
& -\frac{1}{\kappa(\xi,t)}\frac{1}{\kappa(\sigma,t)}(1+\cos(\xi\kappa(\xi,t)-\sigma\kappa(\sigma,t))) \\
& -\frac{1}{\kappa(\eta,t)}\frac{1}{\kappa(\sigma,t)}(1+\cos(\sigma\kappa(\sigma,t)-\eta\kappa(\eta,t))) \\
& \left.+\frac{1}{\kappa(\eta,t)}\left(\frac{1}{\kappa(\sigma,t)}-\frac{1}{\kappa(\xi,t)}\right)\cos(\eta\kappa(\eta,t))\frac{2}{\kappa^2(\sigma,t)}\right]\Big\}.
\end{aligned} \tag{4.17}$$

The total kinetic energy of the system is defined as follows

$$K(t)\triangleq\int_0^{d(t)} K(\sigma,t)\,d\sigma \tag{4.18}$$

where $K(\sigma,t)$ is the kinetic energy of the slice at σ. The upper limit of the integral in (4.18) is the total length of the manipulator, which is a function of time as a result

of the extensible nature of our geometric model. However, the total length of the manipulator in [2] was constant. To facilitate the subsequent development, the total kinetic energy of the system will be rewritten as follows[4]

$$K(t) = \int_0^{d_1} K_1(\sigma, t)\, d\sigma + \int_{d_1}^{d_1+d_2} K_2(\sigma, t)\, d\sigma + \int_{d_1+d_2}^{d_1+d_2+d_3} K_3(\sigma, t)\, d\sigma \tag{4.19}$$

where $K_i(\sigma, t)$ is the kinetic energy of slice σ when σ is a point on Section i, $i = 1, 2, 3$. To facilitate the subsequent development $I_{ijk}(\sigma, \eta, \xi, t)$ is defined as follows

$$I_{ijk}(\sigma, \eta, \xi, t) \triangleq I(\sigma, \eta, \xi, t)|_{\sigma \in \text{ Section } i, \eta \in \text{ Section } j, \xi \in \text{ Section } k} \tag{4.20}$$

where for any $s \in$ Section i means $\dot{l}(s) = \dot{d}_i(t)$ and $\kappa(s) = \kappa_i(t)$. After utilizing (4.16), (4.19), (4.20) along with Property 1, $K_i(\sigma, t)$, $i = 1, 2, 3$ can be evaluated as follows[5]

$$K_1 = \int_0^{\sigma}\int_0^{\sigma} I_{111}\, d\eta d\xi \tag{4.21}$$

$$\begin{aligned} K_2 = &\int_0^{d_1(t)}\int_0^{d_1(t)} I_{211}\, d\eta d\xi \quad + \int_0^{d_1(t)}\int_{d_1(t)}^{\sigma} I_{221}\, d\eta d\xi \\ &+ \int_{d_1(t)}^{\sigma}\int_0^{d_1(t)} I_{212}\, d\eta d\xi \quad + \int_{d_1(t)}^{\sigma}\int_{d_1(t)}^{\sigma} I_{222}\, d\eta d\xi \end{aligned} \tag{4.22}$$

$$\begin{aligned} K_3 = &\int_0^{d_1(t)}\int_0^{d_1(t)} I_{311}\, d\eta d\xi + \int_0^{d_1(t)}\int_{d_1(t)}^{d_2(t)} I_{321}\, d\eta d\xi + \int_0^{d_1(t)}\int_{d_2(t)}^{\sigma} I_{331}\, d\eta d\xi \\ &+ \int_{d_1(t)}^{d_2(t)}\int_0^{d_1(t)} I_{312}\, d\eta d\xi + \int_{d_1(t)}^{d_2(t)}\int_{d_1(t)}^{d_2(t)} I_{322}\, d\eta d\xi + \int_{d_1(t)}^{d_2(t)}\int_{d_2(t)}^{\sigma} I_{332}\, d\eta d\xi \\ &+ \int_{d_2(t)}^{\sigma}\int_0^{d_1(t)} I_{313}\, d\eta d\xi + \int_{d_2(t)}^{\sigma}\int_{d_1(t)}^{d_2(t)} I_{323}\, d\eta d\xi + \int_{d_2(t)}^{\sigma}\int_{d_2(t)}^{\sigma} I_{333}\, d\eta d\xi. \end{aligned} \tag{4.23}$$

[4]For simplicity, the time dependency of the section lengths in (4.19) is dropped.

[5]For simplicity, I_{ijk} is preferred instead of $I_{ijk}(\sigma, \eta, \xi, t)$, in (4.21), (4.22), and (4.23).

To facilitate the subsequent development the joint position vector $q(t) \in \mathbb{R}^6$ is defined as follows

$$q \triangleq \begin{bmatrix} d_1 & d_2 & d_3 & \kappa_1 & \kappa_2 & \kappa_3 \end{bmatrix}^T. \tag{4.24}$$

After utilizing (4.17), (4.19)-(4.23), the total energy of the system can be evaluated as follows

$$\begin{aligned} K(t) &= K_{\dot{d}_1\dot{d}_1}\left(\dot{d}_1\right)^2 + K_{\dot{d}_1\dot{d}_2}\dot{d}_1\dot{d}_2 + K_{\dot{d}_1\dot{d}_3}\dot{d}_1\dot{d}_3 + K_{\dot{d}_1\dot{\kappa}_1}\dot{d}_1\dot{\kappa}_1 + K_{\dot{d}_1\dot{\kappa}_2}\dot{d}_1\dot{\kappa}_2 \\ &+K_{\dot{d}_1\dot{\kappa}_3}\dot{d}_1\dot{\kappa}_3 + K_{\dot{d}_2\dot{d}_2}\left(\dot{d}_2\right)^2 + K_{\dot{d}_2\dot{d}_3}\dot{d}_2\dot{d}_3 + K_{\dot{d}_2\dot{\kappa}_1}\dot{d}_2\dot{\kappa}_1 \\ &+K_{\dot{d}_2\dot{\kappa}_2}\dot{d}_2\dot{\kappa}_2 + K_{\dot{d}_2\dot{\kappa}_3}\dot{d}_2\dot{\kappa}_3 + K_{\dot{d}_3\dot{d}_3}\left(\dot{d}_3\right)^2 + K_{\dot{d}_3\dot{\kappa}_1}\dot{d}_3\dot{\kappa}_1 \\ &+K_{\dot{d}_3\dot{\kappa}_2}\dot{d}_3\dot{\kappa}_2 + K_{\dot{d}_3\dot{\kappa}_3}\dot{d}_3\dot{\kappa}_3 + K_{\dot{\kappa}_1\dot{\kappa}_1}\left(\dot{\kappa}_1\right)^2 + K_{\dot{\kappa}_1\dot{\kappa}_2}\dot{\kappa}_1\dot{\kappa}_2 \\ &+K_{\dot{\kappa}_1\dot{\kappa}_3}\dot{\kappa}_1\dot{\kappa}_3 + K_{\dot{\kappa}_2\dot{\kappa}_2}\left(\dot{\kappa}_2\right)^2 + K_{\dot{\kappa}_2\dot{\kappa}_3}\dot{\kappa}_2\dot{\kappa}_3 + K_{\dot{\kappa}_3\dot{\kappa}_3}\left(\dot{\kappa}_3\right)^2. \end{aligned} \tag{4.25}$$

In (4.25), the terms $K_{\dot{q}_i\dot{q}_j}$ with q_i and q_j being entries of $q(t)$, are presented in Appendix M.

Potential Energy

In this section, three different energy definitions will be introduced for our model. First, gravitational potential energy will be defined and then the elastic potential energy due to both bending and extension will be presented.

Gravitational Potential Energy

The gravitational potential energy of a slice at σ is given as follows [2]

$$P_g(\sigma,t) \triangleq -m(\sigma,t)\ {}^{\sigma}g^T(\sigma,t)\, p(\sigma,t) \tag{4.26}$$

where ${}^{\sigma}g^T(\sigma,t) \in \mathbb{R}^3$ is defined as follows

$${}^{\sigma}g^T(\sigma,t) \triangleq {}^{\sigma}\Phi^T(0,t) \begin{bmatrix} 0 & 0 & -g \end{bmatrix}^T \tag{4.27}$$

where $g \in \mathbb{R}$ is the gravity acceleration constant. After utilizing (4.2), (4.6), (4.27) gravitational potential energy can be calculated as follows

$$P_g(\sigma,t) = \frac{mg}{d(t)\,\kappa(\sigma,t)}\left[\cos\left(\sigma\kappa(\sigma,t)\right) - \cos\left(2\sigma\kappa(\sigma,t)\right)\right]. \tag{4.28}$$

Total gravitational potential energy of the system can be found as a sum of the gravitational energies for every slice

$$P_g(t) \triangleq \int_0^{d(t)} P_g(\sigma, t)\, d\sigma \tag{4.29}$$

where $P_g(\sigma, t)$ is the gravitational potential energy of the slice at σ defined in (4.26) and (4.28). It should be noted that, the upper limit of the integral in (4.29) is the total length of the manipulator, which is a function of time as a result of the extensible nature of our geometric model, while the total length of the manipulator in [2] was constant. To facilitate the subsequent development, the total gravitational potential energy of the system will be rewritten as follows[6]

$$P_g(t) = \int_0^{d_1} P_{g1}(\sigma, t)\, d\sigma + \int_{d_1}^{d_1+d_2} P_{g2}(\sigma, t)\, d\sigma + \int_{d_1+d_2}^{d_1+d_2+d_3} P_{g3}(\sigma, t)\, d\sigma \tag{4.30}$$

where $P_{gi}(\sigma, t)$ is the gravitational potential energy of slice σ when σ is a point on Section i, $i = 1, 2, 3$ which is defined as follows

$$P_{gi}(\sigma, t) = \frac{mg}{d\kappa_i} \left[\cos(\sigma\kappa_i) - \cos(2\sigma\kappa_i)\right]. \tag{4.31}$$

From (4.30) $P_g(t)$ can be calculated as follows

$$\begin{aligned} P_g \;=\; & \frac{mg}{d} \left\{ \frac{1}{\kappa_1^2} \left[\sin(d_1\kappa_1) - \frac{1}{2}\sin(2d_1\kappa_1) \right] \right. \\ & + \frac{1}{\kappa_2^2} \left[\sin((d_1+d_2)\kappa_2) - \frac{1}{2}\sin(2(d_1+d_2)\kappa_2) \right. \\ & \left. - \sin(d_1\kappa_2) + \frac{1}{2}\sin(2d_1\kappa_2) \right] \\ & + \frac{1}{\kappa_3^2} \left[\sin((d_1+d_2+d_3)\kappa_3) - \frac{1}{2}\sin(2(d_1+d_2+d_3)\kappa_3) \right. \\ & \left. \left. - \sin((d_1+d_2)\kappa_3) + \frac{1}{2}\sin(2(d_1+d_2)\kappa_3) \right] \right\} \end{aligned} \tag{4.32}$$

where (4.31) was utilized.

[6]For simplicity, the time dependency of the section lengths in (4.30) is dropped.

Elastic Potential Energy

In this section, potential energy due to extension and bending is discussed.

Elastic Potential Energy due to Bending

The elastic potential energy of the manipulator due to bending is given as follows

$$P_b(t) \triangleq \frac{1}{2}\int_0^{d(t)} k_b(\sigma)\,\beta^2(\sigma,t)\,d\sigma. \tag{4.33}$$

In (4.33), $\beta(\sigma,t)$ is defined as follows

$$\beta(\sigma,t) \triangleq \pi - \frac{1}{2}\alpha(\sigma,t) \tag{4.34}$$

where $\alpha(\sigma,t)$ is defined as follows

$$\alpha(\sigma,t) \triangleq \sigma\kappa(\sigma,t) \tag{4.35}$$

and $k_b(\sigma)$ is the spring constant defined as follows

$$k_b(\sigma) \triangleq k_{bi} \text{ if } \sigma \text{ is a point on Section i, i=1,2,3.} \tag{4.36}$$

This definition of the spring constants allows us to define different spring constants for each section. This definition of the elastic potential energy due to bending provides an improvement over a similar definition introduced in [101]. In [101], the potential energy is in the form of a summation as opposed to the integral form presented in this chapter, and also the spring constant utilized in that derivation is constant for the manipulator. The total elastic potential energy due to bending can be written as follows

$$\begin{aligned} P_b(t) &= \frac{1}{2}k_{b1}\int_0^{d_1}\beta_1^2(\sigma,t)\,d\sigma + \frac{1}{2}k_{b2}\int_{d_1}^{d_1+d_2}\beta_2^2(\sigma,t)\,d\sigma \\ &\quad + \frac{1}{2}k_{b3}\int_{d_1+d_2}^{d_1+d_2+d_3}\beta_3^2(\sigma,t)\,d\sigma \end{aligned} \tag{4.37}$$

where (4.36) was utilized, and from (4.34) and (4.35), $\beta_i(\sigma,t)$, $i=1,2,3$ can be defined as follows

$$\beta_i(\sigma,t) \triangleq \pi - \frac{1}{2}\sigma\kappa_i. \tag{4.38}$$

The total elastic potential energy due to bending evaluated in closed-form is presented as follows

$$\begin{aligned} P_b &= \frac{1}{2}k_{b1}\left\{\pi^2 d_1 - \frac{1}{2}\pi d_1^2\kappa_1 + \frac{1}{12}\pi d_1^3\kappa_1^2\right\} \\ &\quad + \frac{1}{2}k_{b2}\left\{\left[\pi^2(d_1+d_2) - \frac{1}{2}\pi(d_1+d_2)^2\kappa_2 + \frac{1}{12}\pi(d_1+d_2)^3\kappa_2^2\right]\right. \\ &\quad \left. - \left[\pi^2 d_1 - \frac{1}{2}\pi d_1^2\kappa_2 + \frac{1}{12}\pi d_1^3\kappa_2^2\right]\right\} \\ &\quad + \frac{1}{2}k_{b3}\left\{\left[\pi^2(d_1+d_2+d_3) - \frac{1}{2}\pi(d_1+d_2+d_3)^2\kappa_3\right.\right. \\ &\quad \left.\left. + \frac{1}{12}\pi(d_1+d_2+d_3)^3\kappa_3^2\right]\right. \\ &\quad \left. - \left[\pi^2(d_1+d_2) - \frac{1}{2}\pi(d_1+d_2)^2\kappa_3 + \frac{1}{12}\pi(d_1+d_2)^3\kappa_3^2\right]\right\}. \end{aligned} \tag{4.39}$$

Elastic Potential Energy due to Extension

The elastic potential energy of the manipulator due to extension is given as follows

$$P_e \triangleq \frac{1}{2}k_{e1}\left[d_1(t) - d_1^*\right]^2 + \frac{1}{2}k_{e2}\left[d_2(t) - d_2^*\right]^2 + \frac{1}{2}k_{e3}\left[d_3(t) - d_3^*\right]^2 \tag{4.40}$$

where d_i^* is the constant relaxed length of the i^{th} section and k_{ei} are spring constants for each section of the manipulator. This definition of the spring constants provides an improvement on the model in [101] which utilized the same spring constant for that definition.

Lagrangian Representation

The Lagrangian of the system is defined as follows

$$L(t) \triangleq K(t) - P(t) \tag{4.41}$$

where $K(t)$ is the total kinetic energy defined in (4.25) and $P(t)$ represents the total potential energy of the system defined as follows

$$P(t) \triangleq P_g(t) + P_b(t) + P_e(t) \tag{4.42}$$

where $P_g(t)$ is the gravitational potential energy, and $P_b(t)$ and $P_e(t)$ represent elastic potential energy due to extension and bending, respectively. It should be noted that, the potential energy terms $P_g(t)$, $P_b(t)$ and $P_e(t)$, defined in (4.32), (4.39), (4.40) respectively, are functions of only joint position vector $q(t)$ (i.e., they are not functions of the joint velocities or accelerations). Euler-Lagrange equations of motion are defined as follows [59]

$$\frac{d}{dt}\frac{\partial L}{\partial \dot{q}_i} - \frac{\partial L}{\partial q_i} = \tau_i \ , \ i = 1, 2, ..., 6. \tag{4.43}$$

The equations of motion can be rewritten as follows

$$\frac{d}{dt}\frac{\partial K}{\partial \dot{q}_i} - \frac{\partial K}{\partial q_i} - \frac{d}{dt}\frac{\partial P}{\partial \dot{q}_i} + \frac{\partial P}{\partial q_i} = \tau_i \ , \ i = 1, 2, ..., 6. \tag{4.44}$$

where (4.41) was utilized. Since the total potential energy of the system is not a function of the joint velocities, then it is clear that the third term on the left-hand-side of (4.44) is equal to zero for $\forall i$. The final term on the left-hand-side of (4.44) can be written as follows

$$\frac{\partial P}{\partial q_i} = \frac{\partial P_g}{\partial q_i} + \frac{\partial P_b}{\partial q_i} + \frac{\partial P_e}{\partial q_i} \ , \ i = 1, 2, ..., 6. \tag{4.45}$$

In view of the above mentioned facts, the dynamic model of the system is developed as follows

$$M(q)\ddot{q} + V(q, \dot{q})\dot{q} + G(q) + B(q) + E(q) = \tau(t) \tag{4.46}$$

where $M(q)$, $V(q, \dot{q}) \in \mathbb{R}^{6\times 6}$ are inertia matrix and centripetal-coriolis terms, respectively, $\tau(t) \in \mathbb{R}^6$ is the control input, and $G(q)$, $B(q)$, $E(q) \in \mathbb{R}^6$ represent the effects of $P_g(t)$, $P_b(t)$, and $P_e(t)$ respectively.

Remark 1 *The inertia matrix $M(q)$ and the centripetal coriolis terms $V(q,\dot{q})$ satisfy the following property:*

$$\xi^T \left(\dot{M} - 2V \right) \xi = 0, \; \forall \xi \in \mathbb{R}^6. \tag{4.47}$$

When, the matrix $(\dot{M} - 2V)$ is skew-symmetric, then (4.47) is satisfied. The proof of $(\dot{M} - 2V)$ being skew-symmetric is provided in Appendix P.

The terms in (4.46) are of the following form:

$$M \triangleq \begin{bmatrix} 2K_{\dot{d}_1\dot{d}_1} & K_{\dot{d}_1\dot{d}_2} & K_{\dot{d}_1\dot{d}_3} & K_{\dot{d}_1\dot{\kappa}_1} & K_{\dot{d}_1\dot{\kappa}_2} & K_{\dot{d}_1\dot{\kappa}_3} \\ K_{\dot{d}_1\dot{d}_2} & 2K_{\dot{d}_2\dot{d}_2} & K_{\dot{d}_2\dot{d}_3} & K_{\dot{d}_2\dot{\kappa}_1} & K_{\dot{d}_2\dot{\kappa}_2} & K_{\dot{d}_2\dot{\kappa}_3} \\ K_{\dot{d}_1\dot{d}_3} & K_{\dot{d}_2\dot{d}_3} & 2K_{\dot{d}_3\dot{d}_3} & K_{\dot{d}_3\dot{\kappa}_1} & K_{\dot{d}_3\dot{\kappa}_2} & K_{\dot{d}_3\dot{\kappa}_3} \\ K_{\dot{d}_1\dot{\kappa}_1} & K_{\dot{d}_2\dot{\kappa}_1} & K_{\dot{d}_3\dot{\kappa}_1} & 2K_{\dot{\kappa}_1\dot{\kappa}_1} & K_{\dot{\kappa}_1\dot{\kappa}_2} & K_{\dot{\kappa}_1\dot{\kappa}_3} \\ K_{\dot{d}_1\dot{\kappa}_2} & K_{\dot{d}_2\dot{\kappa}_2} & K_{\dot{d}_3\dot{\kappa}_2} & K_{\dot{\kappa}_1\dot{\kappa}_2} & 2K_{\dot{\kappa}_2\dot{\kappa}_2} & K_{\dot{\kappa}_2\dot{\kappa}_3} \\ K_{\dot{d}_1\dot{\kappa}_3} & K_{\dot{d}_2\dot{\kappa}_3} & K_{\dot{d}_3\dot{\kappa}_3} & K_{\dot{\kappa}_1\dot{\kappa}_3} & K_{\dot{\kappa}_2\dot{\kappa}_3} & 2K_{\dot{\kappa}_3\dot{\kappa}_3} \end{bmatrix} \tag{4.48}$$

$$V \triangleq \begin{bmatrix} V_{11} & V_{12} & V_{13} & V_{14} & V_{15} & V_{16} \\ V_{21} & V_{22} & V_{23} & V_{24} & V_{25} & V_{26} \\ V_{31} & V_{32} & V_{33} & V_{34} & V_{35} & V_{36} \\ V_{41} & V_{42} & V_{43} & V_{44} & V_{45} & V_{46} \\ V_{51} & V_{52} & V_{53} & V_{54} & V_{55} & V_{56} \\ V_{61} & V_{62} & V_{63} & V_{64} & V_{65} & V_{66} \end{bmatrix} \tag{4.49}$$

$$G = \begin{bmatrix} G_1 & G_2 & G_3 & G_4 & G_5 & G_6 \end{bmatrix}^T, \tag{4.50}$$

$$B = \begin{bmatrix} B_1 & B_2 & B_3 & B_4 & B_5 & B_6 \end{bmatrix}^T, \tag{4.51}$$

$$E = \begin{bmatrix} E_1 & E_2 & E_3 & E_4 & E_5 & E_6 \end{bmatrix}^T. \tag{4.52}$$

where their individual entries are provided in Appendices M, N, and O.

Numerical Results

To underline the validity of the proposed dynamic model, two numerical simulations are performed. The model is implemented in Matlab 7.0.

First Simulation Run

In the first simulation run, to illustrate the similarities to the physical system, the system is fed with $\tau_6(t)$ being a sinusoid with an amplitude of 10^{-4} [Nm] and a

period of 10 [sec] where the other entries of the control input $\tau(t)$ set to zero. The spring constants are chosen as

$$k_{bi} = 0.001, k_{ei} = 10, \forall i = 1, 2, 3. \tag{4.53}$$

The section lengths and the curvatures are presented in Figures 4.3 and 4.4 respectively. While the changes in the section lengths are negligible (i.e., less than 5mm for each section), the effects observed on the curvatures are decreasing from κ_3, κ_2, κ_1 as expected from a real physical system.

Second Simulation Run

In the second simulation run, a straightforward control scheme for robot manipulators, namely a computed-torque controller is implemented. The tracking error signal $e(t) \in \mathbb{R}^6$ is defined as follows

$$e \triangleq q_d - q \tag{4.54}$$

where $q_d(t) \in \mathbb{R}^6$ is the desired joint positions. The dynamic model presented in (4.46) is rewritten as follows

$$M(q)\ddot{q} + N(q, \dot{q}) = \tau(t) \tag{4.55}$$

where $N(q, \dot{q}) \in \mathbb{R}^6$ represents the other dynamic effects on the left-hand-side of (4.46). The control input $\tau(t)$ is designed as follows [15]

$$\tau \triangleq M(\ddot{q}_d + K_v\dot{e} + K_p e) + N \tag{4.56}$$

where K_v, $K_p \in \mathbb{R}^{6\times6}$ are constant control gain matrices. Since it is not in the scope of this chapter, the stability analysis for the suggested controller is omitted and the reader is referred to Section 4.4 of [15] for a more detailed analysis.

To show the tracking performance of the proposed dynamic model $q_d(t)$ is selected as follows

$$q_d = \begin{bmatrix} 0.35 + 0.01\sin(2\pi t) \\ 0.35 \\ 0.40 + 0.01\sin(2\pi t) \\ 1 + 0.2\sin(2\pi t) \\ 2 + 0.2\sin(2\pi t) \\ 3 \end{bmatrix}. \tag{4.57}$$

The control gains are chosen as follows

$$K_v = I_6, K_p = 100 I_6 \tag{4.58}$$

where $I_6 \in \mathbb{R}^{6\times 6}$ is the standard identity matrix. The spring constants defined in (4.53) are utilized. In Figures 4.5 and 4.6, the section lengths and the curvatures are presented. In Figures 4.7 and 4.8, the tracking error signals for the section lengths and the curvatures are presented, respectively. From Figures 4.7 and 4.8, it is clear that the tracking error signals are driven to zero. The control inputs are presented in Figures 4.9 and 4.10.

Conclusions

A novel dynamic model for planar extensible continuum robot manipulators was derived. First, the kinetic energy of a slice of the continuum robot was evaluated. Then, the total kinetic energy of the manipulator was obtained by utilizing a limit operation (i.e., sum of the kinetic energy of all the slices). Next, the total potential energy of the robot manipulator was considered. First, the gravitational potential energy was calculated. Then, the elastic potential energy terms due to bending and extension effects were derived. Finally, by utilizing the Lagrangian representation, the effects of the total kinetic and potential energy were utilized to derive the dynamic model. Numerical simulation results were presented for a planar 3-section extensible continuum robot manipulator. The results show good consistency with the behavior of continuum robot hardware, and good potential for use in controller implementation.

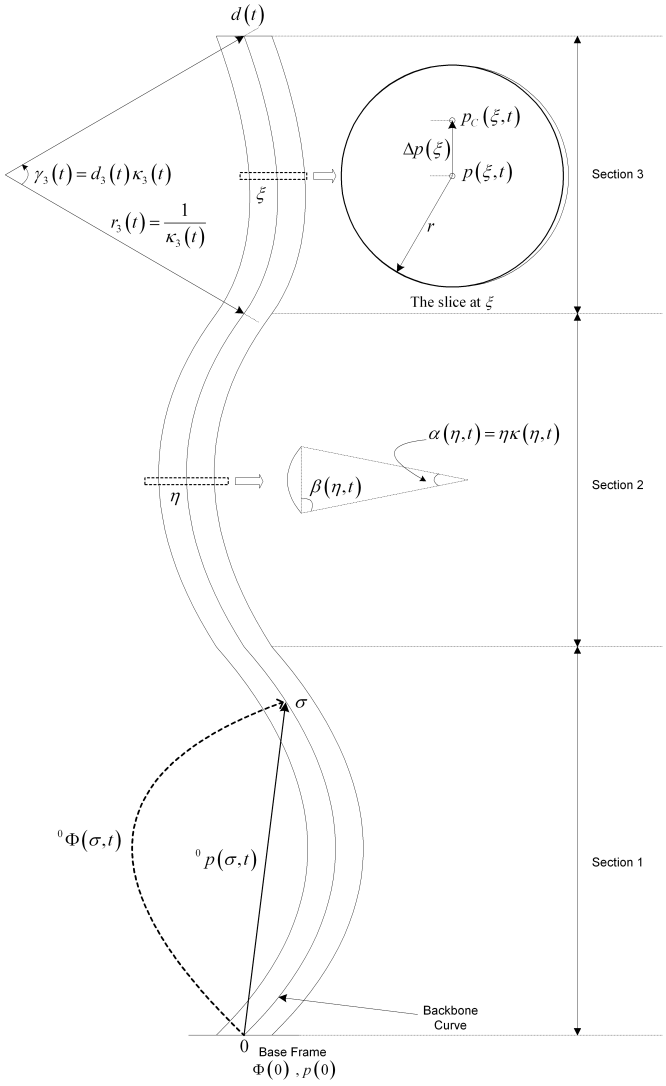

Figure 4.2 Geometry of a 3-Section Extensible Robot Manipulator

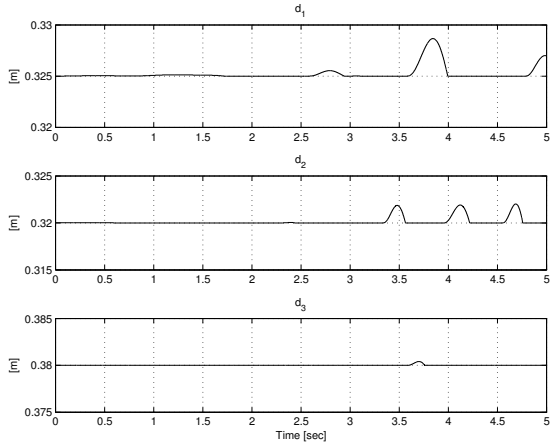

Figure 4.3 The section lengths (first simulation)

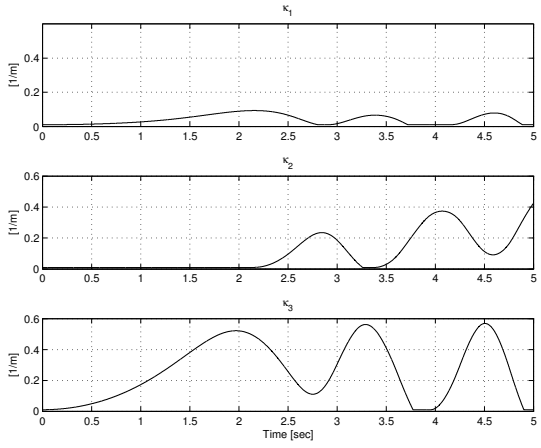

Figure 4.4 The curvatures (first simulation)

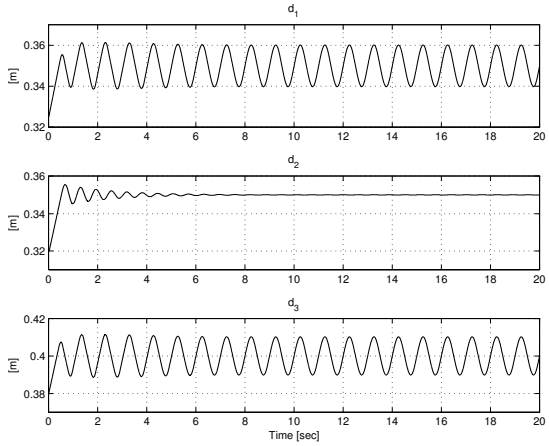

Figure 4.5 The section lengths (second simulation)

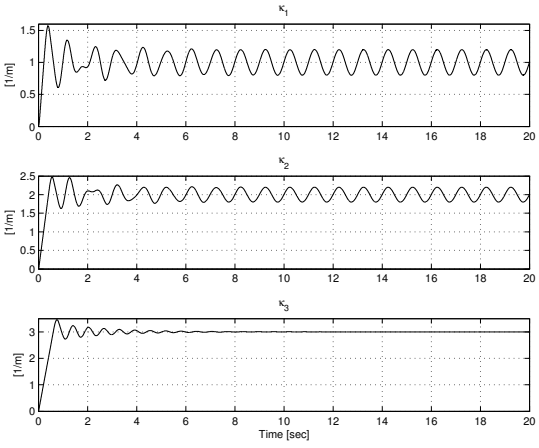

Figure 4.6 The curvatures (second simulation)

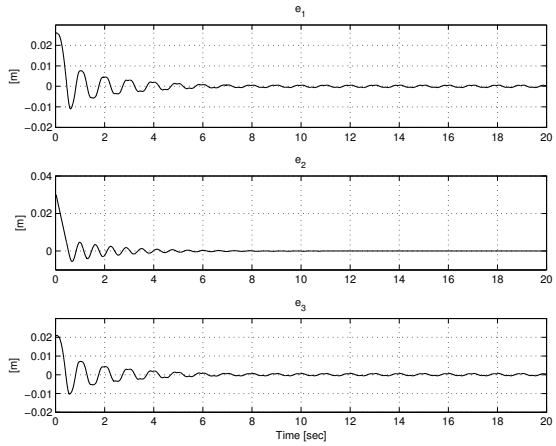

Figure 4.7 The tracking error for the section lengths (second simulation)

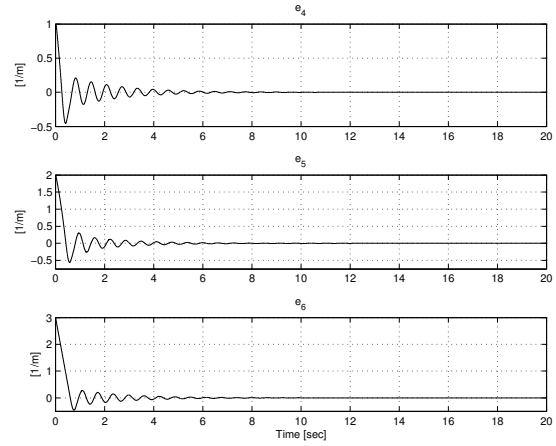

Figure 4.8 The tracking error for the curvatures (second simulation)

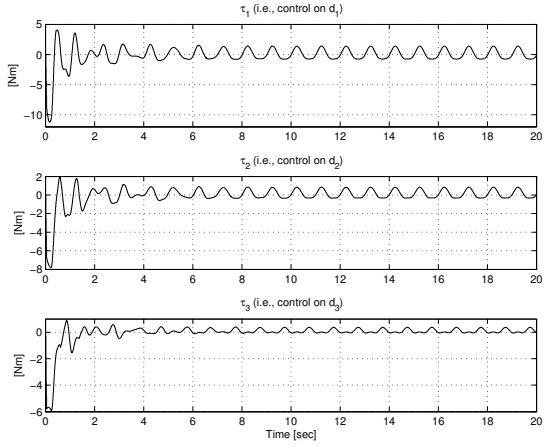

Figure 4.9 The control inputs for section lengths (i.e., $\tau_1(t)$, $\tau_2(t)$, and $\tau_3(t)$ (second simulation))

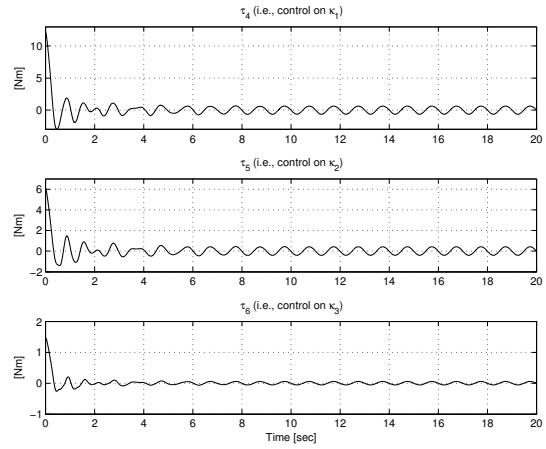

Figure 4.10 The control inputs for curvatures (i.e., $\tau_4(t)$, $\tau_5(t)$, and $\tau_6(t)$ (second simulation))

CHAPTER 5
CONCLUSIONS

This dissertation presents contributions to two research areas: Control of nonlinear systems with applications in robotics and Dynamic modeling for extensible continuum robot manipulators.

In Chapter 1, an adaptive task-space controller for kinematically redundant robot manipulators was designed to encode optional sub-task objectives to make use of the redundancy resolution. This work utilized the adaptive full-state feedback quaternion based controller developed in [1] and focused on the design of a general sub-task controller. This general sub-task controller was developed as to not affect the tracking control objective, and allows for the design of specific sub-task objectives. Four specific sub-tasks were designed as follows: singularity avoidance, joint-limit avoidance, bounding the impact forces, and bounding the potential energy.

In Chapter 2, the human-robot interaction problem was addressed. Two controllers were developed for nonlinear haptic and teleoperator systems that target coordination of the master and slave. The first controller was proven to yield a semi-global asymptotic result in the presence of parametric uncertainty in the master and slave dynamic models provided the user and environmental input forces are measurable. The second controller was proven to yield a global asymptotic result despite unmeasurable user and environmental input forces provided the dynamic models of the master and slave are known. A transformation along with an adjustable target system were utilized that allows the master system's impedance to be adjusted so that matches a desired target system operating in a remote physical/virtual environment. This work also presented an optional strategy to encode a velocity field assist mechanism that provides the user of the system help in controlling the slave system in completing a pre-defined contour following task. For each controller, Lyapunov-based techniques were used to prove the control development implements a stable coordinated teleoperator/haptic system with a user assist mechanism. When the

optional velocity field assist mechanism is disabled, the analysis proved the control development implements a stable passively coordinated teleoperator/haptic system. As an extension of the developments in Chapters 1 and 2, future work will focus on teleoperation with kinematically redundant robot manipulators.

In Chapter 3, the control problem of a class of multi-input multi-output nonlinear systems was addressed. Two controllers were developed for flat MIMO nonlinear systems in the presence of additive disturbances. The robust adaptive controller was proven to yield a semi-global asymptotic tracking result in the presence of parametric uncertainty along with additive disturbances. The adaptive controller and the adaptation law were designed such that, the parameter estimate vector is proven to go to a constant vector. In the second part of the chapter, the learning controller was proven to yield a semi-global asymptotic result in the presence of additive disturbances and when the desired trajectory is periodic. In the development of both controllers, the bounded additive disturbances were assumed to be twice continuously differentiable and have bounded time derivatives up to second order. Since no assumptions were made regarding the periodicity of the disturbances, it is clear that the suggested controllers compensated for both repeating and nonrepeating disturbances. For each controller, Lyapunov-based techniques were used to guarantee that the tracking error is asymptotically driven to zero.

In Chapter 4, a novel dynamic model for planar extensible continuum robot manipulators was derived. First, the kinetic energy of a slice of the continuum robot was evaluated. Then, the total kinetic energy of the manipulator was obtained by utilizing a limit operation (i.e., sum of the kinetic energy of all the slices). Next, the total potential energy of the robot manipulator is considered. First, the gravitational potential energy is calculated. Then, the elastic potential energy terms due to bending and extension effects were derived. Finally, by utilizing the Lagrangian representation, the effects of the total kinetic and potential energy were utilized to derive the dynamic model. Numerical simulation results are presented for a planar

3-section extensible continuum robot manipulator. The results show good consistency with the behavior of continuum robot hardware, and good potential for use in controller implementation. Future work will focus on deriving a three-dimensional dynamic model for extensible continuum robot manipulators.

APPENDICES

Appendix A

Proof of Theorem 2

Let $V_3(t) \in \mathbb{R}$ denotes the following non-negative function

$$V_3 \triangleq \frac{1}{2} y_a^2. \tag{A.1}$$

After taking the time derivative of (A.1), the following simplified expression can be obtained

$$\begin{aligned} \dot{V}_3 &= -k_{s1} \left\| J_s \left(I_n - J^+ J \right) \right\|^2 y_a^2 \\ &\quad + y_a \left[J_s J^+ \Lambda^{-1} \begin{bmatrix} \dot{p}_d + K_1 e_p \\ -R_d^T \omega_d + K_2 e_v \end{bmatrix} - J_s r \right] \end{aligned} \tag{A.2}$$

where (1.44) was utilized. From (1.39), (1.41), (1.56), and the fact that $p(t) \in \mathcal{L}_\infty$ from Theorem 1, Remark 2 can be used to show that $\theta(t) \in \mathcal{L}_\infty$; hence, it is clear that $J_s(\theta) \in \mathcal{L}_\infty$ for all sub-tasks. From Remark 1, it is clear that $J(\theta)$ and $J^+(\theta) \in \mathcal{L}_\infty$ and has full rank. Utilizing these properties we have

$$\left\| J_s \left(I_n - J^+ J \right) \right\|^2 > \bar{\delta} \tag{A.3}$$

where $\bar{\delta} \in \mathbb{R}$ is a positive constant. From the above boundedness statements, and the boundedness assumptions placed on the desired trajectory, the following upper bound can be made

$$\left\| J_s J^+ \Lambda^{-1} \begin{bmatrix} \dot{p}_d + K_1 e_p \\ -R_d^T \omega_d + K_2 e_v \end{bmatrix} - J_s r \right\| \leq \delta_1 \tag{A.4}$$

where $\delta_1 \in \mathbb{R}$ is a positive constant. After applying the bounds defined in (A.3) and (A.4), the expression in (A.2) can be written as follows

$$\dot{V}_3 \leq -k_{s1} \bar{\delta} y_a^2 + \delta_1 y_a. \tag{A.5}$$

The expression in (A.5) can be written as follows

$$\dot{V}_3 \leq -\left(k_{s1} \bar{\delta} - \frac{1}{\delta_2} \right) y_a^2 + \delta_1^2 \delta_2 \tag{A.6}$$

where the following inequality was utilized

$$|\delta_1 y_a| \leq \frac{1}{\delta_2} y_a^2 + \delta_1^2 \delta_2 \tag{A.7}$$

where $\delta_2 \in \mathbb{R}$ is a positive constant. Provided k_{s1}, $\bar{\delta}$, and δ_2 are selected according the following condition

$$\left(k_{s1} \bar{\delta} - \frac{1}{\delta_2} \right) > 0 \text{ then } k_{s1} > \frac{1}{\bar{\delta} \delta_2}, \tag{A.8}$$

the expression in (A.6) can be written as follows

$$\dot{V}_3 \leq -\gamma y_a^2 + \varepsilon \tag{A.9}$$

where $\gamma, \varepsilon \in \mathbb{R}^+$ are bounding constants. After substituting (A.1) into (A.9), the following expression can be written

$$\dot{V}_3 \leq -2\gamma V_3 + \varepsilon. \tag{A.10}$$

After integrating each side of (A.10), the following solution can be written

$$V_3(t) \leq V_3(t_0) \exp(-2\gamma t) + \frac{\varepsilon}{2\gamma} \left(1 - \exp(-2\gamma t) \right). \tag{A.11}$$

From (A.11), it is clear that the following upper bound for $y_a(t)$ can be written

$$|y_a(t)| \leq \sqrt{|y_a^2(t_0)| \exp(-2\gamma t) + \frac{\varepsilon}{\gamma}} \tag{A.12}$$

thus proving that $y_a(t) \in \mathcal{L}_\infty$. From (1.43), it is clear that $h(\theta) \in \mathcal{L}_\infty$. Utilizing the previous bounding statements with (1.44) it is clear that $\dot{y}_a(t) \in \mathcal{L}_\infty$. After taking the time derivative of (1.43), it is clear that $\frac{\partial h(\theta)}{\partial \theta} \in \mathcal{L}_\infty$.

Appendix B

MIF Desired Trajectory Stability Analysis

To prove that $\xi_d(t)$, $\lambda_d(t)$, $\eta_d(t)$, $\dot{\eta}_d(t) \in \mathcal{L}_\infty$, let $V(t) \in \mathbb{R}$ denote the following function

$$V \triangleq V_1 + V_2 \tag{B.1}$$

where $V_1(t) \in \mathbb{R}$ denotes the following non-negative function

$$V_1 \triangleq \frac{1}{2}\eta_d^T M_T \eta_d + \frac{1}{2}\lambda_d^T K_T \lambda_d \tag{B.2}$$

where $\lambda_d(t)$, $\eta_d(t)$, M_T and K_T were introduced in (2.21). The expression given in (B.2) can be lower bounded by the auxiliary function, $V_2(\bar{x}) \in \mathbb{R}$, which is defined as follows

$$V_2 \triangleq 2\varepsilon \eta_d^T M_T \lambda_d \leq V_1 \tag{B.3}$$

where $\bar{x}(t) \in \mathbb{R}^{2n}$ is defined as follows

$$\bar{x} \triangleq \left[\begin{array}{cc} \lambda_d^T & \eta_d^T \end{array} \right]^T \tag{B.4}$$

and $\varepsilon \in \mathbb{R}$ is a positive bounding constant selected according to the following inequality

$$\varepsilon < \frac{\min\left\{\lambda_{\min}\{M_T\}, \lambda_{\min}\{K_T\}\right\}}{4\lambda_{\max}\{M_T\}} \tag{B.5}$$

where $\lambda_{\min}\{\cdot\}$ and $\lambda_{\max}\{\cdot\}$ denote the minimum and maximum eigenvalue of a matrix, respectively. From (B.3) it is clear that $V(t)$ is a non-negative function and bounded by the following inequalities

$$\bar{\lambda}_1 \left\|\bar{x}\right\|^2 \leq V(\bar{x}) \leq \bar{\lambda}_2 \left\|\bar{x}\right\|^2 \tag{B.6}$$

where $\bar{\lambda}_1$, $\bar{\lambda}_2 \in \mathbb{R}$ are positive bounding constants defined as follows, provided that ε is selected according to (B.5)

$$\begin{aligned} \bar{\lambda}_1 &\triangleq \frac{1}{2}\min\left\{\lambda_{\min}\{M_T\}, \lambda_{\min}\{K_T\}\right\} - 2\varepsilon\lambda_{\max}\{M_T\} \\ \bar{\lambda}_2 &\triangleq \frac{1}{2}\max\left\{\lambda_{\max}\{M_T\}, \lambda_{\max}\{K_T\}\right\} + 2\varepsilon\lambda_{\max}\{M_T\}. \end{aligned} \tag{B.7}$$

To facilitate the subsequent analysis, the time derivative of (B.1) can be determined as follows

$$\dot{V} = \eta_d^T M_T \dot{\eta}_d + \lambda_d^T K_T \dot{\lambda}_d + 2\varepsilon \dot{\eta}_d^T M_T \lambda_d + 2\varepsilon \eta_d^T M_T \dot{\lambda}_d. \tag{B.8}$$

After utilizing (2.21) and the fact that $\eta_d(t) = \dot{\lambda}_d(t)$, the expression in (B.8) can be written as

$$\dot{V} = \eta_d^T F - \eta_d^T B_T \eta_d + 2\varepsilon \lambda_d^T F - 2\varepsilon \lambda_d^T B_T \eta_d - 2\varepsilon \lambda_d^T K_T \lambda_d + 2\varepsilon \eta_d^T M_T \eta_d. \tag{B.9}$$

The right-hand side of (B.9) can be upper bounded as follows

$$\begin{aligned} \dot{V} \leq & \frac{1}{\delta_1} \|\eta_d\|^2 + \delta_1 \|F\|^2 - \lambda_{\min}\{B_T\} \|\eta_d\|^2 + 2\varepsilon \left[\delta_2 \|\lambda_d\|^2 + \frac{1}{\delta_2} \|F\|^2 \right] \\ & + 2\varepsilon \lambda_{\max}\{B_T\} \left[\delta_3 \|\lambda_d\|^2 + \frac{1}{\delta_3} \|\eta_d\|^2 \right] \\ & - 2\varepsilon \lambda_{\min}\{K_T\} \|\lambda_d\|^2 + 2\varepsilon \lambda_{\max}\{M_T\} \|\eta_d\|^2 \end{aligned} \tag{B.10}$$

where the following properties were utilized

$$\begin{aligned} \eta_d^T F &\leq \frac{1}{\delta_1} \|\eta_d\|^2 + \delta_1 \|F\|^2 \\ -\eta_d^T B_T \eta_d &\leq -\lambda_{\min}\{B_T\} \|\eta_d\|^2 \\ \lambda_d^T F &\leq \delta_2 \|\lambda_d\|^2 + \frac{1}{\delta_2} \|F\|^2 \\ -\lambda_d^T B_T \eta_d &\leq \lambda_{\max}\{B_T\} \left[\delta_3 \|\lambda_d\|^2 + \frac{1}{\delta_3} \|\eta_d\|^2 \right] \\ -\lambda_d^T K_T \lambda_d &\leq -\lambda_{\min}\{K_T\} \|\lambda_d\|^2 \\ \eta_d^T M_T \eta_d &\leq \lambda_{\max}\{M_T\} \|\eta_d\|^2 \end{aligned}$$

where $\delta_1, \delta_2, \delta_3 \in \mathbb{R}$ are positive bounding constants.

The expression in (B.10) can be rearranged as follows

$$\begin{aligned} \dot{V} \leq & -\left(\lambda_{\min}\{B_T\} - \frac{1}{\delta_1} - \frac{2\varepsilon \lambda_{\max}\{B_T\}}{\delta_3} - 2\varepsilon \lambda_{\max}\{M_T\} \right) \|\eta_d\|^2 \\ & - 2\varepsilon \left(\lambda_{\min}\{K_T\} - \delta_3 \lambda_{\max}\{B_T\} - \delta_2 \right) \|\lambda_d\|^2 + \left(\delta_1 + \frac{2\varepsilon}{\delta_2} \right) \|F\|^2. \end{aligned} \tag{B.11}$$

Provided that ε is selected to satisfy (B.5) and δ_1, δ_2, δ_3, M_T, B_T, K_T are selected to satisfy the following sufficient conditions

$$\lambda_{\min}\{B_T\} > \frac{1}{\delta_1} + \frac{2\varepsilon\lambda_{\max}\{B_T\}}{\delta_3} + 2\varepsilon\lambda_{\max}\{M_T\} \tag{B.12}$$

$$\lambda_{\min}\{K_T\} > \delta_3\lambda_{\max}\{B_T\} + \delta_2 \tag{B.13}$$

along with the Assumption 1, then the right-hand side of (B.11) can be upper bounded as follows

$$\dot{V} \leq -\frac{\min\{\gamma_a, \gamma_b\}}{\bar{\lambda}_2} V + \epsilon \tag{B.14}$$

where (B.4) and (B.6) were utilized, and γ_a, γ_b, $\epsilon \in \mathbb{R}$ denote positive bounding constants.

From (B.1) - (B.3), and (B.6), and the fact that $\mathrm{F}(t) \in \mathcal{L}_\infty$, the expression in (B.14) can be used with the result from [105] to prove that $\bar{x}(t)$, $\lambda_d(t)$, $\eta_d(t) \in \mathcal{L}_\infty$. By utilizing the fact that $\eta_d(t) \in \mathcal{L}_\infty$ along with (2.20) and Remark 2, it is clear that $\xi_d(t)$, $\dot{\xi}_d(t)$, $\varphi\left(\xi_p(t)\right) \in \mathcal{L}_\infty$. Based on (2.21), and the fact that $F(t) \in \mathcal{L}_\infty$ then $\dot{\eta}_d(t) \in \mathcal{L}_\infty$. After utilizing the above boundedness statements along with Remark 2 and the first time derivative of (2.20), it is clear that $\ddot{\xi}_d(t) \in \mathcal{L}_\infty$. The time derivative of (2.21) can be written as follows

$$M_T\ddot{\eta}_d + B_T\dot{\eta}_d + K_T\eta_d = \dot{F} \tag{B.15}$$

where the fact $\eta_d(t) = \dot{\lambda}_d(t)$ was utilized. After utilizing the fact that $\eta_d(t)$, $\dot{\eta}_d(t) \in \mathcal{L}_\infty$, and the assumption that $\dot{F}_H(t)$, $\dot{F}_E(t) \in \mathcal{L}_\infty$ along with (B.15), it is clear that $\ddot{\eta}_d(t) \in \mathcal{L}_\infty$. The second time derivative of (2.20) can be written as follows

$$\dddot{\xi}_d \triangleq \gamma\frac{d^2}{dt^2}\left(\begin{bmatrix} \varphi^T\left(\xi_p\right) & 0_r^T \end{bmatrix}^T\right) + \dddot{\eta}_d. \tag{B.16}$$

After utilizing the above boundedness statements and Remark 2 along with (B.16), then $\dddot{\xi}_d(t) \in \mathcal{L}_\infty$. The time derivative of (B.15) can be written as follows

$$M_T\dddot{\eta}_d + B_T\ddot{\eta}_d + K_T\dot{\eta}_d = \ddot{F} \tag{B.17}$$

After utilizing the fact that $\dot{\eta}_d(t)$, $\ddot{\eta}_d(t) \in \mathcal{L}_\infty$ and the assumption that $\dddot{F}_H(t)$, $\dddot{F}_E(t) \in \mathcal{L}_\infty$, from (B.17) it can be showed that $\dddot{\eta}_d(t) \in \mathcal{L}_\infty$. After taking time derivative of (B.16) and utilizing the facts that $\xi_d(t)$, $\dot{\xi}_d(t)$, $\ddot{\xi}_d(t)$, $\dddot{\xi}_d(t)$, $\dddot{\eta}_d(t) \in \mathcal{L}_\infty$, then it is clear that $\ddddot{\xi}_d(t) \in \mathcal{L}_\infty$. By utilizing the above boundedness statements along with (2.19), it is clear that $x_d(t)$, $\dot{x}_d(t)$, $\ddot{x}_d(t)$, $\dddot{x}_d(t)$, and $\ddddot{x}_d(t) \in \mathcal{L}_\infty$.

Appendix C

Proof of Theorem 3

Lemma 1 *Let the auxiliary functions* $L_1(t)$, $L_2(t) \in \mathbb{R}$ *be defined as follows*

$$L_1 \triangleq r^T \left(N_d - \beta_1 sgn\left(e_2\right) \right) \quad , \quad L_2 \triangleq -\beta_2 \dot{e}_2^T sgn\left(e_2\right) \tag{C.1}$$

where β_1 *and* β_2 *were introduced in (2.34). Provided that* β_1 *is selected to satisfy the following sufficient condition*

$$\beta_1 > \varsigma_1 + \frac{1}{\alpha_1}\varsigma_2 \tag{C.2}$$

where ς_1 *and* ς_2 *were introduced in (2.33), and* α_1 *was introduced in (2.15), then*

$$\int_{t_0}^{t} L_1(\tau)\, d\tau \leq \xi_{b1} \quad , \quad \int_{t_0}^{t} L_2(\tau)\, d\tau \leq \xi_{b2} \tag{C.3}$$

where ξ_{b1}, $\xi_{b2} \in \mathbb{R}$ *are positive constants defined as*

$$\xi_{b1} \triangleq \beta_1 \sum_{i=1}^{2n} \left| e_{2i}(t_0) \right| - e_2^T(t_0) N_d(t_0), \xi_{b2} \triangleq \beta_2 \sum_{i=1}^{2n} \left| e_{2i}(t_0) \right|. \tag{C.4}$$

Proof. After substituting (2.15) into $L_1(t)$ defined in (C.1) and then integrating in time, results in the following expression

$$\begin{aligned} \int_{t_0}^{t} L_1(\tau)\, d\tau &= \alpha_1 \int_{t_0}^{t} e_2^T(\tau) \left[N_d(\tau) - \beta_1 sgn\left(e_2(\tau)\right) \right] d\tau \\ &\quad + \int_{t_0}^{t} \frac{de_2^T(\tau)}{d\tau} N_d(\tau)\, d\tau - \beta_1 \int_{t_0}^{t} \frac{de_2^T(\tau)}{d\tau} sgn\left(e_2(\tau)\right) d\tau. \end{aligned} \tag{C.5}$$

After integrating the second integral on the right side of (C.5) by parts and evaluating the last integral, the following expression is obtained

$$\begin{aligned} \int_{t_0}^{t} L_1(\tau)\, d\tau &= \alpha_1 \int_{t_0}^{t} e_2^T \left(N_d - \frac{1}{\alpha_1} \frac{dN_d}{d\tau} - \beta_1 sgn\left(e_2\right) \right) d\tau \\ &\quad + e_2^T(t) N_d(t) - \beta_1 \sum_{i=1}^{2n} \left| e_{2i}(t) \right| + \xi_{b1}. \end{aligned} \tag{C.6}$$

The right-hand side of (C.6) can be upper bounded as follows

$$\begin{aligned}\int_{t_0}^{t} L_1(\tau)\, d\tau &\leqslant \alpha_1 \int_{t_0}^{t} \sum_{i=1}^{2n} |e_{2i}(\tau)| \left(|N_{d_i}(\tau)| + \frac{1}{\alpha_1} \left| \frac{dN_{d_i}(\tau)}{d\tau} \right| - \beta_1 \right) d\tau \\ &\quad + \sum_{i=1}^{2n} |e_{2i}(t)| \left(|N_{d_i}(t)| - \beta_1 \right) + \xi_{b1}. \end{aligned} \tag{C.7}$$

If β_1 is chosen according to (2.39), then the first inequality in (C.3) can be proven from (C.7). The second inequality in (C.3) can be obtained by integrating the expression for $L_2(t)$ defined in (C.1) as follows

$$\begin{aligned}\int_{t_0}^{t} L_2(\tau)\, d\sigma &= -\beta_2 \int_{t_0}^{t} \dot{e}_2^T(\tau)\, sgn(e_2(\tau))\, d\tau \\ &= \xi_{b2} - \beta_2 \sum_{i=1}^{2n} |e_{2i}(t)| \leq \xi_{b2}. \end{aligned} \tag{C.8}$$

The following is the proof of Theorem 3.

Proof. Let the auxiliary functions $P_1(t)$, $P_2(t) \in \mathbb{R}$ be defined as follows

$$P_1 \triangleq \xi_{b1} - \int_{t_0}^{t} L_1(\tau)\, d\tau \geq 0 \tag{C.9}$$

$$P_2 \triangleq \xi_{b2} - \int_{t_0}^{t} L_2(\tau)\, d\tau \geq 0 \tag{C.10}$$

where $L_1(t)$, $L_2(t)$, ξ_{b1} and ξ_{b2} were defined in Lemma 1. The proof of Lemma 1 ensures that $P_1(t)$ and $P_2(t)$ are non-negative. Let $V(y,t) \in \mathbb{R}$ denote the following non-negative function

$$V \triangleq \frac{1}{2} e_1^T e_1 + \frac{1}{2} e_2^T e_2 + \frac{1}{2} r^T \bar{M} r + P_1 + P_2 \tag{C.11}$$

where $y(t) \in \mathbb{R}^{6n+2}$ is defined as follows

$$y \triangleq \begin{bmatrix} z^T & \sqrt{P_1} & \sqrt{P_2} \end{bmatrix}^T \tag{C.12}$$

where $z(t) \in \mathbb{R}^{6n}$ is defined as follows

$$z \triangleq \begin{bmatrix} e_1^T & e_2^T & r^T \end{bmatrix}^T. \tag{C.13}$$

Because $\bar{M}(x)$ is assumed to be bounded as defined in (2.14), (C.11) is bounded as follows

$$W_1(y) \leq V(y,t) \leq W_2(y) \tag{C.14}$$

where $W_1(y)$, $W_2(y) \in \mathbb{R}$ are defined as

$$W_1(y) \triangleq \lambda_1 \|y(t)\|^2 \quad W_2(y) \triangleq \lambda_2 \|y(t)\|^2 \tag{C.15}$$

where $\lambda_1 \triangleq \frac{1}{2}\min\{1, \bar{m}_1\}$ and $\lambda_2 \triangleq \max\left\{1, \frac{1}{2}\bar{m}_2\right\}$.

After differentiating (C.11) in time, the following expression can be obtained

$$\begin{aligned} \dot{V} &= -\alpha_2 e_1^T e_1 - \alpha_1 e_2^T e_2 - r^T (k_s + 1) r \\ &\quad + e_1^T e_2 + r^T \tilde{N} - r^T \beta_2 sgn(e_2) + \beta_2 \dot{e}_2^T sgn(e_2) \end{aligned} \tag{C.16}$$

where (2.15), (2.16), (2.36), (C.9), and (C.10) were utilized. To facilitate the subsequent analysis, the following inequality can be developed from (2.30) - (2.32) (see Appendix I)

$$\left\| \tilde{N}(\cdot) \right\| \leq \rho(\|z\|)\|z\| \tag{C.17}$$

where $\rho(\cdot)$ is a positive, invertible bounding function that is non-decreasing in $\|z\|$. By utilizing (2.15), (C.17), and the triangle inequality, $\dot{V}(t)$ can be upper bounded as follows

$$\begin{aligned} \dot{V} &\leq -\alpha_2 e_1^T e_1 - \alpha_1 e_2^T e_2 - r^T (k_s + 1) r \\ &\quad + e_1^T e_1 + e_2^T e_2 + \rho(\|z\|)\|r\|\|z\| - \alpha_1 e_2^T \beta_2 sgn(e_2). \end{aligned} \tag{C.18}$$

After utilizing (C.13), the right-hand side of (C.18) can be rearranged as follows

$$\dot{V} \leq -\lambda_3 \|z\|^2 + \left[\rho(\|z\|)\|r\|\|z\| - k_s \|r\|^2\right] - \alpha_1 \beta_2 \sum_{i=1}^{2n} |e_{2i}| \tag{C.19}$$

where $\lambda_3 \triangleq \min\{\alpha_1 - 1,\ \alpha_2 - 1, 1\}$. Completing the squares on the bracketed term in (C.19), yields the following expression

$$\dot{V} \leq -\left(\lambda_3 - \frac{\rho^2(\|z\|)}{4k_s}\right)\|z\|^2 - \alpha_1 \beta_2 \sum_{i=1}^{2n} |e_{2i}|. \tag{C.20}$$

Provided α_1 and α_2 are selected to be greater than 2 and k_s is selected according to the following sufficient condition

$$k_s \geq \frac{\rho^2(\|z\|)}{4\lambda_3} \text{ or } \|z\| \leq \rho^{-1}\left(2\sqrt{k_s\lambda_3}\right) \tag{C.21}$$

then based on (C.20) the following inequality can be developed

$$\dot{V} \leq W(y) - \alpha_1\beta_2 \sum_{i=1}^{2n} |e_{2i}| \tag{C.22}$$

where $W(y) \in \mathbb{R}$ denotes the following non-positive function

$$W(y) \triangleq -\beta_0 \|z\|^2 \tag{C.23}$$

where $\beta_0 \in \mathbb{R}$ is a positive constant. From (C.11)-(C.15) and (C.20)-(C.23) the regions D and S can be defined as follows

$$\mathcal{D} \triangleq \left\{ y \in \mathbb{R}^{6n+2} \mid \|y\| < \rho^{-1}\left(2\sqrt{k_s\lambda_3}\right) \right\} \tag{C.24}$$

$$\mathcal{S} \triangleq \left\{ y \in \mathcal{D} \mid W_2(y) < \lambda_1 \left(\rho^{-1}\left(2\sqrt{k_s\lambda_3}\right)\right)^2 \right\}. \tag{C.25}$$

Note that the region of attraction in (C.25) can be made arbitrarily large to include any initial conditions by increasing the control gain k_s (i.e., a semi-global stability result). Specifically, (C.15) and (C.25) can be used to calculate the region of attraction as follows

$$\begin{aligned} W_2(y(t_0)) &< \lambda_1 \left(\rho^{-1}\left(2\sqrt{k_s\lambda_3}\right)\right)^2 \\ &\implies \|y(t_0)\| < \sqrt{\frac{\lambda_1}{\lambda_2}}\rho^{-1}\left(2\sqrt{k_s\lambda_3}\right), \end{aligned} \tag{C.26}$$

which can be rearranged as

$$k_s \geq \frac{1}{4\lambda_3}\rho^2\left(\sqrt{\frac{\lambda_2}{\lambda_1}}\|y(t_0)\|\right). \tag{C.27}$$

By utilizing (C.4), (C.12) and (C.13) the following explicit expression for $\|y(t_0)\|$ can be derived as follows

$$\|y(t_0)\|^2 = \|e_1(t_0)\|^2 + \|e_2(t_0)\|^2 + \|r(t_0)\|^2 + \xi_{b1} + \xi_{b2}. \tag{C.28}$$

From (C.11), (C.22), (C.25)-(C.27), it is clear that $V(y,t) \in \mathcal{L}_\infty \; \forall y(t_0) \in \mathcal{S}$; hence $e_1(t)$, $e_2(t)$, $r(t)$, $z(t)$, $y(t) \in \mathcal{L}_\infty \; \forall y(t_0) \in \mathcal{S}$. From (C.22), it is easy to show that $e_2(t) \in \mathcal{L}_1 \; \forall y(t_0) \in \mathcal{S}$. The fact that $e_2(t) \in \mathcal{L}_1 \; \forall y(t_0) \in \mathcal{S}$ can be used along with (2.16) to determine that $e_1(t), \dot{e}_1(t) \in \mathcal{L}_1 \; \forall y(t_0) \in \mathcal{S}$. From (2.7), (2.17) and the fact that $x_d(t) \in \mathcal{L}_\infty$, it is clear that $x(t)$, $x_m(t)$, $x_s(t) \in \mathcal{L}_\infty \; \forall y(t_0) \in \mathcal{S}$. From (2.15) and (2.16) it is also clear that $\dot{e}_2(t)$, $\dot{e}_1(t) \in \mathcal{L}_\infty \; \forall y(t_0) \in \mathcal{S}$. Using these boundedness statements, from (2.35) it is clear that $\dot{\bar{u}}(t) \in \mathcal{L}_\infty \; \forall y(t_0) \in \mathcal{S}$. Since $\ddot{e}_1(t) \in \mathcal{L}_\infty$, from the second time derivative of (2.17), and the fact that $\ddot{x}_d(t) \in \mathcal{L}_\infty$ along with (2.27), it is clear that $\bar{u}(t) \in \mathcal{L}_\infty \; \forall y(t_0) \in \mathcal{S}$. The previous boundedness statements can be used along with (2.36), (C.17), and Remark 4 to prove that $\dot{r}(t) \in \mathcal{L}_\infty \; \forall y(t_0) \in \mathcal{S}$. These bounding statements can be used along with the time derivative of (C.23) to prove that $\dot{W}(y(t)) \in \mathcal{L}_\infty \; \forall y(t_0) \in S$; hence, $W(y(t))$ is uniformly continuous. Standard signal chasing arguments can be used to prove that all remaining signals are bounded. A direct application of Theorem 8.4 in [106] can be used to prove that $\|z(t)\| \to 0$ as $t \to \infty \; \forall y(t_0) \in \mathcal{S}$. From (C.13), it is clear that $\|r(t)\| \to 0$ as $t \to \infty \; \forall y(t_0) \in \mathcal{S}$. Based on the definitions given in (2.15) and (2.16), standard linear analysis tools can be used to prove that if $\|r(t)\| \to 0$ then $\|\dot{e}_2(t)\|$, $\|e_2(t)\|$, $\|\dot{e}_1(t)\|$, $\|e_1(t)\| \to 0$ as $t \to \infty \; \forall y(t_0) \in \mathcal{S}$. Based on the definition of $x(t)$ in (2.7) and $e_1(t)$ in (2.17), it is clear that if $\|e_1(t)\| \to 0$ then $x_s(t) \to x_m(t)$ and $x_m(t) \to \xi_d(t)$.

Appendix D

Proof of Theorem 4

Proof. Since the user assist mechanism is disabled (i.e., $\gamma = 0$), the target system defined in (2.20) and (2.21) can be simplified to (2.25). Let $V_p(t) \in \mathbb{R}$ denote the following non-negative function

$$V_p \triangleq \frac{1}{2}\dot{\xi}_d^T M_T \dot{\xi}_d + \frac{1}{2}\xi_d^T K_T \xi_d. \tag{D.1}$$

After differentiating (D.1) in time, the following simplified expression can be obtained

$$\dot{V}_p = \dot{\xi}_d^T F - \dot{\xi}_d^T B_T \dot{\xi}_d \tag{D.2}$$

where (2.25) was utilized. Based on the fact that B_T is a constant positive definite, diagonal matrix, the following inequality can be obtained

$$\dot{V}_p \leq \dot{\xi}_d^T F. \tag{D.3}$$

Integrating both sides of (D.3), results in the following inequality

$$-c_2 \leq V_p(t) - V_p(t_0) \leq \int_{t_0}^{t} \dot{\xi}_d^T(\sigma) F(\sigma) d\sigma \tag{D.4}$$

where $c_2 \in \mathbb{R}$ is a positive bounded constant (since $V_p(t)$ is bounded from the trajectory generation system in (2.25)).

By using the transformation in (2.7), the left-hand side of (2.6) can be expressed as

$$\int_{t_0}^{t} \begin{bmatrix} \dot{x}_m^T(\tau) & \dot{x}_s^T(\tau) \end{bmatrix} \begin{bmatrix} F_H(\tau) \\ F_E(\tau) \end{bmatrix} d\tau = \int_{t_0}^{t} \dot{x}^T \bar{F} d\tau. \tag{D.5}$$

By substituting the time derivative of (2.17) into (D.5), the following expression can be obtained

$$\int_{t_0}^{t} \dot{x}^T(\tau) \bar{F}(\tau) d\tau = \int_{t_0}^{t} \dot{\xi}_d^T(\tau) F(\tau) d\tau - \int_{t_0}^{t} \dot{e}_1^T(\tau) \bar{F}(\tau) d\tau \tag{D.6}$$

where (2.13),(2.19) and (2.22) were utilized. Based on (D.4), it is easy to see that $\int_{t_0}^{t} \dot{\xi}_d^T(\tau) F(\tau) d\tau$ is lower bounded by $-c_2$. The fact that $\dot{e}_1(t) \in \mathcal{L}_1$ (see the proof

for Theorem 3) and the assumption that $\bar{F}(t) \in \mathcal{L}_\infty$ can be used to show that the second integral of (D.6) is bounded. Hence, these facts can be applied to (D.5) and (D.6) to prove that

$$\int_{t_0}^{t} \begin{bmatrix} \dot{x}_m^T(\tau) & \dot{x}_s^T(\tau) \end{bmatrix} \begin{bmatrix} F_H(\tau) \\ F_E(\tau) \end{bmatrix} d\tau \geq -c_3^2 \tag{D.7}$$

where $c_3 \in \mathbb{R}$ is a bounded constant. ■

Appendix E

Proof of Theorem 5

Lemma 2 *Let the auxiliary functions* $L_1(t)$, $L_2(t) \in \mathbb{R}$ *be defined as follows*

$$L_1 \triangleq -r^T\left(\dot{\bar{F}} + \beta_1 sgn(e_2)\right) \quad , \quad L_2 \triangleq -\beta_2 \dot{e}_2^T sgn(e_2) \tag{E.1}$$

where β_1 *and* β_2 *were introduced in (2.67). Provided that* β_1 *is selected to satisfy the following sufficient condition*

$$\beta_1 > \varsigma_3 + \varsigma_4, \tag{E.2}$$

where ς_3 *and* ς_4 *were introduced in (2.70), then*

$$\int_{t_0}^{t} L_1(\tau)\, d\tau \leq \xi_{b1} \quad , \quad \int_{t_0}^{t} L_2(\tau)\, d\tau \leq \xi_{b2} \tag{E.3}$$

where ξ_{b1}, $\xi_{b2} \in \mathbb{R}$ *are positive constants defined as*

$$\xi_{b1} \triangleq \beta_1 \sum_{i=1}^{2n} |e_{2i}(t_0)| - e_2^T(t_0)\left(-\dot{\bar{F}}(t_0)\right), \xi_{b2} \triangleq \beta_2 \sum_{i=1}^{2n} |e_{2i}(t_0)|. \tag{E.4}$$

Proof. After substituting (2.50) into $L_1(t)$ defined in (E.1) and then integrating in time, results in the following expression

$$\begin{aligned} \int_{t_0}^{t} L_1(\tau)\, d\tau &= \int_{t_0}^{t} e_2^T(\tau)\left[-\dot{\bar{F}}(\tau) - \beta_1 sgn(e_2(\tau))\right] d\tau \\ &\quad + \int_{t_0}^{t} \frac{de_2^T(\tau)}{d\tau}\left(-\dot{\bar{F}}(\tau)\right) d\tau - \beta_1 \int_{t_0}^{t} \frac{de_2^T(\tau)}{d\tau} sgn(e_2(\tau))\, d\tau. \end{aligned} \tag{E.5}$$

After integrating the second integral on the right-hand side of (E.5) by parts and evaluating the last integral, the following expression is obtained

$$\begin{aligned} \int_{t_0}^{t} L_1(\tau)\, d\tau &= \int_{t_0}^{t} e_2^T(\tau)\left(-\dot{\bar{F}}(\tau) + \ddot{\bar{F}}(\tau) - \beta_1 sgn(e_2(\tau))\right) d\tau \\ &\quad - e_2^T(t)\,\dot{\bar{F}}(t) - \beta_1 \sum_{i=1}^{2n} |e_{2i}(t)| + \xi_{b1}. \end{aligned} \tag{E.6}$$

The right-hand side of (E.6) can be upper bounded as follows

$$\begin{aligned}\int_{t_0}^{t} L_1(\tau)\, d\tau &\leqslant \int_{t_0}^{t} \sum_{i=1}^{2n} |e_{2i}(\tau)| \left(\left| \dot{\bar{F}}_i(\tau) \right| + \left| \ddot{\bar{F}}_i(\tau) \right| - \beta_1 \right) d\tau \\ &\quad + \sum_{i=1}^{2n} |e_{2i}(t)| \left(\left| \dot{\bar{F}}_i(t) \right| - \beta_1 \right) + \xi_{b1}. \end{aligned} \tag{E.7}$$

If β_1 is chosen to satisfy (E.2), then the first inequality in (E.3) can be proven from (E.7). The second inequality in (E.3) can be obtained by integrating $L_2(t)$, defined in (E.1) as follows

$$\begin{aligned}\int_{t_0}^{t} L_2(\tau)\, d\sigma &= -\beta_2 \int_{t_0}^{t} \dot{e}_2^T(\tau)\, sgn(e_2(\tau))\, d\tau \\ &= \xi_{b2} - \beta_2 \sum_{i=1}^{2n} |e_{2i}(t)| \leq \xi_{b2}. \end{aligned} \tag{E.8}$$

The following is the proof of Theorem 5.

Proof. Let the auxiliary functions $P_1(t)$, $P_2(t) \in \mathbb{R}$ be defined as follows

$$P_1 \triangleq \xi_{b1} - \int_{t_0}^{t} L_1(\tau)\, d\tau \geq 0 \tag{E.9}$$

$$P_2 \triangleq \xi_{b2} - \int_{t_0}^{t} L_2(\tau)\, d\tau \geq 0 \tag{E.10}$$

where $L_1(t)$, $L_2(t)$, ξ_{b1} and ξ_{b2} were defined in Lemma 2. The proof of Lemma 2 ensures that $P_1(t)$ and $P_2(t)$ are non-negative. Let $V_1(y,t) \in \mathbb{R}$ denote the following non-negative function

$$V_1 \triangleq \frac{1}{2} e_2^T e_2 + \frac{1}{2} r^T r + P_1 + P_2 \tag{E.11}$$

where $y(t) \in \mathbb{R}^{4n+2}$ is defined as

$$y \triangleq \left[\begin{array}{cccc} e_2^T & r^T & \sqrt{P_1} & \sqrt{P_2} \end{array} \right]^T. \tag{E.12}$$

Note that (E.11) is bounded by the following inequalities

$$W_3(y) \leq V_1(y,t) \leq W_4(y) \tag{E.13}$$

where $W_3(y)$, $W_4(y) \in \mathbb{R}$ are defined as

$$W_3(y) = \lambda_4 \|y(t)\|^2 \qquad W_4(y) = \lambda_5 \|y(t)\|^2 \tag{E.14}$$

where λ_4, $\lambda_5 \in \mathbb{R}$ are positive bounding constants.

After differentiating (E.11) in time, results in the following expression

$$\dot{V}_1 = -e_2^T e_2 - k_s r^T r - \beta_2 e_2^T sgn(e_2) \tag{E.15}$$

where (2.50), (2.69), (E.9), and (E.10) were utilized. The expression in (E.15) can be rewritten as

$$\dot{V}_1 = -\|e_2\|^2 - k_s \|r\|^2 - \beta_2 \sum_{i=1}^{2n} |e_{2i}|. \tag{E.16}$$

From (E.11) and (E.16), it is clear that $V_1(y,t) \in \mathcal{L}_\infty$; hence, $e_2(t) \in \mathcal{L}_\infty \cap \mathcal{L}_2 \cap \mathcal{L}_1$, $r(t) \in \mathcal{L}_\infty \cap \mathcal{L}_2$, and $y(t) \in \mathcal{L}_\infty$. Since $e_2(t)$, $r(t) \in \mathcal{L}_\infty$, then (2.50) and (2.68) can be used to prove that $\dot{e}_2(t)$, $\dot{\hat{F}}(t) \in \mathcal{L}_\infty$. Given that $e_2(t), r(t)$, $\dot{\hat{F}}(t) \in \mathcal{L}_\infty$ and the assumption that $\dot{\bar{F}}(t) \in \mathcal{L}_\infty$, (2.66) can be used to prove that $\dot{r}(t) \in \mathcal{L}_\infty$. Barbalat's Lemma can be utilized to prove

$$\|e_2(t)\|, \|r(t)\| \to 0 \quad as \quad t \to \infty. \tag{E.17}$$

From (2.50), (2.51), (E.17) and the fact that $\bar{M}(x) \in \mathcal{L}_\infty$, standard linear analysis arguments can be used to prove that $e_1(t)$, $\dot{e}_1(t)$, $\dot{e}_2(t) \in \mathcal{L}_\infty$ and $e_1(t)$, $\dot{e}_1(t) \in \mathcal{L}_1$, and that

$$\|e_1(t)\|, \|\dot{e}_1(t)\|, \|\dot{e}_2(t)\| \to 0 \quad as \quad t \to \infty. \tag{E.18}$$

By using the assumption that $\bar{F}(t) \in \mathcal{L}_\infty$ and the fact that $\dot{e}_2(t) \in \mathcal{L}_\infty$from (2.64) it is clear that $\hat{F}(t) \in \mathcal{L}_\infty$. Since $\hat{F}(t) \in \mathcal{L}_\infty$, (2.55) and the proof in Appendix G can be used to prove that $\lambda_d(t)$, $\eta_d(t)$, $\dot{\eta}_d(t)$, $\xi_d(t)$, $\dot{\xi}_d(t)$, $\ddot{\xi}_d(t) \in \mathcal{L}_\infty$. Using these facts along with (2.48), (2.52) and their first time derivatives, it is clear that $x(t)$, $\dot{x}(t)$, $x_m(t)$, $\dot{x}_m(t)$, $x_s(t)$, $\dot{x}_s(t) \in \mathcal{L}_\infty$. Since $e_1(t)$, $\dot{e}_1(t)$, $\bar{M}(x)$, $\dot{\bar{M}}(x) \in \mathcal{L}_\infty$, it is clear from (2.63) that $\bar{T}_1(t) \in \mathcal{L}_\infty$, and using previously stated bounding

properties, $\bar{T}(t) \in \mathcal{L}_\infty$. It is also possible to state that $\bar{T}_1(t) \in \mathcal{L}_1$, where (2.63) was utilized. Based on the definition of $x(t)$ in (2.48) and the previously stated bounding properties, it is clear that $x_s(t) \to x_m(t)$ and $x_m(t) \to \xi_1(t)$. From these bounding statements and standard signal chasing arguments, all signals can be shown to be bounded. ■

Appendix F

Proof of Theorem 6

Proof. Since the user assist mechanism is disabled (i.e., $\gamma = 0$), the target system defined in (2.54) and (2.55) can be simplified to (2.58). To assist in the subsequent analysis, the following expression can be developed from integration by parts

$$\int_{t_0}^{t} \bar{M}\ddot{e}_1(\tau)\, d\tau = \bar{M}\dot{e}_1(t) - \bar{M}\dot{e}_1(t_0) - \int_{t_0}^{t} \dot{\bar{M}}\, \dot{e}_1(\tau)\, d\tau. \tag{F.1}$$

Since $\bar{M}(x)$, $\dot{\bar{M}}(x)$, $\dot{e}_1(t) \in \mathcal{L}_\infty$, and $\dot{e}_1(t) \in \mathcal{L}_1$, then $\int_{t_0}^{t} \bar{M}\ddot{e}_1(\tau)\, d\tau \in \mathcal{L}_\infty$. After integrating (2.61) as follows

$$\int_{t_0}^{t} \tilde{F}(\tau)\, d\tau = -\int_{t_0}^{t} \bar{M}\ddot{e}_1(\tau)\, d\tau - \int_{t_0}^{t} \bar{T}_1(\tau)\, d\tau \tag{F.2}$$

and using the facts that $\bar{T}_1(t) \in \mathcal{L}_1$ (see proof of Theorem 5) and that $\int_{t_0}^{t} \bar{M}\ddot{e}_1(\tau)\, d\tau \in \mathcal{L}_\infty$, it is clear that $\tilde{F}(t) \in \mathcal{L}_1$, where $\tilde{F}(t) \in \mathbb{R}^{2n}$ is defined as follows

$$\tilde{F} \triangleq \bar{F} - \hat{F}. \tag{F.3}$$

The expression in (F.3) can be decomposed as $\tilde{F}(t) = \left[\begin{array}{cc} \tilde{F}_1^T & \tilde{F}_2^T \end{array}\right]^T$, where $\tilde{F}_1(t)$, $\tilde{F}_2(t) \in \mathbb{R}^n$. After utilizing the fact that $\hat{F}(t_0) = 0_{2n}$, the following can be derived

$$\hat{F}(t) = \int_{t_0}^{t} \dot{\hat{F}}(\tau)\, d\tau. \tag{F.4}$$

From the proof of Theorem 5 (see Appendix E), it is clear that $\hat{F}(t) \in L_\infty$, then from (F.4) it is also clear that $\dot{\hat{F}}(t) \in \mathcal{L}_1$.

By using the transformation in (2.48), the passivity objective in (2.6) can be rewritten as follows

$$\int_{t_0}^{t} \left[\begin{array}{cc} \dot{x}_m^T(\tau) & \dot{x}_s^T(\tau) \end{array}\right] \left[\begin{array}{c} F_H(\tau) \\ F_E(\tau) \end{array}\right] d\tau = \int_{t_0}^{t} \dot{x}^T \bar{F} d\tau - \int_{t_0}^{t} \left[\begin{array}{cc} 0_n^T & \dot{\xi}_2^T \end{array}\right] \bar{F} d\tau. \tag{F.5}$$

By utilizing (F.3) and the time derivative of (2.52), (F.5) can be rewritten as follows

$$\begin{aligned} \int_{t_0}^{t} \dot{x}^T \bar{F} d\tau - \int_{t_0}^{t} \left[\begin{array}{cc} 0_n^T & \dot{\xi}_2^T \end{array}\right] \bar{F} d\tau &= \int_{t_0}^{t} \dot{\xi}_1^T(\tau)\, \tilde{F}_1(\tau)\, d\tau + \int_{t_0}^{t} \dot{\xi}_1^T(\tau)\, \hat{F}_1(\tau)\, d\tau \\ &\quad - \int_{t_0}^{t} \dot{e}_1^T(\tau)\, \bar{F}(\tau)\, d\tau. \end{aligned} \tag{F.6}$$

Following expression can be developed from integration by parts of the second integral at the right-hand side of (F.6)

$$\int_{t_0}^{t} \dot{x}^T \bar{F} d\tau - \int_{t_0}^{t} \left[\begin{array}{cc} 0_n^T & \dot{\xi}_2^T \end{array} \right] \bar{F} d\tau = \int_{t_0}^{t} \dot{\xi}_1^T(\tau) \tilde{F}_1(\tau) d\tau - \int_{t_0}^{t} \xi_1^T(\tau) \dot{\hat{F}}_1(\tau) d\tau + \xi_1^T(t) \hat{F}_1(t) - \int_{t_0}^{t} \dot{e}_1^T(\tau) \bar{F}(\tau) d\tau \quad \text{(F.7)}$$

where $\hat{F}(t_0) = 0_{2n}$ is both utilized. Since $\dot{\xi}_1(t) \in \mathcal{L}_\infty$ and $\tilde{F}(t) \in \mathcal{L}_1$, it is clear that the first integral expression in (F.7) is bounded and a lower negative bound exists. Since $\xi_1(t) \in \mathcal{L}_\infty$ and $\dot{\hat{F}}(t) \in \mathcal{L}_1$ it is clear that the second integral expression in (F.7) is bounded and a lower negative bound exists, and since $\xi_1(t)$, $\hat{F}(t) \in \mathcal{L}_\infty$ then third expression is also bounded and a lower negative bound exists. Finally, because $\dot{e}_1(t) \in \mathcal{L}_1$ and $\bar{F}(t) \in \mathcal{L}_\infty$, it is possible to show that the last integral in (F.7) is also bounded and a lower negative bound exists. Hence, these facts can be applied to (F.5) to prove that

$$\int_{t_0}^{t} \left[\begin{array}{cc} \dot{x}_m^T(\tau) & \dot{x}_s^T(\tau) \end{array} \right] \left[\begin{array}{c} F_H(\tau) \\ F_E(\tau) \end{array} \right] d\tau \geq -c_4^2 \quad \text{(F.8)}$$

where $c_4 \in \mathbb{R}$ is a bounded constant. ■

Appendix G

UMIF Desired Trajectory Stability Analysis

In the proof of Theorem 5 (see Appendix E), it is proven that $e_1(t)$, $e_2(t)$, $r(t)$, $\hat{F}(t)$, $\dot{\hat{F}}(t) \in \mathcal{L}_\infty$ as well as that $\|e_1(t)\|$, $\|e_2(t)\|$, and $\|r(t)\| \to 0$ as $t \to \infty$ regardless of whether or not $x(t)$, $\xi_d(t)$, $\lambda_d(t)$, $\eta_d(t)$, $\dot{\eta}_d(t) \in \mathcal{L}_\infty$. Therefore the fact that $\hat{F}(t) \in \mathcal{L}_\infty$ can be used in the subsequent analysis. To prove that $\lambda_d(t)$, $\eta_d(t) \in \mathcal{L}_\infty$, let $V(t) \in \mathbb{R}$ denote the following function

$$V \triangleq V_1 + V_2 \tag{G.1}$$

where $V_1(t) \in \mathbb{R}$ denotes the following non-negative function

$$V_1 \triangleq \frac{1}{2}\eta_d^T M_T \eta_d + \frac{1}{2}\lambda_d^T K_T \lambda_d \tag{G.2}$$

where $\lambda_d(t)$, $\eta_d(t)$, M_T and K_T were introduced in (2.55). The expression given in (G.2) can be lower bounded by the auxiliary function, $V_2(\bar{x}) \in \mathbb{R}$, defined as follows

$$V_2 \triangleq 2\varepsilon \eta_d^T M_T \lambda_d \leq V_1 \tag{G.3}$$

where $\bar{x}(t) \in \mathbb{R}^{4n}$ is defined as

$$\bar{x} \triangleq \begin{bmatrix} \lambda_d^T & \eta_d^T \end{bmatrix}^T \tag{G.4}$$

and $\varepsilon \in \mathbb{R}$ is a positive bounding constant selected according to the following inequality

$$\varepsilon < \frac{\min\{\lambda_{\min}\{M_T\}, \lambda_{\min}\{K_T\}\}}{4\lambda_{\max}\{M_T\}} \tag{G.5}$$

where $\lambda_{\min}\{\cdot\}$ and $\lambda_{\max}\{\cdot\}$ denote the minimum and maximum eigenvalue of a matrix, respectively. From (G.3) it is clear that $V(t)$ is a non-negative function and bounded by the following inequalities

$$\bar{\lambda}_1 \|\bar{x}\|^2 \leq V(\bar{x}) \leq \bar{\lambda}_2 \|\bar{x}\|^2 \tag{G.6}$$

where $\bar{\lambda}_1$, $\bar{\lambda}_2 \in \mathbb{R}$ are positive constants defined as follows, provided that ε is selected according to (G.5)

$$\begin{aligned} \bar{\lambda}_1 &\triangleq \frac{1}{2}\min\left\{\lambda_{\min}\{M_T\}, \lambda_{\min}\{K_T\}\right\} - 2\varepsilon\lambda_{\max}\{M_T\} \\ \bar{\lambda}_2 &\triangleq \frac{1}{2}\max\left\{\lambda_{\max}\{M_T\}, \lambda_{\max}\{K_T\}\right\} + 2\varepsilon\lambda_{\max}\{M_T\}. \end{aligned} \tag{G.7}$$

To facilitate the subsequent analysis, the time derivative of (G.1) can be determined as follows

$$\begin{aligned} \dot{V} &= \eta_d^T M_T \dot{\eta}_d + \lambda_d^T K_T \dot{\lambda}_d \\ &\quad + 2\varepsilon \dot{\eta}_d^T M_T \lambda_d + 2\varepsilon \eta_d^T M_T \dot{\lambda}_d. \end{aligned} \tag{G.8}$$

After utilizing (2.55) and the fact that $\eta_d(t) = \dot{\lambda}_d(t)$, the expression in (G.8) can be written as

$$\begin{aligned} \dot{V} &= \eta_d^T \left(M_T \bar{M}^{-1}\right) \hat{F} - \eta_d^T B_T \eta_d + 2\varepsilon \lambda_d^T M_T \bar{M}^{-1} \hat{F} \\ &\quad - 2\varepsilon \lambda_d^T B_T \eta_d - 2\varepsilon \lambda_d^T K_T \lambda_d + 2\varepsilon \eta_d^T M_T \eta_d. \end{aligned} \tag{G.9}$$

The right-hand side of (G.9) can be upper bounded as follows

$$\begin{aligned} \dot{V} \leq\ & \xi_{\bar{m}} \lambda_{\max}\{M_T\} \left[\delta_1 \|\eta_d\|^2 + \frac{1}{\delta_1}\left\|\hat{F}\right\|^2\right] - \lambda_{\min}\{B_T\}\|\eta_d\|^2 \\ & + 2\varepsilon \xi_{\bar{m}} \lambda_{\max}\{M_T\} \left[\delta_3 \|\lambda_d\|^2 + \frac{1}{\delta_3}\left\|\hat{F}\right\|^2\right] - 2\varepsilon\lambda_{\min}\{K_T\}\|\lambda_d\|^2 \\ & + 2\varepsilon \lambda_{\max}\{B_T\} \left[\delta_2 \|\lambda_d\|^2 + \frac{1}{\delta_2}\|\eta_d\|^2\right] + 2\varepsilon\lambda_{\max}\{M_T\}\|\eta_d\|^2 \end{aligned} \tag{G.10}$$

where the following properties were utilized

$$\eta_d^T M_T \bar{M}^{-1} \hat{F} \leq \xi_{\bar{m}} \lambda_{\max}\{M_T\} \left[\delta_1 \|\eta_d\|^2 + \frac{1}{\delta_1}\left\|\hat{F}\right\|^2\right] \tag{G.11}$$

$$-\eta_d^T B_T \eta_d \leq -\lambda_{\min}\{B_T\}\|\eta_d\|^2 \tag{G.12}$$

$$2\varepsilon \lambda_d^T M_T \bar{M}^{-1} \hat{F} \leq 2\varepsilon \xi_{\bar{m}} \lambda_{\max}\{M_T\} \left[\delta_3 \|\lambda_d\|^2 + \frac{1}{\delta_3}\left\|\hat{F}\right\|^2\right] \tag{G.13}$$

$$-2\varepsilon \lambda_d^T B_T \eta_d \leq 2\varepsilon \lambda_{\max}\{B_T\} \left[\delta_2 \|\lambda_d\|^2 + \frac{1}{\delta_2}\|\eta_d\|^2\right] \tag{G.14}$$

$$-2\varepsilon \lambda_d^T K_T \lambda_d \leq -2\varepsilon \lambda_{\min}\{K_T\}\|\lambda_d\|^2 \tag{G.15}$$

$$2\varepsilon \eta_d^T M_T \eta_d \leq 2\varepsilon \lambda_{\max}\{M_T\}\|\eta_d\|^2 \tag{G.16}$$

where $\delta_1, \delta_2, \delta_3 \in \mathbb{R}$ denote positive bounding constants and $\xi_{\bar{m}} \in \mathbb{R}$ denotes positive bounding constant defined as

$$\left\| \bar{M}^{-1} \right\|_{\infty} \leq \xi_{\bar{m}} \tag{G.17}$$

where $\left\| \bar{M}^{-1} \right\|_{\infty}$ denotes the induced infinity norm of the bounded matrix $\bar{M}^{-1}(x)$.

The expression in (G.10) can be rearranged as follows

$$\begin{aligned} \dot{V} \leq & -\left(\lambda_{\min}\{B_T\} - \xi_{\bar{m}}\delta_1\lambda_{\max}\{M_T\} \right. \\ & \left. -\frac{2\varepsilon\lambda_{\max}\{B_T\}}{\delta_2} - 2\varepsilon\lambda_{\max}\{M_T\}\right)\|\eta_d\|^2 \\ & -2\varepsilon\left(\lambda_{\min}\{K_T\} - \delta_2\lambda_{\max}\{B_T\} - \xi_{\bar{m}}\delta_3\lambda_{\max}\{M_T\}\right)\|\lambda_d\|^2 \\ & +\xi_{\bar{m}}\lambda_{\max}\{M_T\}\left(\frac{1}{\delta_1} + \frac{2\varepsilon}{\delta_3}\right)\left\|\hat{F}\right\|^2. \end{aligned} \tag{G.18}$$

Provided δ_1, δ_2, δ_3, M_T, B_T, K_T and ε are selected to satisfy (G.5) and the following sufficient conditions

$$\begin{aligned} \lambda_{\min}\{B_T\} &> \xi_{\bar{m}}\delta_1\lambda_{\max}\{M_T\} + \frac{2\varepsilon\lambda_{\max}\{B_T\}}{\delta_2} + 2\varepsilon\lambda_{\max}\{M_T\} \\ \lambda_{\min}\{K_T\} &> \xi_{\bar{m}}\delta_3\lambda_{\max}\{M_T\} + \delta_2\lambda_{\max}\{B_T\} \end{aligned}$$

right-hand side of (G.18) can be upper bounded as follows

$$\dot{V} \leq -\frac{\min\{\gamma_a, \gamma_b\}}{\bar{\lambda}_2}V + \epsilon \tag{G.19}$$

where (G.4) and (G.6) were utilized, and γ_a, γ_b, $\epsilon \in \mathbb{R}$ denote positive bounding constants.

From (G.1) - (G.3), and (G.6), and that $\hat{F}(t) \in \mathcal{L}_{\infty}$ (see Appendix E), the expression in (G.19) can be used with the result from [105] to prove that $\bar{x}(t)$, $\lambda_d(t)$, $\eta_d(t) \in \mathcal{L}_{\infty}$. Based on (2.55), and the fact that $\bar{M}^{-1}(x)$, $\hat{F}(t) \in \mathcal{L}_{\infty}$ then $\dot{\eta}_d(t) \in \mathcal{L}_{\infty}$. After utilizing the fact that $\eta_d(t)$, $\dot{\eta}_d(t) \in \mathcal{L}_{\infty}$ along with the Remark 2, then it is clear that $\xi_d(t)$, $\dot{\xi}_d(t)$, $\ddot{\xi}_d(t) \in \mathcal{L}_{\infty}$. ■

Appendix H

Existence of the Inverse of $\bar{M}M_T^{-1}$

To show that $\left(\bar{M}M_T^{-1}\right)^{-1}$ term introduced at the right-hand side of (2.55) exists, from (2.10) and the fact that M_T is a positive definite, diagonal matrix, then it is clear that

$$\bar{M}M_T^{-1} = S^{-T}\begin{bmatrix} M_1 & 0_{nxn} \\ 0_{nxn} & M_2 \end{bmatrix} S^{-1}M_T^{-1} \tag{H.1}$$

where S, $M_1(\cdot)$ and $M_2(\cdot)$ were introduced in (2.8), (2.1) and (2.2), respectively. From (H.1), it is clear that,

$$\left(\bar{M}M_T^{-1}\right)^{-1} = M_T S\begin{bmatrix} M_1^{-1} & 0_{nxn} \\ 0_{nxn} & M_2^{-1} \end{bmatrix} S^T. \tag{H.2}$$

Appendix I

Upper Bound Development for MIF Analysis

To simplify the following derivations, (2.31) can be rewritten as follows

$$\begin{aligned} N &\triangleq N\left(x, \dot{x}, \ddot{x}, e_1, e_2, r, \dddot{x}_d\right) \\ &= \bar{M}\dddot{x}_d + \dot{\bar{M}}\,\ddot{x} + \dot{\bar{N}} + e_2 + \bar{M}\left(\alpha_1 + \alpha_2\right) r \\ &\quad -\bar{M}\left(\alpha_1^2 + \alpha_1\alpha_2 + \alpha_2^2\right) e_2 + \bar{M}\alpha_2^3 e_1 + \frac{1}{2}\,\dot{\bar{M}}\, r \end{aligned} \tag{I.1}$$

where (2.15) and (2.16) were both utilized. To facilitate the subsequent analysis, the terms $N\left(x, \dot{x}_d, \ddot{x}_d, 0, 0, 0, \dddot{x}_d\right)$, $N\left(x, \dot{x}, \ddot{x}_d, 0, 0, 0, \dddot{x}_d\right)$, $N\left(x, \dot{x}, \ddot{x}, 0, 0, 0, \dddot{x}_d\right)$, $N\left(x, \dot{x}, \ddot{x}, e_1, 0, 0, \dddot{x}_d\right)$, and $N\left(x, \dot{x}, \ddot{x}, e_1, e_2, 0, \dddot{x}_d\right)$ are added and subtracted to the right-hand side of (2.30) as follows

$$\begin{aligned} \tilde{N} &= \left[N\left(x, \dot{x}_d, \ddot{x}_d, 0, 0, 0, \dddot{x}_d\right) - N_d\left(x_d, \dot{x}_d, \ddot{x}_d, 0, 0, 0, \dddot{x}_d\right)\right] \\ &\quad + \left[N\left(x, \dot{x}, \ddot{x}_d, 0, 0, 0, \dddot{x}_d\right) - N\left(x, \dot{x}_d, \ddot{x}_d, 0, 0, 0, \dddot{x}_d\right)\right] \\ &\quad + \left[N\left(x, \dot{x}, \ddot{x}, 0, 0, 0, \dddot{x}_d\right) - N\left(x, \dot{x}, \ddot{x}_d, 0, 0, 0, \dddot{x}_d\right)\right] \\ &\quad + \left[N\left(x, \dot{x}, \ddot{x}, e_1, 0, 0, \dddot{x}_d\right) - N\left(x, \dot{x}, \ddot{x}, 0, 0, 0, \dddot{x}_d\right)\right] \\ &\quad + \left[N\left(x, \dot{x}, \ddot{x}, e_1, e_2, 0, \dddot{x}_d\right) - N\left(x, \dot{x}, \ddot{x}, e_1, 0, 0, \dddot{x}_d\right)\right] \\ &\quad + \left[N\left(x, \dot{x}, \ddot{x}, e_1, e_2, r, \dddot{x}_d\right) - N\left(x, \dot{x}, \ddot{x}, e_1, e_2, 0, \dddot{x}_d\right)\right]. \end{aligned} \tag{I.2}$$

After applying the Mean Value Theorem to each bracketed term of (I.2), the following

expression can be obtained

$$\begin{aligned}
\tilde{N} &= \left.\frac{\partial N\left(\sigma_1, \dot{x}_d, \ddot{x}_d, 0, 0, 0, \dddot{x}_d\right)}{\partial \sigma_1}\right|_{\sigma_1 = v_1} (x - x_d) \\
&+ \left.\frac{\partial N\left(x, \sigma_2, \ddot{x}_d, 0, 0, 0, \dddot{x}_d\right)}{\partial \sigma_2}\right|_{\sigma_2 = v_2} (\dot{x} - \dot{x}_d) \\
&+ \left.\frac{\partial N\left(x, \dot{x}, \sigma_3, 0, 0, 0, \dddot{x}_d\right)}{\partial \sigma_3}\right|_{\sigma_3 = v_3} (\ddot{x} - \ddot{x}_d) \\
&+ \left.\frac{\partial N\left(x, \dot{x}, \ddot{x}, \sigma_4, 0, 0, \dddot{x}_d\right)}{\partial \sigma_4}\right|_{\sigma_4 = v_4} (e_1 - 0) \\
&+ \left.\frac{\partial N\left(x, \dot{x}, \ddot{x}, e_1, \sigma_5, 0, \dddot{x}_d\right)}{\partial \sigma_5}\right|_{\sigma_5 = v_5} (e_2 - 0) \\
&+ \left.\frac{\partial N\left(x, \dot{x}, \ddot{x}, e_1, e_2, \sigma_6, \dddot{x}_d\right)}{\partial \sigma_6}\right|_{\sigma_6 = v_6} (r - 0) \qquad \text{(I.3)}
\end{aligned}$$

where $v_1 \in (x_d, x)$, $v_2 \in (\dot{x}_d, \dot{x})$, $v_3 \in (\ddot{x}_d, \ddot{x})$, $v_4 \in (0, e_1)$, $v_5 \in (0, e_2)$, and $v_6 \in (0, r)$. The right-hand side of (I.3) can be upper bounded as follows

$$\begin{aligned}
\left\|\tilde{N}\right\| &\leq \left\| \left.\frac{\partial N\left(\sigma_1, \dot{x}_d, \ddot{x}_d, 0, 0, 0, \dddot{x}_d\right)}{\partial \sigma_1}\right|_{\sigma_1 = v_1} \right\| \|e_1\| \\
&+ \left\| \left.\frac{\partial N\left(x, \sigma_2, \ddot{x}_d, 0, 0, 0, \dddot{x}_d\right)}{\partial \sigma_2}\right|_{\sigma_2 = v_2} \right\| \|\dot{e}_1\| \\
&+ \left\| \left.\frac{\partial N\left(x, \dot{x}, \sigma_3, 0, 0, 0, \dddot{x}_d\right)}{\partial \sigma_3}\right|_{\sigma_3 = v_3} \right\| \|\ddot{e}_1\| \\
&+ \left\| \left.\frac{\partial N\left(x, \dot{x}, \ddot{x}, \sigma_4, 0, 0, \dddot{x}_d\right)}{\partial \sigma_4}\right|_{\sigma_4 = v_4} \right\| \|e_1\| \\
&+ \left\| \left.\frac{\partial N\left(x, \dot{x}, \ddot{x}, e_1, \sigma_5, 0, \dddot{x}_d\right)}{\partial \sigma_5}\right|_{\sigma_5 = v_5} \right\| \|e_2\| \\
&+ \left\| \left.\frac{\partial N\left(x, \dot{x}, \ddot{x}, e_1, e_2, \sigma_6, \dddot{x}_d\right)}{\partial \sigma_6}\right|_{\sigma_6 = v_6} \right\| \|r\| . \qquad \text{(I.4)}
\end{aligned}$$

The partial derivatives in (I.3) can be calculated by using (I.1) as follows

$$\frac{\partial N\left(\sigma_1, \dot{x}_d, \ddot{x}_d, 0, 0, 0, \dddot{x}_d\right)}{\partial \sigma_1} = \frac{\partial \bar{M}\left(\sigma_1\right)}{\partial \sigma_1}\dddot{x}_d + \frac{\partial\ \dot{\bar{M}}\left(\sigma_1, \dot{x}_d\right)}{\partial \sigma_1}\ddot{x}_d + \frac{\partial\ \dot{\bar{N}}\left(\sigma_1, \dot{x}_d, \ddot{x}_d\right)}{\partial \sigma_1} \tag{I.5}$$

$$\frac{\partial N\left(x, \sigma_2, \ddot{x}_d, 0, 0, 0, \dddot{x}_d\right)}{\partial \sigma_2} = \frac{\partial\ \dot{\bar{M}}\left(x, \sigma_2\right)}{\partial \sigma_2}\ddot{x}_d + \frac{\partial\ \dot{\bar{N}}\left(x, \sigma_2, \ddot{x}_d\right)}{\partial \sigma_2} \tag{I.6}$$

$$\frac{\partial N\left(x, \dot{x}, \sigma_3, 0, 0, 0, \dddot{x}_d\right)}{\partial \sigma_3} = \dot{\bar{M}}\left(x, \dot{x}\right) + \frac{\partial\ \dot{\bar{N}}\left(x, \dot{x}, \sigma_3\right)}{\partial \sigma_3} \tag{I.7}$$

$$\frac{\partial N\left(x, \dot{x}, \ddot{x}, \sigma_4, 0, 0, \dddot{x}_d\right)}{\partial \sigma_4} = \alpha_2^3 \bar{M}\left(x\right) \tag{I.8}$$

$$\frac{\partial N\left(x, \dot{x}, \ddot{x}, e_1, \sigma_5, 0, \dddot{x}_d\right)}{\partial \sigma_5} = I_{2n} - \left(\alpha_1^2 + \alpha_1\alpha_2 + \alpha_2^2\right)\bar{M}\left(x\right) \tag{I.9}$$

$$\frac{\partial N\left(x, \dot{x}, \ddot{x}, e_1, e_2, \sigma_6, \dddot{x}_d\right)}{\partial \sigma_6} = \left(\alpha_1 + \alpha_2\right)\bar{M}\left(x\right) + \frac{1}{2}\ \dot{\bar{M}}\left(x, \dot{x}\right) \tag{I.10}$$

where $I_{2n} \in \mathbb{R}^{2n \times 2n}$ denotes the identity matrix. By defining

$$\begin{array}{ll} v_1 \triangleq x - \tau_1\left(x - x_d\right) & v_2 \triangleq \dot{x} - \tau_2\left(\dot{x} - \dot{x}_d\right) \\ v_3 \triangleq \ddot{x} - \tau_3\left(\ddot{x} - \ddot{x}_d\right) & v_4 \triangleq e_1 - \tau_4\left(e_1 - 0\right) \\ v_5 \triangleq e_2 - \tau_5\left(e_2 - 0\right) & v_6 \triangleq r - \tau_6\left(r - 0\right) \end{array}$$

where $\tau_i \in (0, 1)\ \forall i = 1, 2, ..., 6$, and if the assumptions stated for the system model and the desired trajectory are met, then upper bounds for the right-hand sides of (I.5)-(I.10) can be rewritten as follows

$$\left\| \left. \frac{\partial N\left(\sigma_1, \dot{x}_d, \ddot{x}_d, 0, 0, 0, \dddot{x}_d\right)}{\partial \sigma_1} \right|_{\sigma_1 = v_1} \right\| \leqslant \rho_1\left(x, \dot{x}, \ddot{x}\right) \tag{I.11}$$

$$\left\| \left. \frac{\partial N\left(x, \sigma_2, \ddot{x}_d, 0, 0, 0, \dddot{x}_d\right)}{\partial \sigma_2} \right|_{\sigma_2 = v_2} \right\| \leqslant \rho_2\left(x, \dot{x}, \ddot{x}\right) \tag{I.12}$$

$$\left\| \left. \frac{\partial N\left(x, \dot{x}, \sigma_3, 0, 0, 0, \dddot{x}_d\right)}{\partial \sigma_3} \right|_{\sigma_3 = v_3} \right\| \leqslant \rho_3\left(x, \dot{x}\right) \tag{I.13}$$

$$\left\| \left. \frac{\partial N\left(x, \dot{x}, \ddot{x}, \sigma_4, 0, 0, \dddot{x}_d\right)}{\partial \sigma_4} \right|_{\sigma_4 = v_4} \right\| \leqslant \rho_4\left(x\right) \tag{I.14}$$

$$\left\| \left. \frac{\partial N\left(x, \dot{x}, \ddot{x}, e_1, \sigma_5, 0, \dddot{x}_d\right)}{\partial \sigma_5} \right|_{\sigma_5 = v_5} \right\| \leqslant \rho_5\left(x\right) \tag{I.15}$$

$$\left\| \left. \frac{\partial N\left(x, \dot{x}, \ddot{x}, e_1, e_2, \sigma_6, \dddot{x}_d\right)}{\partial \sigma_6} \right|_{\sigma_6 = v6} \right\| \leqslant \rho_6\left(x, \dot{x}\right) \tag{I.16}$$

where $\rho_i(\cdot)\ \forall i = 1, 2, ..., 6$, are positive nondecreasing functions of $x(t)$, $\dot{x}(t)$, and $\ddot{x}(t)$. After substituting (I.11)-(I.16) into (I.4), $\tilde{N}(\cdot)$ can be rewritten as

$$\begin{aligned} \tilde{N} \leq\ & \left[\rho_1\left(\|e_1\|, \|e_2\|, \|r\|\right) + \rho_4\left(\|e_1\|\right)\right]\|e_1\| + \rho_2\left(\|e_1\|, \|e_2\|, \|r\|\right)\|\dot{e}_1\| \\ & + \rho_3\left(\|e_1\|, \|e_2\|\right)\|\ddot{e}_1\| + \rho_5\left(\|e_1\|\right)\|e_2\| + \rho_6\left(\|e_1\|, \|e_2\|\right)\|r\| \end{aligned} \tag{I.17}$$

where (2.15) and (2.16) were utilized. The expressions in (2.15), (2.16) and (C.13) can be used to rewrite the upper bound for the right-hand side of (I.17) as in (C.17).

Appendix J

Proof of Theorem 7

Lemma 3 *Let the auxiliary functions* $L_1(t)$, $L_2(t) \in \mathbb{R}$ *be defined as follows*

$$L_1 \triangleq r^T(\psi - C_1 Sgn(e_n)) \ , \ L_2 \triangleq -\dot{e}_n^T C_2 Sgn(e_n). \tag{J.1}$$

If C_1 *is selected to satisfy the sufficient condition (3.33), then*

$$\int_{t_0}^{t} L_1(\tau)\, d\tau \leq \zeta_{b1} \quad , \quad \int_{t_0}^{t} L_2(\tau)\, d\tau \leq \zeta_{b2} \tag{J.2}$$

where ζ_{b1}, $\zeta_{b2} \in \mathbb{R}$ *are positive constants defined as*

$$\zeta_{b1} \triangleq \sum_{i=1}^{m} C_{1i} |e_{ni}(t_0)| - e_n^T(t_0)\psi(t_0), \zeta_{b2} \triangleq \sum_{i=1}^{m} C_{2i} |e_{ni}(t_0)|. \tag{J.3}$$

Proof. After substituting (3.13) into (J.1) and then integrating $L_1(t)$ in time, results in the following expression

$$\begin{aligned} \int_{t_0}^{t} L_1(\tau)\, d\tau &= \int_{t_0}^{t} e_n^T(\tau)\Lambda^T[\psi(\tau) - C_1 \mathrm{Sgn}(e_n(\tau))]\, d\tau \\ &\quad + \int_{t_0}^{t} \frac{de_n^T(\tau)}{d\tau}\psi(\tau)\, d\tau - \int_{t_0}^{t} \frac{de_n^T(\tau)}{d\tau} C_1 \mathrm{Sgn}(e_n(\tau))\, d\tau. \end{aligned} \tag{J.4}$$

After integrating the second integral on the right-hand side of (J.4) by parts, the following expression is obtained

$$\begin{aligned} \int_{t_0}^{t} L_1(\tau)\, d\tau &= \int_{t_0}^{t} e_n^T(\tau)\Lambda^T[\psi(\tau) - C_1 \mathrm{Sgn}(e_n(\tau))]\, d\tau + e_n^T(\tau)\psi(\tau)\Big|_{t_0}^{t} \\ &\quad - \int_{t_0}^{t} e_n^T(\tau)\frac{d\psi(\tau)}{d\tau} d\tau - \sum_{i=1}^{m} C_{1i} |e_{ni}(\tau)||_{t_0}^{t} \\ &= \int_{t_0}^{t} e_n^T(\tau)\Lambda^T\left[\psi(\tau) - \Lambda^{-1}\frac{d\psi(\tau)}{d\tau} - C_1 \mathrm{Sgn}(e_n(\tau))\right] d\tau \\ &\quad + e_n^T(t)\psi(t) - e_n^T(t_0)\psi(t_0) - \sum_{i=1}^{m} C_{1i}(|e_{ni}(t)| - |e_{ni}(t_0)|). \end{aligned} \tag{J.5}$$

The right-hand side of (J.5) can be upper-bounded as follows

$$\begin{aligned} \int_{t_0}^{t} L_1(\tau)\, d\tau &\leq \int_{t_0}^{t} \sum_{i=1}^{m} |e_{ni}(\tau)| \Lambda_i \left[|\psi_i(\tau)| + \frac{1}{\Lambda_i}\left|\frac{d\psi_i(\tau)}{d\tau}\right| - C_{1i}\right] d\tau \\ &\quad + \sum_{i=1}^{m} |e_{ni}(t)|(|\psi_i(t)| - C_{1i}) + \zeta_{b1}. \end{aligned} \tag{J.6}$$

If C_1 is chosen according to satisfy (3.33), then the first inequality in (J.2) can be proven from (J.6). The second inequality in (J.2) can be obtained by integrating $L_2(t)$ defined in (J.1) as follows

$$\begin{aligned} \int_{t_0}^{t} L_2(\tau)\, d\tau &= -\int_{t_0}^{t} \dot{e}_n^T(\tau)\, C_2 \mathrm{Sgn}(e_n(\tau))\, d\tau \\ &= \zeta_{b2} - \sum_{i=1}^{m} C_{2i} |e_{ni}(t)| \leq \zeta_{b2}. \end{aligned} \tag{J.7}$$

■

The following is the proof of Theorem 7.

Proof. Let the auxiliary functions $P_1(t)$, $P_2(t) \in \mathbb{R}$ be defined as follows

$$P_1 \triangleq \zeta_{b1} - \int_{t_0}^{t} L_1(\tau)\, d\tau \tag{J.8}$$

$$P_2 \triangleq \zeta_{b2} - \int_{t_0}^{t} L_2(\tau)\, d\tau \tag{J.9}$$

where $L_1(t)$, $L_2(t)$, ζ_{b1} and ζ_{b2} were defined in Lemma 3. The proof of Lemma 3 ensures that $P_1(t)$ and $P_2(t)$ are non-negative. The non-negative function $V(s(t), t) \in \mathbb{R}$ is defined as follows

$$V \triangleq \frac{1}{2}\sum_{i=1}^{n} e_i^T e_i + \frac{1}{2} r^T M r + P_1 + P_2 + \frac{1}{2}\tilde{\theta}^T \Gamma^{-1} \tilde{\theta} \tag{J.10}$$

where $s(t) \in \mathbb{R}^{[(n+1)m+2+p]\times 1}$ is defined as follows

$$s = \begin{bmatrix} z^T & \sqrt{P_1} & \sqrt{P_2} & \tilde{\theta}^T \end{bmatrix}^T. \tag{J.11}$$

After utilizing (3.2), (J.10) can be bounded as follows

$$W_1(s) \leq V(s,t) \leq W_2(s) \tag{J.12}$$

where $W_1(s)$, $W_2(s) \in \mathbb{R}$ are defined as follows

$$W_1(s) \triangleq \lambda_1 \|s\|^2 \quad , \quad W_2(s) \triangleq \lambda_2(\|s\|)\|s\|^2 \tag{J.13}$$

and[7] $\lambda_1, \lambda_2(\cdot) \in \mathbb{R}$ are defined as follows

$$\begin{aligned} \lambda_1 &= \frac{1}{2}\min\left\{1, \underline{m}, \lambda_{\min}\left(\Gamma^{-1}\right)\right\}, \\ \lambda_2 &= \max\left\{1, \frac{1}{2}\bar{m}\left(\|s\|\right), \frac{1}{2}\lambda_{\max}\left(\Gamma^{-1}\right)\right\}. \end{aligned} \tag{J.14}$$

By differentiating (J.10), the following expression can be obtained

$$\dot{V} = -\sum_{i=1}^{n-1} e_i^T e_i - e_n^T \Lambda e_n + e_{n-1}^T e_n - r^T r + r^T \tilde{N} - r^T K r - e_n^T \Lambda C_2 \mathrm{Sgn}\left(e_n\right) \tag{J.15}$$

where (3.6a)-(3.6c), (3.13), (3.29), (3.30) and (J.1) were utilized. By using (3.22), (3.32), and the triangle inequality, an upper-bound on (J.15) can be obtained as follows

$$\begin{aligned} \dot{V} &\leq -\lambda_3 \|z\|^2 + \|r\| \rho\left(\|z\|\right)\|z\| - \lambda_{\min}(K)\|r\|^2 - \sum_{i=1}^{m} \Lambda_i C_{2i} \left|e_{ni}(t)\right| \\ &\leq -\left(\lambda_3 - \frac{\rho^2\left(\|z\|\right)}{4\lambda_{\min}(K)}\right)\|z\|^2 - \sum_{i=1}^{m} \Lambda_i C_{2i} \left|e_{ni}(t)\right| \end{aligned} \tag{J.16}$$

where $\lambda_3 \triangleq \min\left\{\frac{1}{2}, \lambda_{\min}(\Lambda) - \frac{1}{2}\right\}$. The following inequality can be developed

$$\dot{V} \leq W(s) - \sum_{i=1}^{m} \Lambda_i C_{2i} \left|e_{ni}(t)\right| \tag{J.17}$$

where $W(s) \in \mathbb{R}$ denotes the following non-positive function

$$W(s) \triangleq -\beta_0 \|z\|^2 \tag{J.18}$$

with $\beta_0 \in \mathbb{R}$ being a positive constant, and provided that $\lambda_{\min}(K)$ is selected according to the following sufficient condition

$$\lambda_{\min}(K) \geq \frac{\rho^2\left(\|z\|\right)}{4\lambda_3} \text{ or } \|z\| \leq \rho^{-1}\left(2\sqrt{\lambda_3 \lambda_{\min}(K)}\right). \tag{J.19}$$

[7] Using (3.4) and (3.6a)-(3.6c) it can be shown that $\left\|(x, \dot{x}, ..., x^{(n-1)})\right\| \leq \vartheta(\|\mathbf{s}\|)$ where $\vartheta(\cdot)$ is some positive function. Thus, $\bar{m}(x, \dot{x}, ..., x^{(n-1)}) \leq \bar{m}(\|s\|)$.

Based on (J.10)-(J.14) and (J.16)-(J.18) the regions D and S can be defined as follows

$$\mathcal{D} = \left\{ s : \|s\| < \rho^{-1}\left(2\sqrt{\lambda_3 \lambda_{\min}(K)}\right)\right\} \tag{J.20}$$

$$\mathcal{S} = \left\{ s \in \mathcal{D} : W_2(s) < \lambda_1\left(\rho^{-1}\left(2\sqrt{\lambda_3 \lambda_{\min}(K)}\right)\right)^2\right\} \tag{J.21}$$

Note that the region of attraction in (J.21) can be made arbitrarily large to include any initial conditions by increasing $\lambda_{\min}(K)$ (i.e., a semi-global stability result). Specifically, (J.13) and (J.21) can be used to calculate the region of attraction as follows

$$\begin{aligned} W_2(s(t_0)) &< \lambda_1\left(\rho^{-1}\left(2\sqrt{\lambda_3 \lambda_{\min}(K)}\right)\right)^2 \\ \Longrightarrow \|s(t_0)\| &< \sqrt{\frac{\lambda_1}{\lambda_2(\|s(t_0)\|)}}\rho^{-1}\left(2\sqrt{\lambda_3 \lambda_{\min}(K)}\right) \end{aligned} \tag{J.22}$$

which can be rearranged as

$$\lambda_{\min}(K) \geq \frac{1}{4\lambda_3}\rho^2\left(\sqrt{\frac{\lambda_2(\|s(t_0)\|)}{\lambda_1}}\|s(t_0)\|\right). \tag{J.23}$$

By utilizing (3.23), (J.3) and (J.11) the following explicit expression for $\|s(t_0)\|$ can be derived as follows

$$\|s(t_0)\|^2 = \sum_{i=1}^{n}\|e_i(t_0)\|^2 + \|r(t_0)\|^2 + \zeta_{b1} + \zeta_{b2} + \|\theta\|^2. \tag{J.24}$$

From (J.10), (J.17), (J.21)-(J.23), it is clear that $V(s,t) \in \mathcal{L}_\infty$ $\forall s(t_0) \in \mathcal{S}$; hence $s(t)$, $z(t)$, $\tilde{\theta}(t) \in \mathcal{L}_\infty$ $\forall s(t_0) \in \mathcal{S}$. From (J.17) it is easy to prove that $e_n(t) \in \mathcal{L}_1$ $\forall s(t_0) \in \mathcal{S}$. From (3.13), it is clear that $\dot{e}_n(t) \in \mathcal{L}_\infty$ $\forall s(t_0) \in \mathcal{S}$. By using (3.4), (3.5) and (3.7), it can be proved that $x^{(i)}(t) \in \mathcal{L}_\infty$, $i = 0, 1, ..., n$, $\forall s(t_0) \in \mathcal{S}$. Then, it is clear that $M(t)$, $\dot{M}(t)$, $f(t) \in \mathcal{L}_\infty$ $\forall s(t_0) \in \mathcal{S}$. The facts that $r(t)$, $\dot{\tilde{\theta}}(t) \in \mathcal{L}_\infty$ $\forall s(t_0) \in \mathcal{S}$ can be used along with (3.31) and (3.29) to prove that $\hat{\theta}(t)$, $\dot{\hat{\theta}}(t) \in \mathcal{L}_\infty$ $\forall s(t_0) \in \mathcal{S}$. After using these boundedness statements along with (3.11) and (3.28), it is clear that $u(t)$, $\dot{u}(t) \in \mathcal{L}_\infty$ $\forall s(t_0) \in \mathcal{S}$. The previous boundedness statements and Remarks 1, 2, 3 can be used along with (3.17), to prove that $\dot{r}(t) \in \mathcal{L}_\infty$ $\forall s(t_0) \in \mathcal{S}$.

These boundedness statements can be used along with the time derivative of (J.18) to prove that $\dot{W}(s(t)) \in \mathcal{L}_\infty \ \forall s(t_0) \in \mathcal{S}$; hence $W(s(t))$ is uniformly continuous. Standard signal chasing algorithms can be used to prove that all remaining signals are bounded. A direct application of Theorem 8.4 in [106] can be used to prove that $\|z(t)\| \to 0$ as $t \to \infty \ \forall s(t_0) \in \mathcal{S}$. Based on the definition of $z(t)$, it is easy to show that $\|e_i(t)\|, \|r(t)\| \to 0$ as $t \to \infty \ \forall s(t_0) \in \mathcal{S}$, $i = 1, 2, ..., n$. From (3.13), it is clear that $\|\dot{e}_n(t)\| \to 0$ as $t \to \infty \ \forall s(t_0) \in \mathcal{S}$. By utilizing (3.7) recursively it can be proven that $\left\|e_1^{(i)}(t)\right\| \to 0$ as $t \to \infty$, $i = 1, 2, ..., n \ \forall s(t_0) \in \mathcal{S}$. ■

Appendix K

Proof of Theorem 8

Proof. The fact that $W_r(t)$ is a function of only $x_r(t)$ and its time derivatives, can be used along with the boundedness expression in (3.5), to show that $W_r(t), \dot{W}_r(t) \in \mathcal{L}_\infty$. After considering the fact that $e_n(t) \in \mathcal{L}_1$ (see the proof of Theorem 7), it is clear that $W_r^T(t)\Lambda e_n(t)$, $\dot{W}_r^T(t) e_n(t) \in \mathcal{L}_1$. This assures the existence of the limits for the first and second terms in (3.26), i.e., $\lim_{t\to\infty} \int_{t_0}^{t} W_r^T(\tau)\Lambda e_n(\tau)\, d\tau$ and $\lim_{t\to\infty} \int_{t_0}^{t} \dot{W}_r^T(\tau) e_n(\tau)\, d\tau$ exist (see Theorem 3.1 of [71]). Based on the fact that $e_n(t) \to 0$ as $t \to \infty$ $\forall s(t_0) \in \mathcal{S}$ (see the proof of Theorem 7) then it is clear that $\lim_{t\to\infty} W_r^T(t) e_n(t) = 0$. Utilizing the above facts along with the fact that $W_r^T(t_0) e_n(t_0)$ is constant, it follows that $\lim_{t\to\infty} \hat{\theta}(t) = \hat{\theta}_\infty$. ■

Appendix L

Proof of Theorem 9

Proof. Let $V(s,t) \in \mathbb{R}$ denotes the following non-negative function

$$V \triangleq \frac{1}{2}\sum_{i=1}^{n} e_i^T e_i + \frac{1}{2} r^T M r + P_1 + V_g \tag{L.1}$$

where $P_1(t)$ was defined in Lemma 3 and $V_g(t) \in \mathbb{R}$ is a non-negative function defined as follows

$$V_g \triangleq \frac{1}{2k_L}\int_{t-T}^{t} \tilde{N}_r^T(\tau)\,\tilde{N}_r(\tau)\,d\tau \tag{L.2}$$

where $s(t)$ is defined as follows

$$s \triangleq \begin{bmatrix} z^T & \sqrt{P_1} & \sqrt{V_g} \end{bmatrix}^T. \tag{L.3}$$

After utilizing (3.2), (L.1) can be bounded as follows

$$W_1(s) \leq V(s,t) \leq W_2(s) \tag{L.4}$$

where $W_1(s)$, $W_2(s) \in \mathbb{R}$ are defined as follows

$$W_1(s) \triangleq \lambda_1 \|s\|^2 \quad , \quad W_2(s) \triangleq \lambda_2(\|s\|)\|s\|^2 \tag{L.5}$$

and $\lambda_1, \lambda_2(\cdot) \in \mathbb{R}$ are defined as follows

$$\lambda_1 \triangleq \frac{1}{2}\min\{1, \underline{m}\} \ , \ \lambda_2 \triangleq \max\left\{1, \frac{1}{2}\bar{m}(\|s\|)\right\}. \tag{L.6}$$

After taking the time derivative of (L.1), the following expression can be obtained

$$\dot{V} = -\sum_{i=1}^{n-1} e_i^T e_i - e_n^T \Lambda e_n + e_{n-1}^T e_n - r^T r + r^T \tilde{N} - r^T K r - \frac{k_L}{2} r^T r \tag{L.7}$$

where (3.6a)-(3.6c), (3.13), (3.46), (3.48) and (J.1) were utilized. By (3.22), (3.32) and the triangle inequality, an upper-bound on (L.7) can be obtained as follows

$$\begin{aligned} \dot{V} &\leq -\lambda_3 \|z\|^2 + \|r\|\rho(\|z\|)\|z\| - \left(\lambda_{\min}(K) + \frac{k_L}{2}\right)\|r\|^2 \\ &\leq -\left(\lambda_4 - \frac{\rho^2(\|z\|)}{4\lambda_{\min}(K)}\right)\|z\|^2 \end{aligned} \tag{L.8}$$

where $\lambda_3 \triangleq \min\left\{\frac{1}{2}, \lambda_{\min}(\Lambda) - \frac{1}{2}\right\}$ and $\lambda_4 \triangleq \min\left\{\lambda_3, \frac{k_L}{2}\right\}$. The following inequality can be developed

$$\dot{V} \leq W(s) \leq \bar{W}(s) \tag{L.9}$$

where $W(s), \bar{W}(s) \in \mathbb{R}$ denote the following non-positive functions

$$W(s) \triangleq -\beta_0 \|z\|^2 \quad , \quad \bar{W}(s) \triangleq -\beta_0 \|e_1\|^2 \tag{L.10}$$

with $\beta_0 \in \mathbb{R}$ being a positive constant, and provided that $\lambda_{\min}(K)$ is selected according to the following sufficient condition

$$\lambda_{\min}(K) \geq \frac{\rho^2(\|z\|)}{4\lambda_4} \text{ or } \|z\| \leq \rho^{-1}\left(2\sqrt{\lambda_4 \lambda_{\min}(K)}\right). \tag{L.11}$$

Based on (L.1)-(L.6) and (L.8)-(L.10), the regions D and S can be defined as follows

$$\mathcal{D} = \left\{s : \|s\| < \rho^{-1}\left(2\sqrt{\lambda_4 \lambda_{\min}(K)}\right)\right\} \tag{L.12}$$

$$\mathcal{S} = \left\{s \in \mathcal{D} : W_2(s) < \lambda_1\left(\rho^{-1}\left(2\sqrt{\lambda_4 \lambda_{\min}(K)}\right)\right)^2\right\} \tag{L.13}$$

Note that the region of attraction in (L.13) can be made arbitrarily large to include any initial conditions by increasing $\lambda_{\min}(K)$ (i.e., a semi-global stability result). Specifically, (L.5) and (L.13) can be used to calculate the region of attraction as follows

$$\begin{aligned} W_2(s(t_0)) &< \lambda_1\left(\rho^{-1}\left(2\sqrt{\lambda_4 \lambda_{\min}(K)}\right)\right)^2 \\ &\implies \|s(t_0)\| < \sqrt{\frac{\lambda_1}{\lambda_2(\|s(t_0)\|)}}\rho^{-1}\left(2\sqrt{\lambda_4 \lambda_{\min}(K)}\right), \end{aligned} \tag{L.14}$$

which can be rearranged as

$$\lambda_{\min}(K) \geq \frac{1}{4\lambda_4}\rho^2\left(\sqrt{\frac{\lambda_2(\|s(t_0)\|)}{\lambda_1}}\|s(t_0)\|\right). \tag{L.15}$$

By utilizing (3.23), (J.3) and (L.3) the following explicit expression for $\|s(t_0)\|$ can be derived as follows

$$\|s(t_0)\|^2 = \sum_{i=1}^{n} \|e_i(t_0)\|^2 + \|r(t_0)\|^2 + \zeta_{b1}. \tag{L.16}$$

From (L.1), (L.9), (L.13)-(L.15), it is clear that $V(s,t) \in \mathcal{L}_\infty \ \forall s(t_0) \in \mathcal{S}$; hence $s(t), z(t) \in \mathcal{L}_\infty \ \forall s(t_0) \in \mathcal{S}$. From (3.13), it is clear that $\dot{e}_n(t) \in \mathcal{L}_\infty \ \forall s(t_0) \in \mathcal{S}$. Using (3.4) and (3.39), it can be proved that $x^{(i)}(t) \in \mathcal{L}_\infty$, $i = 0, 1, ..., n$, $\forall s(t_0) \in \mathcal{S}$. Then, it is clear that $M(t), \dot{M}(t), f(t) \in \mathcal{L}_\infty \ \forall s(t_0) \in \mathcal{S}$. By using these boundedness statements along with (3.11) it is clear that $u(t) \in \mathcal{L}_\infty \ \forall s(t_0) \in \mathcal{S}$. These boundedness statements can be used along with the time derivative of (L.10) to prove that $\dot{\bar{W}}(s(t)) \in \mathcal{L}_\infty \ \forall s(t_0) \in \mathcal{S}$; hence $\bar{W}(s(t))$ is uniformly continuous. A direct application of Theorem 8.4 in [106] can be used to prove that $\|e_1(t)\| \to 0$ as $t \to \infty \ \forall s(t_0) \in \mathcal{S}$. It should be noted that for finite time the subsequent analysis can be easily extended to prove that $\hat{N}_r(t)$, $\dot{u}(t)$, $\dot{r}(t)$, $\tilde{N}_r(t)$ are bounded. ■

Remark 1 *It should be noted that when $\hat{W}_r(t)$ is designed as follows*

$$\hat{W}_r(t) \triangleq \int_{t_0}^{t} \left[Sat_\beta\left(\hat{N}_r(\tau - T)\right) + k_L \Lambda e_n(\tau) \right] d\tau + k_L e_n(t) - k_L e_n(t_0) \qquad \text{(L.17)}$$

where $\hat{N}_r(t)$ was introduced in (3.43) and $Sat_\beta(\cdot) \in \mathbb{R}^m$ is a saturation function vector, then the previous analysis can be modified to prove that $\hat{N}_r(t)$, $\dot{u}(t)$, $\dot{r}(t)$, $\tilde{N}_r(t)$ are bounded for all time and thus $\left\| e_1^{(i)}(t) \right\|$ converge to zero for $i = 1, ..., n$.

Appendix M

Entries of the Inertia Matrix

The entries of the inertia matrix are defined as follows[8]

$$K_{\dot{d}_1\dot{d}_1} = \frac{m}{d\kappa_1^2} r_{20} \tag{M.1}$$

$$K_{\dot{d}_1\dot{d}_2} = \frac{m}{d}\left\{r_8 + r_9 - r_{23} - r_{24}\right\} \tag{M.2}$$

$$K_{\dot{d}_1\dot{d}_3} = \frac{m}{d}\left\{r_{16} + r_{10} - r_{25}\right\} \tag{M.3}$$

$$\begin{aligned} K_{\dot{d}_1\dot{\kappa}_1} &= \frac{m}{d}\left\{-\frac{1}{\kappa_1^3} r_1 - \frac{d_1}{\kappa_2 d_3} r_{23} - \frac{d_1}{\kappa_2\left(d_2+d_3\right)} r_{24} - \frac{2}{\kappa_1^3} r_{20}\right. \\ &\left. -\frac{d_1}{\kappa_3 d_3} r_{25} - d_1 r_4 + \frac{d_1}{\kappa_1}\left[\frac{d_3+d_2}{\kappa_1} - \frac{d_2}{\kappa_2} - \frac{d_3}{\kappa_3}\right]\sin\left(d_1\kappa_1\right)\right\} \end{aligned} \tag{M.4}$$

$$\begin{aligned} K_{\dot{d}_1\dot{\kappa}_2} &= \frac{m}{d}\left\{-\frac{2}{\kappa_2} r_8 - \frac{2}{\kappa_2} r_9 - \frac{d_2}{\kappa_3 d_3} r_{25} - d_2 r_4 + \frac{1}{\kappa_2} r_{24}\right. \\ &\left. + \frac{d_3 - d_2}{\kappa_2 d_3} r_{23} - \frac{1}{\kappa_1} d_2 d_3\left(\frac{1}{\kappa_3} - \frac{1}{\kappa_2}\right)\sin\left(d_1\kappa_1\right)\right\} \end{aligned} \tag{M.5}$$

$$K_{\dot{d}_1\dot{\kappa}_3} = \frac{m}{d}\left\{-\frac{2}{\kappa_3} r_{16} - \frac{2}{\kappa_3} r_{10} + \frac{1}{\kappa_3} r_{25} - d_3 r_4\right\} \tag{M.6}$$

$$K_{\dot{d}_2\dot{d}_2} = \frac{m}{d\kappa_2^2} r_{21} \tag{M.7}$$

$$K_{\dot{d}_2\dot{d}_3} = \frac{m}{d}\left\{r_{26} - r_{11}\right\} \tag{M.8}$$

$$\begin{aligned} K_{\dot{d}_2\dot{\kappa}_1} &= \frac{m}{d}\left\{\frac{1}{\kappa_1} r_{24} + \frac{d_1}{\kappa_2^3} r_5 + \frac{d_1}{\kappa_3 d_3} r_{26} - \frac{d_1}{\kappa_2} r_{13} + \frac{1}{\kappa_1} r_{23} + \frac{d_1}{\kappa_1} r_{13}\right. \\ &-\kappa_1\kappa_2\left(\frac{d_1\left(d_1+d_2+d_3\right)}{\kappa_1} + \frac{1}{\kappa_1^2\kappa_2} - \frac{d_1 d_3}{\kappa_3}\right) r_8 - \frac{1}{\kappa_1} r_9 + \frac{d_1}{\kappa_3^2} r_6 \\ &\left. + \frac{d_1}{\kappa_2}\left(\frac{d_1}{\kappa_1} + \frac{d_2}{\kappa_2}\right)\sin\left(d_1\kappa_2\right) - \frac{d_1\left(d_1+d_2\right)}{\kappa_2\kappa_1}\sin\left(\left(d_1+d_2\right)\kappa_2\right)\right\} \end{aligned} \tag{M.9}$$

$$\begin{aligned} K_{\dot{d}_2\dot{\kappa}_2} &= \frac{m}{d}\left\{\frac{d_2}{\kappa_3 d_3} r_{26} + \frac{d_2}{\kappa_3^2} r_6 - \frac{1}{\kappa_2^3} r_2 - \frac{2}{\kappa_2^3} r_{21}\right. \\ &\left. + d_2 d_3\kappa_1\kappa_2\left(\frac{1}{\kappa_3} - \frac{1}{\kappa_2}\right) r_8\right\} \end{aligned} \tag{M.10}$$

[8]The calculation of the these terms was done by MAPLE 9.5.

$$K_{\dot{d}_2\dot{\kappa}_3} = \frac{m}{d\kappa_3}\left\{\frac{d_3}{\kappa_3}r_6 - r_{26} + 2r_{11}\right\} \tag{M.11}$$

$$K_{\dot{d}_3\dot{d}_3} = \frac{m}{d\kappa_3^2}r_{22} \tag{M.12}$$

$$\begin{aligned} K_{\dot{d}_3\dot{\kappa}_1} &= \frac{m}{d}\left\{\frac{d_1}{\kappa_3^3}r_7 - \frac{1}{\kappa_1}r_{10} - \frac{1}{\kappa_1}r_{16} + \frac{1}{\kappa_1}r_{25}\right. \\ &\quad \left. + d_1\left(\frac{1}{\kappa_1} - \frac{1}{\kappa_3}\right)\left[r_{14} - \frac{d_3}{\kappa_3}\sin\left(\left(d_1+d_2\right)\kappa_3\right)\right]\right\} \end{aligned} \tag{M.13}$$

$$\begin{aligned} K_{\dot{d}_3\dot{\kappa}_2} &= \frac{m}{d}\left\{\frac{d_2}{\kappa_3^3}r_7 - \frac{1}{\kappa_2}r_{26} + \frac{1}{\kappa_2}r_{11}\right. \\ &\quad \left. + d_2\left(\frac{1}{\kappa_2} - \frac{1}{\kappa_3}\right)\left[r_{14} - \frac{d_3}{\kappa_3}\sin\left(\left(d_1+d_2\right)\kappa_3\right)\right]\right\} \end{aligned} \tag{M.14}$$

$$K_{\dot{d}_3\dot{\kappa}_3} = \frac{m}{d\kappa_3^3}\left\{-r_3 - 2r_{22}\right\} \tag{M.15}$$

$$\begin{aligned} K_{\dot{\kappa}_1\dot{\kappa}_1} &= \frac{m}{d}\left\{\frac{d_1}{\kappa_1\kappa_2 d_3}r_{23} + \frac{d_1}{\kappa_1\kappa_2\left(d_2+d_3\right)}r_{24} + \frac{d_1}{\kappa_1\kappa_3 d_3}r_{25} + \frac{d_1}{\kappa_1}r_4\right. \\ &\quad + d_1^2\kappa_1\left(\frac{1}{\kappa_2} - \frac{1}{\kappa_1}\right)r_8 + d_1^2\kappa_1\left(\frac{1}{\kappa_3} - \frac{1}{\kappa_1}\right)r_{16} + \frac{1}{\kappa_1^4}r_1 \\ &\quad + \frac{1}{\kappa_1^4}r_{20} + \frac{d_1}{\kappa_1^2}\left(\frac{d_2}{\kappa_2} + \frac{d_3}{\kappa_3} - \frac{d_2+d_3}{\kappa_1}\right)\sin\left(d_1\kappa_1\right) \\ &\quad \left. + d_1^2\left[\frac{d_2}{\kappa_2^2} - \frac{d_2}{\kappa_1\kappa_2} - \frac{d_3}{\kappa_1\kappa_3} + \frac{d_3}{\kappa_3^2} + \frac{d_3+d_2}{2\kappa_1^2} + \frac{d_1}{6\kappa_1^2}\right]\right\} \end{aligned} \tag{M.16}$$

$$\begin{aligned} K_{\dot{\kappa}_1\dot{\kappa}_2} &= \frac{m}{d}\left\{\left[\frac{d_2+d_3}{\kappa_1^2} + \frac{2d_1}{\kappa_2}\left(\frac{1}{\kappa_2} - \frac{1}{\kappa_1}\right)\right]r_{13} + \frac{d_2}{\kappa_1}r_4 + \frac{d_2}{\kappa_1\kappa_3 d_3}r_{25}\right. \\ &\quad + \frac{2d_2}{\kappa_1\kappa_2 d_3}r_{23} + \left(d_2+d_3\right)r_{17} + d_1d_2\kappa_1\left(\frac{2}{\kappa_3} - \frac{1}{\kappa_2} - \frac{1}{\kappa_1}\right)r_{16} \\ &\quad + \frac{2}{\kappa_1\kappa_2}r_9 + \kappa_1\left[-\frac{d_1d_2}{\kappa_2} + \frac{d_1\left(d_3+d_2\right)}{\kappa_1} - \frac{d_1d_3}{\kappa_3} + \frac{2}{\kappa_1^2\kappa_2}\right]r_8 \\ &\quad - \frac{d_1}{\kappa_2\kappa_3 d_3}r_{26} - \frac{d_1}{\kappa_2\kappa_3^2}r_6 + \frac{d_1}{\kappa_2^4}\cos\left(d_2\kappa_2\right) \\ &\quad - \frac{2d_1d_2}{\kappa_2^2}\left(\frac{1}{\kappa_2} - \frac{1}{\kappa_1}\right)\sin\left(\left(d_1+d_2\right)\kappa_2\right) - \frac{d_2d_3}{\kappa_1^2}\left(\frac{1}{\kappa_2} - \frac{1}{\kappa_3}\right)\sin\left(d_1\kappa_1\right) \\ &\quad \left. - \frac{d_1}{\kappa_2^4} + \frac{d_1d_2^2}{2\kappa_2^2} - d_1d_2d_3\left(\frac{1}{\kappa_1\kappa_3} + \frac{1}{\kappa_2\kappa_3} - \frac{1}{\kappa_1\kappa_2} - \frac{2}{\kappa_3^2}\right)\right\} \end{aligned} \tag{M.17}$$

$$K_{\dot{\kappa}_1\dot{\kappa}_3} = \frac{m}{d}\left\{\frac{2}{\kappa_1\kappa_3}r_{10} + d_3 r_{18} - d_3 r_{15} + \frac{2}{\kappa_1\kappa_3}r_{16} - \frac{d_1}{\kappa_3^4}r_7 \right. \tag{M.18}$$
$$\left. + d_1 d_3\left(\frac{1}{\kappa_1} - \frac{1}{\kappa_3}\right)r_{19} + \frac{2d_1}{\kappa_3}\left(\frac{1}{\kappa_3} - \frac{1}{\kappa_1}\right)r_{14} + \frac{d_1 d_3^2}{2\kappa_3^2}\right\}$$

$$K_{\dot{\kappa}_2\dot{\kappa}_2} = \frac{m}{d}\left\{-\frac{d_2}{\kappa_2\kappa_3 d_3}r_{26} - \frac{d_2}{\kappa_2\kappa_3^2}r_6 - d_2^2\kappa_1\left(\frac{1}{\kappa_2} - \frac{1}{\kappa_3}\right)r_{16}\right.$$
$$+\frac{1}{\kappa_2^4}r_{21} + \frac{1}{\kappa_2^4}r_2 + d_2 d_3\kappa_1\left(\frac{1}{\kappa_2} - \frac{1}{\kappa_3}\right)r_8$$
$$\left. + \frac{d_2^2\left(d_2 + 3d_3\right)}{6\kappa_2^2} + \frac{d_3 d_2^2}{\kappa_3}\left(\frac{1}{\kappa_3} - \frac{1}{\kappa_2}\right)\right\} \tag{M.19}$$

$$K_{\dot{\kappa}_2\dot{\kappa}_3} = \frac{m}{d}\left\{-\frac{d_2}{\kappa_3^4}r_7 - \frac{2d_2}{\kappa_3}\left(\frac{1}{\kappa_2} - \frac{1}{\kappa_3}\right)r_{14} - \frac{d_3}{\kappa_2\kappa_3^2}r_6\right. \tag{M.20}$$
$$\left. + \frac{1}{\kappa_2\kappa_3}r_{26} - \frac{2}{\kappa_2\kappa_3}r_{11} - d_2 d_3\left(\frac{1}{\kappa_3} - \frac{1}{\kappa_2}\right)r_{19} + \frac{d_2 d_3^2}{2\kappa_3^2}\right\}$$

$$K_{\dot{\kappa}_3\dot{\kappa}_3} = \frac{m}{d\kappa_3^2}\left\{\frac{1}{\kappa_3^2}r_3 + \frac{d_3^3}{6} + \frac{1}{\kappa_3^2}r_{22}\right\}. \tag{M.21}$$

The time-varying functions $r_i(t)$, $i = 1, ..., 26$, in (M.1)-(M.21) are introduced to simplify the calculations. They are defined as follows

$$r_1 = d_1\cos\left(d_1\kappa_1\right) - \frac{1}{\kappa_1}\sin\left(d_1\kappa_1\right) \tag{M.22}$$

$$r_2 = d_2\cos\left(d_2\kappa_2\right) - \frac{1}{\kappa_2}\sin\left(d_2\kappa_2\right) \tag{M.23}$$

$$r_3 = d_3\cos\left(d_3\kappa_3\right) - \frac{1}{\kappa_3}\sin\left(d_3\kappa_3\right) \tag{M.24}$$

$$r_4 = \frac{1}{\kappa_1\kappa_3^2}\left[\cos\left(d\kappa_3\right) - \cos\left(d_1\kappa_1 - d\kappa_3\right)\right] \tag{M.25}$$

$$r_5 = 1 - \cos\left(d_2\kappa_2\right) \tag{M.26}$$

$$r_6 = \frac{1}{\kappa_2}\left[\cos\left(\left(d_1 + d_2\right)\kappa_2 - d\kappa_3\right) - \cos\left(d_1\kappa_2 - d\kappa_3\right)\right] \tag{M.27}$$

$$r_7 = 1 - \cos\left(d_3\kappa_3\right) \tag{M.28}$$

$$r_8 = \frac{1}{\kappa_1\kappa_2^2}\left[\sin\left(d_1\kappa_2\right) - \sin\left(\left(d_1 + d_2\right)\kappa_2\right)\right] \tag{M.29}$$

$$r_9 = \frac{1}{\kappa_1\kappa_2^2}\left[\sin\left(d_1\left(\kappa_1-\kappa_2\right)\right)-\sin\left(d_1\kappa_1-\left(d_1+d_2\right)\kappa_2\right)\right] \tag{M.30}$$

$$r_{10} = \frac{1}{\kappa_1\kappa_3^2}\left[\sin\left(d_1\kappa_1-\left(d_1+d_2\right)\kappa_3\right)-\sin\left(d_1\kappa_1-d\kappa_3\right)\right] \tag{M.31}$$

$$\begin{aligned} r_{11} \;=\; & \frac{1}{\kappa_2\kappa_3^2}\left[\sin\left(d_1\kappa_2-\left(d_1+d_2\right)\kappa_3\right)-\sin\left(d_1\kappa_2-d\kappa_3\right)\right. \\ & \left.+\sin\left(\left(d_1+d_2\right)\kappa_2-d\kappa_3\right)-\sin\left(d_1+d_2\right)\left(\kappa_2-\kappa_3\right)\right] \end{aligned} \tag{M.32}$$

$$r_{12} = \frac{1}{\kappa_3^2}\left[\sin\left(\left(d_1+d_2\right)\kappa_3\right)-\sin\left(d\kappa_3\right)\right] \tag{M.33}$$

$$r_{13} = \frac{1}{\kappa_2^2}\left[\cos\left(d_1\kappa_2\right)-\cos\left(\left(d_1+d_2\right)\kappa_2\right)\right] \tag{M.34}$$

$$r_{14} = \frac{1}{\kappa_3^2}\left[\cos\left(\left(d_1+d_2\right)\kappa_3\right)-\cos\left(d\kappa_3\right)\right] \tag{M.35}$$

$$r_{15} = \frac{1}{\kappa_1^2\kappa_3^2}\left[\cos\left(d_1\kappa_1-\left(d_1+d_2\right)\kappa_3\right)+\cos\left(d_1\kappa_1-d\kappa_3\right)\right] \tag{M.36}$$

$$r_{16} = \frac{1}{\kappa_1\kappa_3^2}\left[\sin\left(\left(d_1+d_2\right)\kappa_3\right)-\sin\left(d\kappa_3\right)\right] \tag{M.37}$$

$$r_{17} = \frac{1}{\kappa_1^2\kappa_2^2}\left[\cos\left(\left(d_1+d_2\right)\kappa_2-d_1\kappa_1\right)-\cos\left(d_1\left(\kappa_2-\kappa_1\right)\right)\right] \tag{M.38}$$

$$r_{18} = \frac{1}{\kappa_1^2\kappa_3^2}\left[\cos\left(d\kappa_3\right)+\cos\left(\left(d_1+d_2\right)\kappa_3\right)\right] \tag{M.39}$$

$$r_{19} = \frac{1}{\kappa_3^2}\left[\sin\left(d\kappa_3\right)+\sin\left(\left(d_1+d_2\right)\kappa_3\right)\right] \tag{M.40}$$

$$r_{20} = -\left(d_2+d_3\right)\cos\left(d_1\kappa_1\right)+d_1+d_2+d_3-\frac{1}{\kappa_1}\sin\left(d_1\kappa_1\right) \tag{M.41}$$

$$r_{21} = -d_3\cos\left(d_2\kappa_2\right)+d_2+d_3-\frac{1}{\kappa_2}\sin\left(d_2\kappa_2\right) \tag{M.42}$$

$$r_{22} = d_3-\frac{1}{\kappa_3}\sin\left(d_3\kappa_3\right) \tag{M.43}$$

$$r_{23} = \frac{d_3}{\kappa_1\kappa_2}\left[\cos\left(\left(d_1+d_2\right)\kappa_2\right)-\cos\left(d_1\kappa_1-\left(d_1+d_2\right)\kappa_2\right)\right] \tag{M.44}$$

$$r_{24} = \frac{d_2+d_3}{\kappa_1\kappa_2}\left[\cos\left(d_1\left(\kappa_1-\kappa_2\right)\right)-\cos\left(d_1\kappa_2\right)\right] \tag{M.45}$$

$$r_{25} = \frac{d_3}{\kappa_1\kappa_3}\left[\cos\left(d_1\kappa_1-\left(d_1+d_2\right)\kappa_3\right)-\cos\left(\left(d_1+d_2\right)\kappa_3\right)\right] \tag{M.46}$$

$$r_{26} = \frac{d_3}{\kappa_2\kappa_3}\left[\cos\left(d_1\kappa_2-\left(d_1+d_2\right)\kappa_3\right)-\cos\left(d_1+d_2\right)\left(\kappa_2-\kappa_3\right)\right]. \tag{M.47}$$

Appendix N

Entries of the Centripetal-Coriolis Matrix

The elements of the centripetal-coriolis matrix $V(q, \dot{q})$ are defined as follows

$$V_{11} \triangleq \frac{\partial K_{\dot{d}_1\dot{d}_1}}{\partial d_1}\dot{d}_1 + \frac{\partial K_{\dot{d}_1\dot{d}_1}}{\partial d_2}\dot{d}_2 + \frac{\partial K_{\dot{d}_1\dot{d}_1}}{\partial d_3}\dot{d}_3 + \frac{\partial K_{\dot{d}_1\dot{d}_1}}{\partial \kappa_1}\dot{\kappa}_1 \tag{N.1}$$

$$\begin{aligned} V_{12} \triangleq\ & \frac{\partial K_{\dot{d}_1\dot{d}_2}}{\partial d_2}\dot{d}_2 - \frac{\partial K_{\dot{d}_2\dot{d}_2}}{\partial d_1}\dot{d}_2 + \frac{\partial K_{\dot{d}_1\dot{d}_1}}{\partial d_2}\dot{d}_1 + \frac{\partial K_{\dot{d}_1\dot{d}_2}}{\partial d_3}\dot{d}_3 \\ & + \frac{\partial K_{\dot{d}_1\dot{d}_2}}{\partial \kappa_1}\dot{\kappa}_1 + \frac{\partial K_{\dot{d}_1\dot{d}_2}}{\partial \kappa_2}\dot{\kappa}_2 - \frac{\partial K_{\dot{d}_2\dot{\kappa}_1}}{\partial d_1}\dot{\kappa}_1 - \frac{\partial K_{\dot{d}_2\dot{\kappa}_2}}{\partial d_1}\dot{\kappa}_2 \end{aligned} \tag{N.2}$$

$$\begin{aligned} V_{13} \triangleq\ & \frac{\partial K_{\dot{d}_1\dot{d}_3}}{\partial d_3}\dot{d}_3 - \frac{\partial K_{\dot{d}_3\dot{d}_3}}{\partial d_1}\dot{d}_3 + \frac{\partial K_{\dot{d}_1\dot{d}_1}}{\partial d_3}\dot{d}_1 + \frac{\partial K_{\dot{d}_1\dot{d}_3}}{\partial d_2}\dot{d}_2 \\ & - \frac{\partial K_{\dot{d}_2\dot{d}_3}}{\partial d_1}\dot{d}_2 + \frac{\partial K_{\dot{d}_1\dot{d}_3}}{\partial \kappa_1}\dot{\kappa}_1 + \frac{\partial K_{\dot{d}_1\dot{d}_3}}{\partial \kappa_3}\dot{\kappa}_3 - \frac{\partial K_{\dot{d}_3\dot{\kappa}_1}}{\partial d_1}\dot{\kappa}_1 - \frac{\partial K_{\dot{d}_3\dot{\kappa}_2}}{\partial d_1}\dot{\kappa}_2 \end{aligned} \tag{N.3}$$

$$\begin{aligned} V_{14} \triangleq\ & \frac{\partial K_{\dot{d}_1\dot{\kappa}_1}}{\partial \kappa_1}\dot{\kappa}_1 - \frac{\partial K_{\dot{\kappa}_1\dot{\kappa}_1}}{\partial d_1}\dot{\kappa}_1 + \frac{\partial K_{\dot{d}_1\dot{d}_1}}{\partial \kappa_1}\dot{d}_1 + \frac{\partial K_{\dot{d}_1\dot{\kappa}_1}}{\partial d_2}\dot{d}_2 \\ & + \frac{\partial K_{\dot{d}_1\dot{\kappa}_1}}{\partial d_3}\dot{d}_3 + \frac{\partial K_{\dot{d}_1\dot{\kappa}_1}}{\partial \kappa_2}\dot{\kappa}_2 + \frac{\partial K_{\dot{d}_1\dot{\kappa}_1}}{\partial \kappa_3}\dot{\kappa}_3 - \frac{\partial K_{\dot{\kappa}_1\dot{\kappa}_3}}{\partial d_1}\dot{\kappa}_3 \end{aligned} \tag{N.4}$$

$$\begin{aligned} V_{15} \triangleq\ & \frac{\partial K_{\dot{d}_1\dot{\kappa}_2}}{\partial \kappa_2}\dot{\kappa}_2 - \frac{\partial K_{\dot{\kappa}_2\dot{\kappa}_2}}{\partial d_1}\dot{\kappa}_2 + \frac{\partial K_{\dot{d}_1\dot{\kappa}_2}}{\partial d_2}\dot{d}_2 + \frac{\partial K_{\dot{d}_1\dot{\kappa}_2}}{\partial d_3}\dot{d}_3 \\ & + \frac{\partial K_{\dot{d}_1\dot{\kappa}_2}}{\partial \kappa_1}\dot{\kappa}_1 + \frac{\partial K_{\dot{d}_1\dot{\kappa}_2}}{\partial \kappa_3}\dot{\kappa}_3 - \frac{\partial K_{\dot{\kappa}_1\dot{\kappa}_2}}{\partial d_1}\dot{\kappa}_1 - \frac{\partial K_{\dot{\kappa}_2\dot{\kappa}_3}}{\partial d_1}\dot{\kappa}_3 \end{aligned} \tag{N.5}$$

$$\begin{aligned} V_{16} \triangleq\ & \frac{\partial K_{\dot{d}_1\dot{\kappa}_3}}{\partial \kappa_3}\dot{\kappa}_3 - \frac{\partial K_{\dot{\kappa}_3\dot{\kappa}_3}}{\partial d_1}\dot{\kappa}_3 + \frac{\partial K_{\dot{d}_1\dot{\kappa}_3}}{\partial d_2}\dot{d}_2 + \frac{\partial K_{\dot{d}_1\dot{\kappa}_3}}{\partial d_3}\dot{d}_3 \\ & + \frac{\partial K_{\dot{d}_1\dot{\kappa}_3}}{\partial \kappa_1}\dot{\kappa}_1 - \frac{\partial K_{\dot{d}_2\dot{\kappa}_3}}{\partial d_1}\dot{d}_2 - \frac{\partial K_{\dot{d}_3\dot{\kappa}_3}}{\partial d_1}\dot{d}_3 \end{aligned} \tag{N.6}$$

$$V_{21} \triangleq \frac{\partial K_{\dot{d}_1\dot{d}_2}}{\partial d_1}\dot{d}_1 - \frac{\partial K_{\dot{d}_1\dot{d}_1}}{\partial d_2}\dot{d}_1 + \frac{\partial K_{\dot{d}_2\dot{d}_2}}{\partial d_1}\dot{d}_2 + \frac{\partial K_{\dot{d}_2\dot{\kappa}_1}}{\partial d_1}\dot{\kappa}_1 + \frac{\partial K_{\dot{d}_2\dot{\kappa}_2}}{\partial d_1}\dot{\kappa}_2 \tag{N.7}$$

$$V_{22} \triangleq \frac{\partial K_{\dot{d}_2\dot{d}_2}}{\partial d_1}\dot{d}_1 + \frac{\partial K_{\dot{d}_2\dot{d}_2}}{\partial d_2}\dot{d}_2 + \frac{\partial K_{\dot{d}_2\dot{d}_2}}{\partial d_3}\dot{d}_3 + \frac{\partial K_{\dot{d}_2\dot{d}_2}}{\partial \kappa_2}\dot{\kappa}_2 \tag{N.8}$$

$$
\begin{aligned}
V_{23} \triangleq\ & \frac{\partial K_{\dot{d}_2\dot{d}_3}}{\partial d_3}\dot{d}_3 - \frac{\partial K_{\dot{d}_3\dot{d}_3}}{\partial d_2}\dot{d}_3 + \frac{\partial K_{\dot{d}_2\dot{d}_2}}{\partial d_3}\dot{d}_2 + \frac{\partial K_{\dot{d}_1\dot{d}_2}}{\partial d_3}\dot{d}_1 \\
& + \frac{\partial K_{\dot{d}_2\dot{d}_3}}{\partial d_1}\dot{d}_1 - \frac{\partial K_{\dot{d}_1\dot{d}_3}}{\partial d_2}\dot{d}_1 + \frac{\partial K_{\dot{d}_2\dot{d}_3}}{\partial \kappa_2}\dot{\kappa}_2 + \frac{\partial K_{\dot{d}_2\dot{d}_3}}{\partial \kappa_3}\dot{\kappa}_3 \\
& - \frac{\partial K_{\dot{d}_3\dot{\kappa}_1}}{\partial d_2}\dot{\kappa}_1 - \frac{\partial K_{\dot{d}_3\dot{\kappa}_2}}{\partial d_2}\dot{\kappa}_2 - \frac{\partial K_{\dot{d}_3\dot{\kappa}_3}}{\partial d_2}\dot{\kappa}_3
\end{aligned} \tag{N.9}
$$

$$
\begin{aligned}
V_{24} \triangleq\ & \frac{\partial K_{\dot{d}_2\dot{\kappa}_1}}{\partial \kappa_1}\dot{\kappa}_1 - \frac{\partial K_{\dot{\kappa}_1\dot{\kappa}_1}}{\partial d_2}\dot{\kappa}_1 + \frac{\partial K_{\dot{d}_2\dot{\kappa}_1}}{\partial d_3}\dot{d}_3 + \frac{\partial K_{\dot{d}_2\dot{\kappa}_1}}{\partial \kappa_2}\dot{\kappa}_2 \\
& + \frac{\partial K_{\dot{d}_2\dot{\kappa}_1}}{\partial \kappa_3}\dot{\kappa}_3 + \frac{\partial K_{\dot{d}_1\dot{d}_2}}{\partial \kappa_1}\dot{d}_1 - \frac{\partial K_{\dot{d}_1\dot{\kappa}_1}}{\partial d_2}\dot{d}_1 - \frac{\partial K_{\dot{\kappa}_1\dot{\kappa}_2}}{\partial d_2}\dot{\kappa}_2
\end{aligned} \tag{N.10}
$$

$$
\begin{aligned}
V_{25} \triangleq\ & \frac{\partial K_{\dot{d}_2\dot{\kappa}_2}}{\partial \kappa_2}\dot{\kappa}_2 - \frac{\partial K_{\dot{\kappa}_2\dot{\kappa}_2}}{\partial d_2}\dot{\kappa}_2 + \frac{\partial K_{\dot{d}_2\dot{d}_2}}{\partial \kappa_2}\dot{d}_2 + \frac{\partial K_{\dot{d}_2\dot{\kappa}_2}}{\partial d_3}\dot{d}_3 \\
& + \frac{\partial K_{\dot{d}_2\dot{\kappa}_2}}{\partial \kappa_3}\dot{\kappa}_3 + \frac{\partial K_{\dot{d}_1\dot{d}_2}}{\partial \kappa_2}\dot{d}_1 - \frac{\partial K_{\dot{d}_1\dot{\kappa}_2}}{\partial d_2}\dot{d}_1
\end{aligned} \tag{N.11}
$$

$$
\begin{aligned}
V_{26} \triangleq\ & \frac{\partial K_{\dot{d}_2\dot{\kappa}_3}}{\partial \kappa_3}\dot{\kappa}_3 - \frac{\partial K_{\dot{\kappa}_3\dot{\kappa}_3}}{\partial d_2}\dot{\kappa}_3 + \frac{\partial K_{\dot{d}_2\dot{\kappa}_3}}{\partial d_1}\dot{d}_1 + \frac{\partial K_{\dot{d}_2\dot{\kappa}_3}}{\partial d_3}\dot{d}_3 \\
& + \frac{\partial K_{\dot{d}_2\dot{\kappa}_3}}{\partial \kappa_2}\dot{\kappa}_2 - \frac{\partial K_{\dot{d}_1\dot{\kappa}_3}}{\partial d_2}\dot{d}_1 - \frac{\partial K_{\dot{\kappa}_1\dot{\kappa}_3}}{\partial d_2}\dot{\kappa}_1 - \frac{\partial K_{\dot{\kappa}_2\dot{\kappa}_3}}{\partial d_2}\dot{\kappa}_2
\end{aligned} \tag{N.12}
$$

$$
\begin{aligned}
V_{31} \triangleq\ & \frac{\partial K_{\dot{d}_1\dot{d}_3}}{\partial d_1}\dot{d}_1 - \frac{\partial K_{\dot{d}_1\dot{d}_1}}{\partial d_3}\dot{d}_1 + \frac{\partial K_{\dot{d}_3\dot{d}_3}}{\partial d_1}\dot{d}_3 \\
& + \frac{\partial K_{\dot{d}_2\dot{d}_3}}{\partial d_1}\dot{d}_2 + \frac{\partial K_{\dot{d}_3\dot{\kappa}_1}}{\partial d_1}\dot{\kappa}_1 + \frac{\partial K_{\dot{d}_3\dot{\kappa}_2}}{\partial d_1}\dot{\kappa}_2
\end{aligned} \tag{N.13}
$$

$$
\begin{aligned}
V_{32} \triangleq\ & \frac{\partial K_{\dot{d}_2\dot{d}_3}}{\partial d_2}\dot{d}_2 - \frac{\partial K_{\dot{d}_2\dot{d}_2}}{\partial d_3}\dot{d}_2 + \frac{\partial K_{\dot{d}_3\dot{d}_3}}{\partial d_2}\dot{d}_3 + \frac{\partial K_{\dot{d}_1\dot{d}_3}}{\partial d_2}\dot{d}_1 \\
& - \frac{\partial K_{\dot{d}_1\dot{d}_2}}{\partial d_3}\dot{d}_1 + \frac{\partial K_{\dot{d}_3\dot{\kappa}_1}}{\partial d_2}\dot{\kappa}_1 + \frac{\partial K_{\dot{d}_3\dot{\kappa}_2}}{\partial d_2}\dot{\kappa}_2 + \frac{\partial K_{\dot{d}_3\dot{\kappa}_3}}{\partial d_2}\dot{\kappa}_3
\end{aligned} \tag{N.14}
$$

$$
V_{33} \triangleq \frac{\partial K_{\dot{d}_3\dot{d}_3}}{\partial d_1}\dot{d}_1 + \frac{\partial K_{\dot{d}_3\dot{d}_3}}{\partial d_2}\dot{d}_2 + \frac{\partial K_{\dot{d}_3\dot{d}_3}}{\partial d_3}\dot{d}_3 + \frac{\partial K_{\dot{d}_3\dot{d}_3}}{\partial \kappa_3}\dot{\kappa}_3 \tag{N.15}
$$

$$
\begin{aligned}
V_{34} \triangleq\ & \frac{\partial K_{\dot{d}_3\dot{\kappa}_1}}{\partial \kappa_1}\dot{\kappa}_1 - \frac{\partial K_{\dot{\kappa}_1\dot{\kappa}_1}}{\partial d_3}\dot{\kappa}_1 + \frac{\partial K_{\dot{d}_3\dot{\kappa}_1}}{\partial \kappa_3}\dot{\kappa}_3 + \frac{\partial K_{\dot{d}_1\dot{d}_3}}{\partial \kappa_1}\dot{d}_1 \\
& - \frac{\partial K_{\dot{d}_1\dot{\kappa}_1}}{\partial d_3}\dot{d}_1 - \frac{\partial K_{\dot{d}_2\dot{\kappa}_1}}{\partial d_3}\dot{d}_2 - \frac{\partial K_{\dot{\kappa}_1\dot{\kappa}_2}}{\partial d_3}\dot{\kappa}_2
\end{aligned} \tag{N.16}
$$

$$V_{35} \triangleq \frac{\partial K_{\dot{d}_3\dot{\kappa}_2}}{\partial \kappa_2}\dot{\kappa}_2 - \frac{\partial K_{\dot{\kappa}_2\dot{\kappa}_2}}{\partial d_3}\dot{\kappa}_2 + \frac{\partial K_{\dot{d}_3\dot{\kappa}_2}}{\partial \kappa_3}\dot{\kappa}_3 - \frac{\partial K_{\dot{d}_1\dot{\kappa}_2}}{\partial d_3}\dot{d}_1 + \frac{\partial K_{\dot{d}_2\dot{d}_3}}{\partial \kappa_2}\dot{d}_2 - \frac{\partial K_{\dot{d}_2\dot{\kappa}_2}}{\partial d_3}\dot{d}_2 - \frac{\partial K_{\dot{\kappa}_2\dot{\kappa}_3}}{\partial d_3}\dot{\kappa}_3 \tag{N.17}$$

$$V_{36} \triangleq \frac{\partial K_{\dot{d}_3\dot{\kappa}_3}}{\partial \kappa_3}\dot{\kappa}_3 - \frac{\partial K_{\dot{\kappa}_3\dot{\kappa}_3}}{\partial d_3}\dot{\kappa}_3 + \frac{\partial K_{\dot{d}_3\dot{d}_3}}{\partial \kappa_3}\dot{d}_3 + \frac{\partial K_{\dot{d}_3\dot{\kappa}_3}}{\partial d_1}\dot{d}_1 + \frac{\partial K_{\dot{d}_1\dot{d}_3}}{\partial \kappa_3}\dot{d}_1 - \frac{\partial K_{\dot{d}_1\dot{\kappa}_3}}{\partial d_3}\dot{d}_1 + \frac{\partial K_{\dot{d}_2\dot{d}_3}}{\partial \kappa_3}\dot{d}_2 - \frac{\partial K_{\dot{d}_2\dot{\kappa}_3}}{\partial d_3}\dot{d}_2 - \frac{\partial K_{\dot{\kappa}_1\dot{\kappa}_3}}{\partial d_3}\dot{\kappa}_1 \tag{N.18}$$

$$V_{41} \triangleq \frac{\partial K_{\dot{d}_1\dot{\kappa}_1}}{\partial d_1}\dot{d}_1 - \frac{\partial K_{\dot{d}_1\dot{d}_1}}{\partial \kappa_1}\dot{d}_1 + \frac{\partial K_{\dot{\kappa}_1\dot{\kappa}_1}}{\partial d_1}\dot{\kappa}_1 + \frac{\partial K_{\dot{\kappa}_1\dot{\kappa}_3}}{\partial d_1}\dot{\kappa}_3 \tag{N.19}$$

$$V_{42} \triangleq \frac{\partial K_{\dot{d}_2\dot{\kappa}_1}}{\partial d_2}\dot{d}_2 + \frac{\partial K_{\dot{\kappa}_1\dot{\kappa}_1}}{\partial d_2}\dot{\kappa}_1 - \frac{\partial K_{\dot{d}_1\dot{d}_2}}{\partial \kappa_1}\dot{d}_1 + \frac{\partial K_{\dot{d}_1\dot{\kappa}_1}}{\partial d_2}\dot{d}_1 + \frac{\partial K_{\dot{d}_2\dot{\kappa}_1}}{\partial d_1}\dot{d}_1 + \frac{\partial K_{\dot{\kappa}_1\dot{\kappa}_2}}{\partial d_2}\dot{\kappa}_2 \tag{N.20}$$

$$V_{43} \triangleq \frac{\partial K_{\dot{d}_3\dot{\kappa}_1}}{\partial d_3}\dot{d}_3 + \frac{\partial K_{\dot{\kappa}_1\dot{\kappa}_1}}{\partial d_3}\dot{\kappa}_1 - \frac{\partial K_{\dot{d}_1\dot{d}_3}}{\partial \kappa_1}\dot{d}_1 + \frac{\partial K_{\dot{d}_1\dot{\kappa}_1}}{\partial d_3}\dot{d}_1 + \frac{\partial K_{\dot{d}_2\dot{\kappa}_1}}{\partial d_3}\dot{d}_2 + \frac{\partial K_{\dot{d}_3\dot{\kappa}_1}}{\partial d_1}\dot{d}_1 + \frac{\partial K_{\dot{d}_3\dot{\kappa}_1}}{\partial d_2}\dot{d}_2 + \frac{\partial K_{\dot{\kappa}_1\dot{\kappa}_2}}{\partial d_3}\dot{\kappa}_2 \tag{N.21}$$

$$V_{44} \triangleq \frac{\partial K_{\dot{\kappa}_1\dot{\kappa}_1}}{\partial d_1}\dot{d}_1 + \frac{\partial K_{\dot{\kappa}_1\dot{\kappa}_1}}{\partial d_2}\dot{d}_2 + \frac{\partial K_{\dot{\kappa}_1\dot{\kappa}_1}}{\partial d_3}\dot{d}_3 + \frac{\partial K_{\dot{\kappa}_1\dot{\kappa}_1}}{\partial \kappa_1}\dot{\kappa}_1 + \frac{\partial K_{\dot{\kappa}_1\dot{\kappa}_1}}{\partial \kappa_2}\dot{\kappa}_2 + \frac{\partial K_{\dot{\kappa}_1\dot{\kappa}_1}}{\partial \kappa_3}\dot{\kappa}_3 \tag{N.22}$$

$$V_{45} \triangleq \frac{\partial K_{\dot{\kappa}_1\dot{\kappa}_2}}{\partial \kappa_2}\dot{\kappa}_2 + \frac{\partial K_{\dot{\kappa}_1\dot{\kappa}_1}}{\partial \kappa_2}\dot{\kappa}_1 + \frac{\partial K_{\dot{\kappa}_1\dot{\kappa}_2}}{\partial \kappa_3}\dot{\kappa}_3 + \frac{\partial K_{\dot{\kappa}_1\dot{\kappa}_2}}{\partial d_1}\dot{d}_1 + \frac{\partial K_{\dot{d}_1\dot{\kappa}_1}}{\partial \kappa_2}\dot{d}_1 - \frac{\partial K_{\dot{d}_1\dot{\kappa}_2}}{\partial \kappa_1}\dot{d}_1 + \frac{\partial K_{\dot{d}_2\dot{\kappa}_1}}{\partial \kappa_2}\dot{d}_2 \tag{N.23}$$

$$V_{46} \triangleq \frac{\partial K_{\dot{\kappa}_1\dot{\kappa}_3}}{\partial \kappa_3}\dot{\kappa}_3 + \frac{\partial K_{\dot{\kappa}_1\dot{\kappa}_1}}{\partial \kappa_3}\dot{\kappa}_1 + \frac{\partial K_{\dot{\kappa}_1\dot{\kappa}_3}}{\partial d_2}\dot{d}_2 + \frac{\partial K_{\dot{\kappa}_1\dot{\kappa}_3}}{\partial d_3}\dot{d}_3 + \frac{\partial K_{\dot{d}_1\dot{\kappa}_1}}{\partial \kappa_3}\dot{d}_1 - \frac{\partial K_{\dot{d}_1\dot{\kappa}_3}}{\partial \kappa_1}\dot{d}_1 + \frac{\partial K_{\dot{d}_2\dot{\kappa}_1}}{\partial \kappa_3}\dot{d}_2 + \frac{\partial K_{\dot{d}_3\dot{\kappa}_1}}{\partial \kappa_3}\dot{d}_3 \tag{N.24}$$

$$V_{51} \triangleq \frac{\partial K_{\dot{d}_1\dot{\kappa}_2}}{\partial d_1}\dot{d}_1 + \frac{\partial K_{\dot{\kappa}_2\dot{\kappa}_2}}{\partial d_1}\dot{\kappa}_2 + \frac{\partial K_{\dot{\kappa}_1\dot{\kappa}_2}}{\partial d_1}\dot{\kappa}_1 + \frac{\partial K_{\dot{\kappa}_2\dot{\kappa}_3}}{\partial d_1}\dot{\kappa}_3 \tag{N.25}$$

$$V_{52} \triangleq \frac{\partial K_{\dot{d}_2\dot{\kappa}_2}}{\partial d_2}\dot{d}_2 - \frac{\partial K_{\dot{d}_2\dot{d}_2}}{\partial \kappa_2}\dot{d}_2 + \frac{\partial K_{\dot{\kappa}_2\dot{\kappa}_2}}{\partial d_2}\dot{\kappa}_2 - \frac{\partial K_{\dot{d}_1\dot{d}_2}}{\partial \kappa_2}\dot{d}_1 + \frac{\partial K_{\dot{d}_1\dot{\kappa}_2}}{\partial d_2}\dot{d}_1 + \frac{\partial K_{\dot{d}_2\dot{\kappa}_2}}{\partial d_1}\dot{d}_1 \quad \text{(N.26)}$$

$$V_{53} \triangleq \frac{\partial K_{\dot{d}_3\dot{\kappa}_2}}{\partial d_3}\dot{d}_3 + \frac{\partial K_{\dot{\kappa}_2\dot{\kappa}_2}}{\partial d_3}\dot{\kappa}_2 + \frac{\partial K_{\dot{d}_1\dot{\kappa}_2}}{\partial d_3}\dot{d}_1 - \frac{\partial K_{\dot{d}_2\dot{d}_3}}{\partial \kappa_2}\dot{d}_2 + \frac{\partial K_{\dot{d}_2\dot{\kappa}_2}}{\partial d_3}\dot{d}_2 + \frac{\partial K_{\dot{d}_3\dot{\kappa}_2}}{\partial d_1}\dot{d}_1 + \frac{\partial K_{\dot{d}_3\dot{\kappa}_2}}{\partial d_2}\dot{d}_2 + \frac{\partial K_{\dot{\kappa}_2\dot{\kappa}_3}}{\partial d_3}\dot{\kappa}_3 \quad \text{(N.27)}$$

$$V_{54} \triangleq \frac{\partial K_{\dot{\kappa}_1\dot{\kappa}_2}}{\partial \kappa_1}\dot{\kappa}_1 - \frac{\partial K_{\dot{\kappa}_1\dot{\kappa}_1}}{\partial \kappa_2}\dot{\kappa}_1 - \frac{\partial K_{\dot{d}_1\dot{\kappa}_1}}{\partial \kappa_2}\dot{d}_1 + \frac{\partial K_{\dot{d}_1\dot{\kappa}_2}}{\partial \kappa_1}\dot{d}_1 - \frac{\partial K_{\dot{d}_2\dot{\kappa}_1}}{\partial \kappa_2}\dot{d}_2 + \frac{\partial K_{\dot{\kappa}_1\dot{\kappa}_2}}{\partial d_2}\dot{d}_2 + \frac{\partial K_{\dot{\kappa}_1\dot{\kappa}_2}}{\partial d_3}\dot{d}_3 \quad \text{(N.28)}$$

$$V_{55} \triangleq \frac{\partial K_{\dot{\kappa}_2\dot{\kappa}_2}}{\partial d_1}\dot{d}_1 + \frac{\partial K_{\dot{\kappa}_2\dot{\kappa}_2}}{\partial d_2}\dot{d}_2 + \frac{\partial K_{\dot{\kappa}_2\dot{\kappa}_2}}{\partial d_3}\dot{d}_3 + \frac{\partial K_{\dot{\kappa}_2\dot{\kappa}_2}}{\partial \kappa_2}\dot{\kappa}_2 + \frac{\partial K_{\dot{\kappa}_2\dot{\kappa}_2}}{\partial \kappa_3}\dot{\kappa}_3 \quad \text{(N.29)}$$

$$V_{56} \triangleq \frac{\partial K_{\dot{\kappa}_2\dot{\kappa}_3}}{\partial \kappa_3}\dot{\kappa}_3 + \frac{\partial K_{\dot{\kappa}_2\dot{\kappa}_2}}{\partial \kappa_3}\dot{\kappa}_2 + \frac{\partial K_{\dot{\kappa}_1\dot{\kappa}_2}}{\partial \kappa_3}\dot{\kappa}_1 + \frac{\partial K_{\dot{\kappa}_2\dot{\kappa}_3}}{\partial d_2}\dot{d}_2 + \frac{\partial K_{\dot{d}_1\dot{\kappa}_2}}{\partial \kappa_3}\dot{d}_1 + \frac{\partial K_{\dot{d}_2\dot{\kappa}_2}}{\partial \kappa_3}\dot{d}_2 - \frac{\partial K_{\dot{d}_2\dot{\kappa}_3}}{\partial \kappa_2}\dot{d}_2 + \frac{\partial K_{\dot{d}_3\dot{\kappa}_2}}{\partial \kappa_3}\dot{d}_3 \quad \text{(N.30)}$$

$$V_{61} \triangleq \frac{\partial K_{\dot{d}_1\dot{\kappa}_3}}{\partial d_1}\dot{d}_1 + \frac{\partial K_{\dot{\kappa}_3\dot{\kappa}_3}}{\partial d_1}\dot{\kappa}_3 + \frac{\partial K_{\dot{d}_2\dot{\kappa}_3}}{\partial d_1}\dot{d}_2 + \frac{\partial K_{\dot{d}_3\dot{\kappa}_3}}{\partial d_1}\dot{d}_3 \quad \text{(N.31)}$$

$$V_{62} \triangleq \frac{\partial K_{\dot{d}_2\dot{\kappa}_3}}{\partial d_2}\dot{d}_2 + \frac{\partial K_{\dot{\kappa}_3\dot{\kappa}_3}}{\partial d_2}\dot{\kappa}_3 + \frac{\partial K_{\dot{d}_1\dot{\kappa}_3}}{\partial d_2}\dot{d}_1 + \frac{\partial K_{\dot{\kappa}_1\dot{\kappa}_3}}{\partial d_2}\dot{\kappa}_1 + \frac{\partial K_{\dot{\kappa}_2\dot{\kappa}_3}}{\partial d_2}\dot{\kappa}_2 \quad \text{(N.32)}$$

$$V_{63} \triangleq \frac{\partial K_{\dot{d}_3\dot{\kappa}_3}}{\partial d_3}\dot{d}_3 - \frac{\partial K_{\dot{d}_3\dot{d}_3}}{\partial \kappa_3}\dot{d}_3 + \frac{\partial K_{\dot{\kappa}_3\dot{\kappa}_3}}{\partial d_3}\dot{\kappa}_3 - \frac{\partial K_{\dot{d}_1\dot{d}_3}}{\partial \kappa_3}\dot{d}_1 + \frac{\partial K_{\dot{d}_1\dot{\kappa}_3}}{\partial d_3}\dot{d}_1 - \frac{\partial K_{\dot{d}_2\dot{d}_3}}{\partial \kappa_3}\dot{d}_2 + \frac{\partial K_{\dot{d}_2\dot{\kappa}_3}}{\partial d_3}\dot{d}_2 + \frac{\partial K_{\dot{d}_3\dot{\kappa}_3}}{\partial d_2}\dot{d}_2 + \frac{\partial K_{\dot{\kappa}_1\dot{\kappa}_3}}{\partial d_3}\dot{\kappa}_1 \quad \text{(N.33)}$$

$$V_{64} \triangleq \frac{\partial K_{\dot{\kappa}_1\dot{\kappa}_3}}{\partial \kappa_1}\dot{\kappa}_1 - \frac{\partial K_{\dot{\kappa}_1\dot{\kappa}_1}}{\partial \kappa_3}\dot{\kappa}_1 - \frac{\partial K_{\dot{d}_1\dot{\kappa}_1}}{\partial \kappa_3}\dot{d}_1 + \frac{\partial K_{\dot{d}_1\dot{\kappa}_3}}{\partial \kappa_1}\dot{d}_1 - \frac{\partial K_{\dot{d}_2\dot{\kappa}_1}}{\partial \kappa_3}\dot{d}_2 - \frac{\partial K_{\dot{d}_3\dot{\kappa}_1}}{\partial \kappa_3}\dot{d}_3 + \frac{\partial K_{\dot{\kappa}_1\dot{\kappa}_3}}{\partial d_1}\dot{d}_1 \quad \text{(N.34)}$$

$$V_{65} \triangleq \frac{\partial K_{\dot{\kappa}_2\dot{\kappa}_3}}{\partial \kappa_2}\dot{\kappa}_2 - \frac{\partial K_{\dot{\kappa}_2\dot{\kappa}_2}}{\partial \kappa_3}\dot{\kappa}_2 - \frac{\partial K_{\dot{\kappa}_1\dot{\kappa}_2}}{\partial \kappa_3}\dot{\kappa}_1 - \frac{\partial K_{\dot{d}_1\dot{\kappa}_2}}{\partial \kappa_3}\dot{d}_1 - \frac{\partial K_{\dot{d}_2\dot{\kappa}_2}}{\partial \kappa_3}\dot{d}_2 + \frac{\partial K_{\dot{d}_2\dot{\kappa}_3}}{\partial \kappa_2}\dot{d}_2 - \frac{\partial K_{\dot{d}_3\dot{\kappa}_2}}{\partial \kappa_3}\dot{d}_3 + \frac{\partial K_{\dot{\kappa}_2\dot{\kappa}_3}}{\partial d_1}\dot{d}_1 + \frac{\partial K_{\dot{\kappa}_2\dot{\kappa}_3}}{\partial d_3}\dot{d}_3 \quad \text{(N.35)}$$

$$V_{66} \triangleq \frac{\partial K_{\dot{\kappa}_3\dot{\kappa}_3}}{\partial d_1}\dot{d}_1 + \frac{\partial K_{\dot{\kappa}_3\dot{\kappa}_3}}{\partial d_2}\dot{d}_2 + \frac{\partial K_{\dot{\kappa}_3\dot{\kappa}_3}}{\partial d_3}\dot{d}_3 + \frac{\partial K_{\dot{\kappa}_3\dot{\kappa}_3}}{\partial \kappa_3}\dot{\kappa}_3. \quad \text{(N.36)}$$

Appendix O

Entries of $G(q)$, $B(q)$, and $E(q)$

Gravitational Terms

The entries of $G(q)$ are given as follows

$$\begin{aligned}
G_1 \triangleq\ & \frac{mg}{d}\left\{\frac{1}{\kappa_1}\left[\cos\left(d_1\kappa_1\right)-\cos\left(2d_1\kappa_1\right)\right]\right. \\
& +\frac{1}{\kappa_2}\left[\cos\left(\left(d_1+d_2\right)\kappa_2\right)-\cos\left(2\left(d_1+d_2\right)\kappa_2\right)-\cos\left(d_1\kappa_2\right)+\cos\left(2d_1\kappa_2\right)\right] \\
& +\frac{1}{\kappa_3}\left[\cos\left(\left(d_1+d_2+d_3\right)\kappa_3\right)-\cos\left(2\left(d_1+d_2+d_3\right)\kappa_3\right)\right. \\
& \left.\left.-\cos\left(\left(d_1+d_2\right)\kappa_3\right)+\cos\left(2\left(d_1+d_2\right)\kappa_3\right)\right]\right\} \\
& -\frac{mg}{d^2}\left\{\frac{1}{\kappa_1^2}\left[\sin\left(d_1\kappa_1\right)-\frac{1}{2}\sin\left(2d_1\kappa_1\right)\right]\right. \\
& +\frac{1}{\kappa_2^2}\left[\sin\left(\left(d_1+d_2\right)\kappa_2\right)-\frac{1}{2}\sin\left(2\left(d_1+d_2\right)\kappa_2\right)-\sin\left(d_1\kappa_2\right)\right. \\
& \left.+\frac{1}{2}\sin\left(2d_1\kappa_2\right)\right]+\frac{1}{\kappa_3^2}\left[\sin\left(\left(d_1+d_2+d_3\right)\kappa_3\right)\right. \\
& -\frac{1}{2}\sin\left(2\left(d_1+d_2+d_3\right)\kappa_3\right) \\
& \left.\left.\left.-\sin\left(\left(d_1+d_2\right)\kappa_3\right)+\frac{1}{2}\sin\left(2\left(d_1+d_2\right)\kappa_3\right)\right]\right\}
\end{aligned}$$

$$\begin{aligned}
G_2 \triangleq\ & \frac{mg}{d}\left\{\frac{1}{\kappa_2}\left[\cos\left(\left(d_1+d_2\right)\kappa_2\right)-\cos\left(2\left(d_1+d_2\right)\kappa_2\right)\right]\right. \\
& +\frac{1}{\kappa_3}\left[\cos\left(\left(d_1+d_2+d_3\right)\kappa_3\right)-\cos\left(2\left(d_1+d_2+d_3\right)\kappa_3\right)\right. \\
& \left.\left.-\cos\left(\left(d_1+d_2\right)\kappa_3\right)+\cos\left(2\left(d_1+d_2\right)\kappa_3\right)\right]\right\} \\
& -\frac{mg}{d^2}\left\{\frac{1}{\kappa_1^2}\left[\sin\left(d_1\kappa_1\right)-\frac{1}{2}\sin\left(2d_1\kappa_1\right)\right]\right. \\
& +\frac{1}{\kappa_2^2}\left[\sin\left(\left(d_1+d_2\right)\kappa_2\right)-\frac{1}{2}\sin\left(2\left(d_1+d_2\right)\kappa_2\right)-\sin\left(d_1\kappa_2\right)+\frac{1}{2}\sin\left(2d_1\kappa_2\right)\right] \\
& +\frac{1}{\kappa_3^2}\left[\sin\left(\left(d_1+d_2+d_3\right)\kappa_3\right)-\frac{1}{2}\sin\left(2\left(d_1+d_2+d_3\right)\kappa_3\right)\right. \\
& \left.\left.-\sin\left(\left(d_1+d_2\right)\kappa_3\right)+\frac{1}{2}\sin\left(2\left(d_1+d_2\right)\kappa_3\right)\right]\right\}
\end{aligned}$$

$$
\begin{aligned}
G_3 \triangleq\ & \frac{mg}{d}\frac{1}{\kappa_3}\left[\cos\left(\left(d_1+d_2+d_3\right)\kappa_3\right)-\cos\left(2\left(d_1+d_2+d_3\right)\kappa_3\right)\right] \\
& -\frac{mg}{d^2}\left\{\frac{1}{\kappa_1^2}\left[\sin\left(d_1\kappa_1\right)-\frac{1}{2}\sin\left(2d_1\kappa_1\right)\right]\right. \\
& +\frac{1}{\kappa_2^2}\left[\sin\left(\left(d_1+d_2\right)\kappa_2\right)-\frac{1}{2}\sin\left(2\left(d_1+d_2\right)\kappa_2\right)-\sin\left(d_1\kappa_2\right)+\frac{1}{2}\sin\left(2d_1\kappa_2\right)\right] \\
& +\frac{1}{\kappa_3^2}\left[\sin\left(\left(d_1+d_2+d_3\right)\kappa_3\right)-\frac{1}{2}\sin\left(2\left(d_1+d_2+d_3\right)\kappa_3\right)\right. \\
& \left.\left.-\sin\left(\left(d_1+d_2\right)\kappa_3\right)+\frac{1}{2}\sin\left(2\left(d_1+d_2\right)\kappa_3\right)\right]\right\}
\end{aligned}
$$

$$
G_4 \triangleq -\frac{2mg}{d\kappa_1^3}\left[\sin\left(d_1\kappa_1\right)-\frac{1}{2}\sin\left(2d_1\kappa_1\right)\right]+\frac{mgd_1}{\kappa_1^2}\left[\cos\left(d_1\kappa_1\right)-\sin\left(2d_1\kappa_1\right)\right]
$$

$$
\begin{aligned}
G_5 \triangleq\ & -\frac{2mg}{d\kappa_2^3}\left[\sin\left(\left(d_1+d_2\right)\kappa_2\right)-\frac{1}{2}\sin\left(2\left(d_1+d_2\right)\kappa_2\right)\right. \\
& \left.-\sin\left(d_1\kappa_2\right)+\frac{1}{2}\sin\left(2d_1\kappa_2\right)\right] \\
& +\frac{mg}{d\kappa_2^2}\left\{\left(d_1+d_2\right)\left[\cos\left(\left(d_1+d_2\right)\kappa_2\right)-\cos\left(2\left(d_1+d_2\right)\kappa_2\right)\right]\right. \\
& \left.-d_1\left[\cos\left(d_1\kappa_2\right)-\cos\left(2d_1\kappa_2\right)\right]\right\}
\end{aligned}
$$

$$
\begin{aligned}
G_6 \triangleq\ & -\frac{2mg}{d\kappa_3^3}\left[\sin\left(\left(d_1+d_2+d_3\right)\kappa_3\right)-\frac{1}{2}\sin\left(2\left(d_1+d_2+d_3\right)\kappa_3\right)\right. \\
& \left.-\sin\left(\left(d_1+d_2\right)\kappa_3\right)+\frac{1}{2}\sin\left(2\left(d_1+d_2\right)\kappa_3\right)\right] \\
& +\frac{mg}{d\kappa_3^2}\left\{\left(d_1+d_2+d_3\right)\left[\cos\left(\left(d_1+d_2+d_3\right)\kappa_3\right)-\cos\left(2\left(d_1+d_2+d_3\right)\kappa_3\right)\right]\right. \\
& \left.-\left(d_1+d_2\right)\left[\cos\left(\left(d_1+d_2\right)\kappa_3\right)-\cos\left(2\left(d_1+d_2\right)\kappa_3\right)\right]\right\}
\end{aligned}
$$

Bending Terms

The entries of $B\left(q\right)$ are given as follows

$$
\begin{aligned}
B_1 =\ & \frac{1}{2}k_{b1}\left(\pi-\frac{1}{2}d_1\kappa_1\right)^2+\frac{1}{2}k_{b2}\left\{\left(\pi-\frac{1}{2}\left(d_1+d_2\right)\kappa_2\right)^2-\left(\pi-\frac{1}{2}d_1\kappa_2\right)^2\right\} \\
& +\frac{1}{2}k_{b3}\left\{\left(\pi-\frac{1}{2}\left(d_1+d_2+d_3\right)\kappa_3\right)^2-\left(\pi-\frac{1}{2}\left(d_1+d_2\right)\kappa_3\right)^2\right\}
\end{aligned}
$$

$$\begin{aligned} B_2 &= \frac{1}{2}k_{b2}\left(\pi - \frac{1}{2}\left(d_1+d_2\right)\kappa_2\right)^2 \\ &\quad + \frac{1}{2}k_{b3}\left\{\left(\pi - \frac{1}{2}\left(d_1+d_2+d_3\right)\kappa_3\right)^2 - \left(\pi - \frac{1}{2}\left(d_1+d_2\right)\kappa_3\right)^2\right\} \end{aligned}$$

$$B_3 = \frac{1}{2}k_{b3}\left(\pi - \frac{1}{2}\left(d_1+d_2+d_3\right)\kappa_3\right)^2$$

$$B_4\left(t\right) = \frac{1}{2}k_{b1}\left[-\frac{1}{2}\pi d_1^2 + \frac{1}{6}\pi d_1^3\kappa_1\right]$$

$$B_5\left(t\right) = \frac{1}{2}k_{b2}\left\{\left[-\frac{1}{2}\pi\left(d_1+d_2\right)^2 + \frac{1}{6}\pi\left(d_1+d_2\right)^3\kappa_2\right] - \left[-\frac{1}{2}\pi d_1^2 + \frac{1}{6}\pi d_1^3\kappa_2\right]\right\}$$

$$\begin{aligned} B_6\left(t\right) &= \frac{1}{2}k_{b3}\left\{\left[-\frac{1}{2}\pi\left(d_1+d_2+d_3\right)^2 + \frac{1}{6}\pi\left(d_1+d_2+d_3\right)^3\kappa_3\right]\right. \\ &\quad \left. - \left[-\frac{1}{2}\pi\left(d_1+d_2\right)^2 + \frac{1}{6}\pi\left(d_1+d_2\right)^3\kappa_3\right]\right\} \end{aligned}$$

Extension Terms

The entries of $E\left(q\right)$ are given as follows

$$E_1 = k_{e1}\left(d_1\left(t\right) - d_1^*\right)$$

$$E_2 = k_{e2}\left(d_2\left(t\right) - d_2^*\right)$$

$$E_3 = k_{e3}\left(d_3\left(t\right) - d_3^*\right)$$

$$E_4 = 0,\ E_5 = 0,\ E_6 = 0$$

Appendix P

Skew-Symmetry Property

For $\left(\dot{M}-2V\right)$ to be skew-symmetric, the following should be satisfied

$$\left(\dot{M}-2V\right)+\left(\dot{M}-2V\right)^{T}=0_{6\times 6} \tag{P.1}$$

where $0_{6\times 6}\in\mathbb{R}^{6\times 6}$ is a matrix of zeros. Since the inertia matrix is symmetric, the following can be obtained

$$\dot{M}=V+V^{T} \tag{P.2}$$

where (P.1) is utilized. From (P.2), for $\left(\dot{M}-2V\right)$ to be skew-symmetric the following conditions for diagonal and off-diagonal elements should be satisfied

$$\dot{M}_{ii}=2V_{ii}\quad,\quad i=1,...,6 \tag{P.3}$$

$$\dot{M}_{ji}=V_{ij}+V_{ji}\quad,\quad j=1,...,(i-1)\,. \tag{P.4}$$

The time derivatives of the diagonal entries of the inertia matrix are given as follows

$$\dot{M}_{11}=2\left(\frac{\partial K_{\dot{d}_1\dot{d}_1}}{\partial d_1}\dot{d}_1+\frac{\partial K_{\dot{d}_1\dot{d}_1}}{\partial d_2}\dot{d}_2+\frac{\partial K_{\dot{d}_1\dot{d}_1}}{\partial d_3}\dot{d}_3+\frac{\partial K_{\dot{d}_1\dot{d}_1}}{\partial \kappa_1}\dot{\kappa}_1\right) \tag{P.5}$$

$$\dot{M}_{22}=2\left(\frac{\partial K_{\dot{d}_2\dot{d}_2}}{\partial d_1}\dot{d}_1+\frac{\partial K_{\dot{d}_2\dot{d}_2}}{\partial d_2}\dot{d}_2+\frac{\partial K_{\dot{d}_2\dot{d}_2}}{\partial d_3}\dot{d}_3+\frac{\partial K_{\dot{d}_2\dot{d}_2}}{\partial \kappa_2}\dot{\kappa}_2\right) \tag{P.6}$$

$$\dot{M}_{33}=2\left(\frac{\partial K_{\dot{d}_3\dot{d}_3}}{\partial d_1}\dot{d}_1+\frac{\partial K_{\dot{d}_3\dot{d}_3}}{\partial d_2}\dot{d}_2+\frac{\partial K_{\dot{d}_3\dot{d}_3}}{\partial d_3}\dot{d}_3+\frac{\partial K_{\dot{d}_3}}{\partial \kappa_3}\dot{\kappa}_3\right) \tag{P.7}$$

$$\begin{aligned}\dot{M}_{44} &= 2\left(\frac{\partial K_{\dot{\kappa}_1\dot{\kappa}_1}}{\partial d_1}\dot{d}_1+\frac{\partial K_{\dot{\kappa}_1\dot{\kappa}_1}}{\partial d_2}\dot{d}_2+\frac{\partial K_{\dot{\kappa}_1\dot{\kappa}_1}}{\partial d_3}\dot{d}_3\right.\\ &\quad\left.+\frac{\partial K_{\dot{\kappa}_1\dot{\kappa}_1}}{\partial \kappa_1}\dot{\kappa}_1+\frac{\partial K_{\dot{\kappa}_1\dot{\kappa}_1}}{\partial \kappa_2}\dot{\kappa}_2+\frac{\partial K_{\dot{\kappa}_1\dot{\kappa}_1}}{\partial \kappa_3}\dot{\kappa}_3\right)\end{aligned} \tag{P.8}$$

$$\begin{aligned}\dot{M}_{55} &= 2\left(\frac{\partial K_{\dot{\kappa}_2\dot{\kappa}_2}}{\partial d_1}\dot{d}_1+\frac{\partial K_{\dot{\kappa}_2\dot{\kappa}_2}}{\partial d_2}\dot{d}_2+\frac{\partial K_{\dot{\kappa}_2\dot{\kappa}_2}}{\partial d_3}\dot{d}_3\right.\\ &\quad\left.+\frac{\partial K_{\dot{\kappa}_2\dot{\kappa}_2}}{\partial \kappa_2}\dot{\kappa}_2+\frac{\partial K_{\dot{\kappa}_2\dot{\kappa}_2}}{\partial \kappa_3}\dot{\kappa}_3\right)\end{aligned} \tag{P.9}$$

$$\dot{M}_{66} = 2\left(\frac{\partial K_{\dot{\kappa}_3\dot{\kappa}_3}}{\partial d_1}\dot{d}_1 + \frac{\partial K_{\dot{\kappa}_3\dot{\kappa}_3}}{\partial d_2}\dot{d}_2 + \frac{\partial K_{\dot{\kappa}_3\dot{\kappa}_3}}{\partial d_3}\dot{d}_3 + \frac{\partial K_{\dot{\kappa}_3\dot{\kappa}_3}}{\partial \kappa_3}\dot{\kappa}_3\right). \tag{P.10}$$

After comparing (P.5)-(P.10) with (N.1), (N.8), (N.15), (N.22), (N.29), and (N.36), it is clear that (P.3) is satisfied. The time derivatives of the off-diagonal entries of the inertia matrix are given as follows

$$\dot{M}_{12} = \frac{\partial K_{\dot{d}_1\dot{d}_2}}{\partial d_1}\dot{d}_1 + \frac{\partial K_{\dot{d}_1\dot{d}_2}}{\partial d_2}\dot{d}_2 + \frac{\partial K_{\dot{d}_1\dot{d}_2}}{\partial d_3}\dot{d}_3 + \frac{\partial K_{\dot{d}_1\dot{d}_2}}{\partial \kappa_1}\dot{\kappa}_1 + \frac{\partial K_{\dot{d}_1\dot{d}_2}}{\partial \kappa_2}\dot{\kappa}_2 \tag{P.11}$$

$$\dot{M}_{13} = \frac{\partial K_{\dot{d}_1\dot{d}_3}}{\partial d_1}\dot{d}_1 + \frac{\partial K_{\dot{d}_1\dot{d}_3}}{\partial d_2}\dot{d}_2 + \frac{\partial K_{\dot{d}_1\dot{d}_3}}{\partial d_3}\dot{d}_3 + \frac{\partial K_{\dot{d}_1\dot{d}_3}}{\partial \kappa_1}\dot{\kappa}_1 + \frac{\partial K_{\dot{d}_1\dot{d}_3}}{\partial \kappa_3}\dot{\kappa}_3 \tag{P.12}$$

$$\begin{aligned}\dot{M}_{14} &= \frac{\partial K_{\dot{d}_1\dot{\kappa}_1}}{\partial d_1}\dot{d}_1 + \frac{\partial K_{\dot{d}_1\dot{\kappa}_1}}{\partial d_2}\dot{d}_2 + \frac{\partial K_{\dot{d}_1\dot{\kappa}_1}}{\partial d_3}\dot{d}_3 \\ &\quad + \frac{\partial K_{\dot{d}_1\dot{\kappa}_1}}{\partial \kappa_1}\dot{\kappa}_1 + \frac{\partial K_{\dot{d}_1\dot{\kappa}_1}}{\partial \kappa_2}\dot{\kappa}_2 + \frac{\partial K_{\dot{d}_1\dot{\kappa}_1}}{\partial \kappa_3}\dot{\kappa}_3\end{aligned} \tag{P.13}$$

$$\begin{aligned}\dot{M}_{15} &= \frac{\partial K_{\dot{d}_1\dot{\kappa}_2}}{\partial d_1}\dot{d}_1 + \frac{\partial K_{\dot{d}_1\dot{\kappa}_2}}{\partial d_2}\dot{d}_2 + \frac{\partial K_{\dot{d}_1\dot{\kappa}_2}}{\partial d_3}\dot{d}_3 \\ &\quad + \frac{\partial K_{\dot{d}_1\dot{\kappa}_2}}{\partial \kappa_1}\dot{\kappa}_1 + \frac{\partial K_{\dot{d}_1\dot{\kappa}_2}}{\partial \kappa_2}\dot{\kappa}_2 + \frac{\partial K_{\dot{d}_1\dot{\kappa}_2}}{\partial \kappa_3}\dot{\kappa}_3\end{aligned} \tag{P.14}$$

$$\dot{M}_{16} = \frac{\partial K_{\dot{d}_1\dot{\kappa}_3}}{\partial d_1}\dot{d}_1 + \frac{\partial K_{\dot{d}_1\dot{\kappa}_3}}{\partial d_2}\dot{d}_2 + \frac{\partial K_{\dot{d}_1\dot{\kappa}_3}}{\partial d_3}\dot{d}_3 + \frac{\partial K_{\dot{d}_1\dot{\kappa}_3}}{\partial \kappa_1}\dot{\kappa}_1 + \frac{\partial K_{\dot{d}_1\dot{\kappa}_3}}{\partial \kappa_3}\dot{\kappa}_3 \tag{P.15}$$

$$\dot{M}_{23} = \frac{\partial K_{\dot{d}_2\dot{d}_3}}{\partial d_1}\dot{d}_1 + \frac{\partial K_{\dot{d}_2\dot{d}_3}}{\partial d_2}\dot{d}_2 + \frac{\partial K_{\dot{d}_2\dot{d}_3}}{\partial d_3}\dot{d}_3 + \frac{\partial K_{\dot{d}_2\dot{d}_3}}{\partial \kappa_2}\dot{\kappa}_2 + \frac{\partial K_{\dot{d}_2\dot{d}_3}}{\partial \kappa_3}\dot{\kappa}_3 \tag{P.16}$$

$$\begin{aligned}\dot{M}_{24} &= \frac{\partial K_{\dot{d}_2\dot{\kappa}_1}}{\partial d_1}\dot{d}_1 + \frac{\partial K_{\dot{d}_2\dot{\kappa}_1}}{\partial d_2}\dot{d}_2 + \frac{\partial K_{\dot{d}_2\dot{\kappa}_1}}{\partial d_3}\dot{d}_3 \\ &\quad + \frac{\partial K_{\dot{d}_2\dot{\kappa}_1}}{\partial \kappa_1}\dot{\kappa}_1 + \frac{\partial K_{\dot{d}_2\dot{\kappa}_1}}{\partial \kappa_2}\dot{\kappa}_2 + \frac{\partial K_{\dot{d}_2\dot{\kappa}_1}}{\partial \kappa_3}\dot{\kappa}_3\end{aligned} \tag{P.17}$$

$$\dot{M}_{25} = \frac{\partial K_{\dot{d}_2\dot{\kappa}_2}}{\partial d_1}\dot{d}_1 + \frac{\partial K_{\dot{d}_2\dot{\kappa}_2}}{\partial d_2}\dot{d}_2 + \frac{\partial K_{\dot{d}_2\dot{\kappa}_2}}{\partial d_3}\dot{d}_3 + \frac{\partial K_{\dot{d}_2\dot{\kappa}_2}}{\partial \kappa_2}\dot{\kappa}_2 + \frac{\partial K_{\dot{d}_2\dot{\kappa}_2}}{\partial \kappa_3}\dot{\kappa}_3 \tag{P.18}$$

$$\dot{M}_{26} = \frac{\partial K_{\dot{d}_2\dot{\kappa}_3}}{\partial d_1}\dot{d}_1 + \frac{\partial K_{\dot{d}_2\dot{\kappa}_3}}{\partial d_2}\dot{d}_2 + \frac{\partial K_{\dot{d}_2\dot{\kappa}_3}}{\partial d_3}\dot{d}_3 + \frac{\partial K_{\dot{d}_2\dot{\kappa}_3}}{\partial \kappa_2}\dot{\kappa}_2 + \frac{\partial K_{\dot{d}_2\dot{\kappa}_3}}{\partial \kappa_3}\dot{\kappa}_3 \tag{P.19}$$

$$\dot{M}_{34} = \frac{\partial K_{\dot{d}_3\dot{\kappa}_1}}{\partial d_1}\dot{d}_1 + \frac{\partial K_{\dot{d}_3\dot{\kappa}_1}}{\partial d_2}\dot{d}_2 + \frac{\partial K_{\dot{d}_3\dot{\kappa}_1}}{\partial d_3}\dot{d}_3 + \frac{\partial K_{\dot{d}_3\dot{\kappa}_1}}{\partial \kappa_1}\dot{\kappa}_1 + \frac{\partial K_{\dot{d}_3\dot{\kappa}_1}}{\partial \kappa_3}\dot{\kappa}_3 \tag{P.20}$$

$$\dot{M}_{35} = \frac{\partial K_{\dot{d}_3\dot{\kappa}_2}}{\partial d_1}\dot{d}_1 + \frac{\partial K_{\dot{d}_3\dot{\kappa}_2}}{\partial d_2}\dot{d}_2 + \frac{\partial K_{\dot{d}_3\dot{\kappa}_2}}{\partial d_3}\dot{d}_3 + \frac{\partial K_{\dot{d}_3\dot{\kappa}_2}}{\partial \kappa_2}\dot{\kappa}_2 + \frac{\partial K_{\dot{d}_3\dot{\kappa}_2}}{\partial \kappa_3}\dot{\kappa}_3 \tag{P.21}$$

$$\dot{M}_{36} = \frac{\partial K_{\dot{d}_3\dot{\kappa}_3}}{\partial d_1}\dot{d}_1 + \frac{\partial K_{\dot{d}_3\dot{\kappa}_3}}{\partial d_2}\dot{d}_2 + \frac{\partial K_{\dot{d}_3\dot{\kappa}_3}}{\partial d_3}\dot{d}_3 + \frac{\partial K_{\dot{d}_3\dot{\kappa}_3}}{\partial \kappa_3}\dot{\kappa}_3 \tag{P.22}$$

$$\begin{aligned}\dot{M}_{45} &= \frac{\partial K_{\dot{\kappa}_1\dot{\kappa}_2}}{\partial d_1}\dot{d}_1 + \frac{\partial K_{\dot{\kappa}_1\dot{\kappa}_2}}{\partial d_2}\dot{d}_2 + \frac{\partial K_{\dot{\kappa}_1\dot{\kappa}_2}}{\partial d_3}\dot{d}_3 \\ &\quad + \frac{\partial K_{\dot{\kappa}_1\dot{\kappa}_2}}{\partial \kappa_1}\dot{\kappa}_1 + \frac{\partial K_{\dot{\kappa}_1\dot{\kappa}_2}}{\partial \kappa_2}\dot{\kappa}_2 + \frac{\partial K_{\dot{\kappa}_1\dot{\kappa}_2}}{\partial \kappa_3}\dot{\kappa}_3\end{aligned} \tag{P.23}$$

$$\dot{M}_{46} = \frac{\partial K_{\dot{\kappa}_1\dot{\kappa}_3}}{\partial d_1}\dot{d}_1 + \frac{\partial K_{\dot{\kappa}_1\dot{\kappa}_3}}{\partial d_2}\dot{d}_2 + \frac{\partial K_{\dot{\kappa}_1\dot{\kappa}_3}}{\partial d_3}\dot{d}_3 + \frac{\partial K_{\dot{\kappa}_1\dot{\kappa}_3}}{\partial \kappa_1}\dot{\kappa}_1 + \frac{\partial K_{\dot{\kappa}_1\dot{\kappa}_3}}{\partial \kappa_3}\dot{\kappa}_3 \tag{P.24}$$

$$\dot{M}_{56} = \frac{\partial K_{\dot{\kappa}_2\dot{\kappa}_3}}{\partial d_1}\dot{d}_1 + \frac{\partial K_{\dot{\kappa}_2\dot{\kappa}_3}}{\partial d_2}\dot{d}_2 + \frac{\partial K_{\dot{\kappa}_2\dot{\kappa}_3}}{\partial d_3}\dot{d}_3 + \frac{\partial K_{\dot{\kappa}_2\dot{\kappa}_3}}{\partial \kappa_2}\dot{\kappa}_2 + \frac{\partial K_{\dot{\kappa}_2\dot{\kappa}_3}}{\partial \kappa_3}\dot{\kappa}_3. \tag{P.25}$$

After comparing (P.11)-(P.25) with the corresponding entries of $V(q, \dot{q})$, then it is clear that (P.4) is satisfied.

BIBLIOGRAPHY

[1] W. Dixon, A. Behal, D. Dawson, and S. Nagarkatti, *Nonlinear Control of Engineering Systems: A Lyapunov-Based Approach*. Boston, MA: Birkhauser, 2003.

[2] H. Mochiyama and T. Suzuki, "Dynamics modelling of a hyper-flexible manipulator," in *Proc. of the 41st SICE Annual Conference*, Osaka, Japan, 2002, pp. 1505–1510.

[3] F. Caccavale, C. Natale, B. Siciliano, and L. Villani, "Resolved-acceleration control of robot manipulators: A critical review with experiments," *Robotica*, vol. 16, no. 5, pp. 565–573, 1998.

[4] O. Khatib, "Dynamic control of manipulators in operational space," in *IFTOMM Cong. Theory of Machines and Mechanisms*, New Delhi, India, 1983, pp. 1–10.

[5] J. Yuan, "Closed-loop manipulator control using quaternion feedback," *IEEE Trans. Robot. Automat.*, vol. 4, no. 4, pp. 434–440, 1988.

[6] Y. Nakamura, *Advanced Robotics Redundancy and Optimization*. Reading, MA: Addison-Wesley, 1991.

[7] D. Nenchev, "Redundancy resolution through local optimization: A review," *Journal of Robotic Systems*, vol. 6, no. 6, pp. 769–798, 1989.

[8] B. Siciliano, "Kinematic control of redundant robot manipulators: A tutorial," *J. Intelligent and Robotic Systems*, vol. 3, no. 3, pp. 201–212, 1990.

[9] R. Colbaugh and K. Glass, "Robust adaptive control of redundant manipulators," *J. Intelligent and Robotic Systems*, vol. 14, no. 1, pp. 68–88, 1995.

[10] P. Hsu, J. Hauser, and S. Sastry, "Dynamic control of redundant manipulators," *Journal of Robotic Systems*, vol. 6, no. 3, pp. 133–148, 1989.

[11] Z. Peng and N. Adachi, "Compliant motion control of kinematically redundant manipulators," *IEEE Trans. Robot. Automat.*, vol. 9, no. 6, pp. 831–837, 1993.

[12] H. Seraji, "Configuration control of redundant manipulators: Theory and implementation," *IEEE Trans. Robot. Automat.*, vol. 5, no. 4, pp. 472–490, 1989.

[13] T. Yoshikawa, "Analysis and control of robot manipulators with redundancy," in *Robotics Research - The First International Symp.*, Cambridge, MA, 1994, pp. 735–747.

[14] E. Zergeroglu, D. Dawson, I. Walker, and A. Behal, "Nonlinear tracking control of kinematically redundant robot manipulators," in *Proc. American Control Conf.*, Chicago, IL, 2000, pp. 2513–2517.

[15] F. Lewis, D. Dawson, and C. Abdallah, *Robot Manipulator Control: Theory and Practice*. New York, NY: Marcel Dekker, Inc., 2004.

[16] F. Lizarralde and J. Wen, "Attitude control without angular velocity measurement: A passivity approach," *IEEE Trans. Automat. Contr.*, vol. 41, no. 3, pp. 468–472, 1996.

[17] P. Hughes, *Spacecraft Attitude Dynamics*. New York, NY: Wiley, 1994.

[18] A. Klumpp, "Singularity-free extraction of a quaternion from a directional cosine matrix," *J. Spacecraft and Rockets*, vol. 13, no. 12, pp. 754–755, 1976.

[19] J. Ahmed, V. Coppola, and D. Bernstein, "Adaptive asymptotic tracking of spacecraft attitude motion with inertia matrix identification," *J. Guidance, Control, and Dynamics*, vol. 21, no. 5, pp. 684–691, 1998.

[20] J. Kuipers, *Quaternions and Rotation Sequences*. Princeton, NJ: Princeton University Press, 1999.

[21] D. Dawson, M. Bridges, and Z.Qu, *Nonlinear Control of Robotic Systems for Environmental Waste and Restoration*. Englewood Cliffs, NJ: Prentice-Hall, 1995.

[22] L. Sciavicco and B. Sicilano, *Modeling and Control of Robot Manipulators*. New York, NY: McGraw-Hill Co., 1996.

[23] I. Walker, "Impact configurations and measures for kinematically redundant and multiple armed robot systems," *IEEE Trans. Robot. Automat.*, vol. 10, no. 5, pp. 670–683, 1994.

[24] H. Khalil, "Adaptive output feedback control of nonlinear systems represented by input-output models," *IEEE Trans. Automat. Contr.*, vol. 41, no. 2, pp. 177–188, 1996.

[25] E. Faulring, K. Lynch, J. Colgate, and M. Peshkin, "Haptic interaction with constrained dynamic systems," in *Proc. IEEE Int. Conf. Robot. Autom.*, Barcelona, Spain, 2005, pp. 2458–2464.

[26] T. B. Sheridan, *Telerobotics, Automation, and Human Supervisory Control*. Cambridge, MA: MIT Press, 1992.

[27] R. V. der Linde, P. Lammertse, E. Frederiksen, and B. Ruiter, "The hapticmaster, a new high-performance haptic interface," in *Proc. EuroHaptics*, Edinburgh, U.K., 2002, pp. 1–5.

[28] B. Hannaford, "A design framework for teleoperators with kinesthetic feedback," *IEEE Trans. Robot. Automat.*, vol. 5, no. 4, pp. 426–434, 1989.

[29] J. Colgate, "Robust impedance shaping telemanipulation," *IEEE Trans. Robot. Automat.*, vol. 9, no. 4, pp. 374–384, 1993.

[30] K. Fite, L. Shao, and M. Goldfarb, "Loop shaping for transparency and stability robustness in bilateral telemanipulation," *IEEE Trans. Robot. Automat.*, vol. 20, no. 3, pp. 620–624, 2004.

[31] D. Lawrence, "Stability and transparency in bilateral teleoperation," *IEEE Trans. Robot. Automat.*, vol. 9, no. 5, pp. 624–637, 1993.

[32] S. Salcudean, M. Zhu, W.-H. Zhu, and K. Hashtrudi-Zaad, "Transparent bilateral teleoperation under position and rate control," *Int. J. Robotics Research*, vol. 19, no. 12, pp. 1185–1202, 2000.

[33] Y. Yokokohji and T. Yoshikawa, "Bilateral control of master-slave manipulators for ideal kinesthetic coupling-formulation and experiment," *IEEE Trans. Robot. Automat.*, vol. 10, no. 5, pp. 605–620, 1994.

[34] N. Chopra, M. Spong, and R. Lozano, "Adaptive coordination control of bilateral teleoperators with time delay," in *Proc. IEEE Int. Conf. Decision and Control*, Nassau, Bahamas, 2004, pp. 4540–4547.

[35] K. Hashtrudi-Zaad and S. Salcudean, "Adaptive transparent impedance reflecting teleoperation," in *Proc. IEEE Int. Conf. Robot. Autom.*, Minneapolis, MN, 1996, pp. 1369–1374.

[36] H.-K. Lee and M. J. Chung, "Adaptive controller of a master-slave system for transparent teleoperation," *Journal of Robotic Systems*, vol. 15, no. 8, pp. 465–475, 1998.

[37] J.-H. Ryu and D.-S. Kwon, "A novel adaptive bilateral control scheme using similar closed-loop dynamic characteristics of master/slave manipulators," *Journal of Robotic Systems*, vol. 18, no. 9, pp. 533–543, 2001.

[38] M. Shi, G. Tao, H. Liu, and J. Downs, "Adaptive control of teleoperation systems," in *Proc. IEEE Int. Conf. Decision and Control*, Phoenix, AZ, 1999, pp. 791–796.

[39] W.-H. Zhu and S. Salcudean, "Stability guaranteed teleoperation: An adaptive motion/force control approach," *IEEE Trans. Automat. Contr.*, vol. 45, no. 11, pp. 1951–1969, 2000.

[40] R. Anderson and M. Spong, "Bilateral control of teleoperators with time delay," *IEEE Trans. Automat. Contr.*, vol. 34, no. 5, pp. 494–501, 1989.

[41] G. Niemeyer and J.-J. Slotine, "Stable adaptive teleoperation," *IEEE J. Oceanic Eng.*, vol. 16, no. 1, pp. 152–162, 1991.

[42] N. Chopra, M. Spong, R. Ortega, and N. Barabanov, "On position tracking in bilateral teleoperation," in *Proc. American Control Conf.*, Boston, MA, 2004, pp. 5244–5249.

[43] G. Niemeyer and J.-J. Slotine, "Designing force reflecting teleoperators with large time delays to appear as virtual tools," in *Proc. IEEE Int. Conf. Robot. Autom.*, Albuquerque, NM, 1997, pp. 2212–2218.

[44] N. Chopra, M. Spong, S. Hirche, and M. Buss, "Bilateral teleoperation over the internet: the time varying delay problem," in *Proc. American Control Conf.*, Denver, CO, 2003, pp. 155–160.

[45] D. Lee and P. Li, "Passive bilateral feedforward control of linear dynamically similar teleoperated manipulators," *IEEE Trans. Robot. Automat.*, vol. 19, no. 3, pp. 443–456, 2003.

[46] ——, "Passive coordination control of nonlinear bilateral teleoperated manipulators," in *Proc. IEEE Int. Conf. Robot. Autom.*, Washington, DC, 2002, pp. 3278–3283.

[47] ——, "Passive tool dynamics rendering for nonlinear bilateral teleoperated manipulators," in *Proc. IEEE Int. Conf. Robot. Autom.*, Washington, DC, 2002, pp. 3284–3289.

[48] ——, "Toward robust passivity: a passive control implementation structure for mechanical teleoperators," in *Proc. IEEE VR Symposium on Haptic Interfaces for Virtual Environment and Teleoperator Systems*, Los Angeles, CA, 2003, pp. 132–139.

[49] ——, "Passive bilateral control and tool dynamics rendering for nonlinear mechanical teleoperators," *IEEE Trans. Robot. Automat.*, vol. 21, no. 5, pp. 936–951, 2005.

[50] D. Lee and M. Spong, "Bilateral teleoperation of multiple cooperative robots over delayed communication networks: Theory," in *Proc. IEEE Int. Conf. Robot. Autom.*, Barcelona, Spain, 2005, pp. 360–365.

[51] D. Lee, O. Martinez-Palafox, and M. Spong, "Bilateral teleoperation of multiple cooperative robots over delayed communication networks: Application," in *Proc. IEEE Int. Conf. Robot. Autom.*, Barcelona, Spain, 2005, pp. 366–371.

[52] B. Hannaford and J.-H. Ryu, "Time domain passivity control of haptic interfaces," *IEEE Trans. Robot. Automat.*, vol. 18, no. 1, pp. 1–10, 2002.

[53] J.-H. Ryu, C. Preusche, B. Hannaford, and G. Hirzinger, "Time domain passivity control with reference energy following," *IEEE Trans. Contr. Syst. Technol.*, vol. 13, no. 5, pp. 737–742, 2005.

[54] M. McIntyre, W. Dixon, D. Dawson, and E. Tatlicioglu, "Passive coordination of nonlinear bilateral teleoperated manipulators," *Robotica*, vol. 24, no. 4, pp. 463–476, 2006.

[55] Z. Qu and J.-X. Xu, "Model-based learning controls and their comparisons using lyapunov direct method," *Asian J. Control*, vol. 4, no. 1, pp. 99–110, 2002.

[56] B. Xian, M. de Queiroz, and D. Dawson, "A continuous control mechanism for uncertain nonlinear systems," in *Control, Stabilization, and Nonsmooth Analysis, Lecture Notes in Control and Information Sciences.* Heidelberg, Germany: Springer-Verlag, 2004, pp. 251–262.

[57] P. Li and R. Horowitz, "Passive velocity field control of mechanical manipulators," *IEEE Trans. Robot. Automat.*, vol. 15, no. 4, pp. 751–763, 1999.

[58] I. Cervantes, R. Kelly, J. Alvarez-Ramirez, and J. Moreno, "A robust velocity field control," *IEEE Trans. Contr. Syst. Technol.*, vol. 10, no. 6, pp. 888–894, 2002.

[59] M. W. Spong and M. Vidyasagar, *Robot Dynamics and Control.* New York, NY: John Wiley and Sons, Inc., 1989.

[60] R. Ortega, A. Loria, P. Nicklasson, and H. Sira-Ramirez, *Passivity-based Control of Euler-Lagrange Systems*. London: Springer-Verlag, 1998.

[61] M. Fliess, J. Levine, P. Martin, and P. Rouchon, "Flatness and defect of non-linear systems: Introductory theory and examples," *Int. J. Control*, vol. 61, no. 6, pp. 1327–1361, 1995.

[62] K. Glass, R. Colbaugh, and K. Wedeward, "Control of differentially flat mechanical systems in the presence of uncertainty," in *Proc. American Control Conf.*, Albuquerque, NM, 1997, pp. 3836–3838.

[63] Y. Zhang and P. Ioannou, "A new class of nonlinear robust adaptive controllers," *Int. J. Control*, vol. 65, no. 5, pp. 745–769, 1996.

[64] M. Polycarpou and P. Ioannou, "A robust adaptive nonlinear control design," *Automatica*, vol. 33, no. 3, pp. 423–427, 1996.

[65] R. Freeman, M. Krstic, and P. Kokotovic, "Robustness of adaptive nonlinear control to bounded uncertainties," *Automatica*, vol. 34, no. 10, p. 1998, 1227-1230.

[66] M. Krstic, I. Kanellakopoulos, and P. Kokotovic, *Nonlinear and Adaptive Control Design*. New York, NY: John Wiley and Sons, 1995.

[67] F. Ikhouane and M. Krstic, "Robustness of the tuning functions adaptive backstepping designs for linear systems," *IEEE Trans. Automat. Contr.*, vol. 43, no. 3, pp. 431–437, 1998.

[68] R. Marino and P. Tomei, "Robust adaptive state-feedback tracking for nonlinear systems," *IEEE Trans. Automat. Contr.*, vol. 43, no. 1, pp. 84–89, 1998.

[69] Z. Pan and T. Basar, "Adaptive controller design for tracking and disturbance attenuation in parametric strict-feedback nonlinear systems," *IEEE Trans. Automat. Contr.*, vol. 43, no. 8, pp. 1066–1083, 1998.

[70] S. Ge and J. Wang, "Robust adaptive tracking for time-varying uncertain nonlinear systems with unknown control coefficients," *IEEE Trans. Automat. Contr.*, vol. 48, no. 8, p. 2003, 1462-1469.

[71] M. Krstic, "Invariant manifolds and asymptotic properties of adaptive nonlinear stabilizers," *IEEE Trans. Automat. Contr.*, vol. 41, no. 6, pp. 817–829, 1996.

[72] Z. Cai, M. de Queiroz, and D. Dawson, "Robust adaptive asymptotic tracking of nonlinear systems with additive disturbance," *IEEE Trans. Automat. Contr.*, vol. 51, no. 3, pp. 524–529, 2006.

[73] D. A. Bristow, M. Tharayil, and A. G. Alleyne, "A survey of iterative learning control," *IEEE Control Syst. Mag.*, vol. 26, no. 3, pp. 96–114, 2006.

[74] W. Dixon, E. Zergeroglu, D. Dawson, and B. Kostic, "Repetitive learning control: A lyapunov-based approach," *IEEE Trans. Syst., Man, Cybern. B*, vol. 32, no. 4, pp. 538–545, 2002.

[75] G. Hillerstrom and K. Walgama, "Repetitive control theory and applications - a survey," in *Proc. 13th IFAC World Congress*, San Francisco, CA, 1996, pp. 1–6.

[76] B. Xian, D. Dawson, M. de Queiroz, and J. Chen, "A continuous asymptotic tracking control strategy for uncertain nonlinear systems," *IEEE Trans. Automat. Contr.*, vol. 49, no. 7, pp. 1206–1211, 2004.

[77] W. J. Book, "Recursive lagrangian dynamics of flexible manipulator arms," *Int. J. Robotics Research*, vol. 3, no. 3, pp. 87–1010, 1984.

[78] G. Robinson and J. Davies, "Continuum robots - a state of the art," in *Proc. IEEE Int. Conf. Robot. Autom.*, Detroit, MI, 1999, pp. 2849–2854.

[79] V. Anderson and R. Horn, "Tensor arm manipulator design," *Transactions of the ASME*, vol. 67-DE-57, pp. 1–12, 1967.

[80] G. Chen, P. Tu, T. Herve, and C. Prelle, "Design and modeling of a micro-robotic manipulator for colonoscopy," in *Proc. of the 41st SICE Annual Conference*, Annecy, France, 2005, pp. 109–114.

[81] G. Chirikjian and J. Burdick, "A hyper-redundant manipulator," *IEEE Robot. Automat. Mag.*, vol. 1, no. 4, pp. 22–29, 1994.

[82] S. Hirose, *Biologically Inspired Robots*. New York, NY: Oxford University Press, 1993.

[83] M. Ivanescu and V. Stoian, "A variable structure controller for a tentacle manipulator," in *Proc. IEEE Int. Conf. Robot. Autom.*, Nagoya, Japan, 1995, pp. 3155–3160.

[84] D. Lane, J. Davies, G. Robinson, D. O'Brien, J. Sneddon, E. Seaton, and A. Elfstrom, "The amadeus dextrous subsea hand: Design, modeling, and sensor processing," *IEEE J. Oceanic Eng.*, vol. 24, no. 1, pp. 96–111, 1999.

[85] R. Cieslak and A. Morecki, "Elephant trunk type elastic manipulator a tool for bulk and liquid type materials transportation," *Robotica*, vol. 17, no. 1, pp. 11–16, 1999.

[86] H. Tsukagoshi, A. Kitagawa, and M. Segawa, "Active hose: An artificial elephant's nose with maneuverability for rescue operation," in *Proc. IEEE Int. Conf. Robot. Autom.*, Seoul, Korea, 2001, pp. 2454–2459.

[87] W. McMahan, B. Jones, V. Chitrakaran, M. Csencsits, M. Grissom, M. Pritts, C. Rahn, and I. Walker, "Field trials and testing of the octarm continuum manipulator," in *Proc. IEEE Int. Conf. Robot. Autom.*, Orlando, FL, 2006, pp. 2336–2341.

[88] H. Ohno and S. Hirose, "Design of slim slime robot and its gait of locomotion," in *Proc. IEEE/RSJ Int. Conf. Intell. Robots Syst.*, Maui, HI, 2001, pp. 707–715.

[89] K. Suzumori, S. Iikura, and H. Tanaka, "Development of flexible microactuator and its applications to robotic mechanisms," in *Proc. IEEE Int. Conf. Robot. Autom.*, Sacramento, CA, 1991, pp. 1622–1627.

[90] R. Buckingham and A. Graham, "Snaking around in a nuclear jungle," *Industrial Robot: An International Journal*, vol. 32, no. 2, pp. 120–127, 2005.

[91] G. Immega and K. Antonelli, "The ksi tentacle manipulator," in *Proc. IEEE Int. Conf. Robot. Autom.*, Nagoya, Japan, 1995, pp. 3149–3154.

[92] W. McMahan, B. Jones, and I. Walker, "Robotic manipulators inspired by cephalopod limbs," *J. Engineering Design and Innovation*, vol. 1P-01P2, 2005.

[93] I. Walker, C. Carreras, R. McDonnell, and G. Grimes, "Extension versus bending for continuum robots," *Intl. J. Advanced Robotic Systems*, vol. 3, no. 2, pp. 171–178, 2006.

[94] B. Jones and I. Walker, "Limiting-case analysis of continuum trunk kinematics," in *Proc. IEEE Int. Conf. Robot. Autom.*, Rome, Italy, 2007, pp. 1363–1368.

[95] ——, "Kinematics for multi-section continuum robots," *IEEE Transactions on Robotics*, vol. 22, no. 1, pp. 43–55, 2006.

[96] W. Khalil, G. Gallot, O. Ibrahim, and F. Boyer, "Dynamic modeling of a 3-d serial eel-like robot," in *Proc. IEEE Int. Conf. Robot. Autom.*, Barcelona, Spain, 2005, pp. 1282–1287.

[97] F. Matsuno and H. Sato, "Trajectory tracking control of snake robots based on dynamic model," in *Proc. IEEE Int. Conf. Robot. Autom.*, Barcelona, Spain, 2005, pp. 3040–3045.

[98] Y. Yekutieli, R. Sagiv-Zohar, R. Aharonov, Y. Engel, B. Hochner, and T. Flash, "Dynamic model of the octopus arm. i. biomechanics of the octopus arm reaching movement," *Journal of Neurophysiology*, vol. 94, pp. 1443–1458, 2005.

[99] G. Chirikjian and J. Burdick, "A modal approach to hyper-redundant manipulator kinematics," *IEEE Trans. Robot. Automat.*, vol. 10, no. 3, pp. 343–354, 1994.

[100] G. Chirikjian, "Hyper-redundant manipulator dynamics: A continuum approximation," *Advanced Robotics*, vol. 9, no. 3, pp. 217–243, 1995.

[101] M. Ivanescu, N. Popescu, and D. Popescu, "A variable length tentacle manipulator control system," in *Proc. IEEE Int. Conf. Robot. Autom.*, Barcelona, Spain, 2005, pp. 3274–3279.

[102] ——, "A variable length tentacle manipulator control system," in *Proc. IEEE Int. Conf. Robot. Autom.*, Barcelona, Spain, 2005, pp. 3274–3279.

[103] H. Mochiyama, "Hyper-flexible robotic manipulators," in *Proc. IEEE Int. Symposium on Micro-NanoMechatronics and Human Science*, Nagoya, Japan, 2005, pp. 41–46.

[104] H. Mochiyama and T. Suzuki, "Kinematics and dynamics of a cable-like hyper-flexible manipulator," in *Proc. IEEE Int. Conf. Robot. Autom.*, Taipei, Taiwan, 2003, pp. 3672–3677.

[105] M. Corless and G. Leitmann, "Continuous state feedback guaranteeing uniform ultimate boundedness for uncertain dynamic systems," *IEEE Trans. Automat. Contr.*, vol. 26, no. 5, pp. 1139–1144, 1981.

[106] H. K. Khalil, *Nonlinear Systems, 3rd Edition.* New York, NY: Prentice Hall, 2002.